1987

Identification of endmembers for magma mixing in Little Sitkin Volcano, Alaska

Douglas A. Wolf
University at Albany, State University of New York

IDENTIFICATION OF ENDMEMBERS FOR MAGMA MIXING IN LITTLE SITKIN VOLCANO, ALASKA

A thesis presented to the Faculty

of the State University of New York

at Albany

in partial fulfillment of the requirements

for the degree of

Master of Science

Douglas A. Wolf

1987

IDENTIFICATION OF ENDMEMBERS FOR MAGMA MIXING IN LITTLE SITKIN VOLCANO, ALASKA

Abstract of

a thesis presented to the Faculty

of the State University of New York

at Albany

in partial fulfillment of the requirements

for the degree of

Master of Science

Douglas A. Wolf

1987

ABSTRACT

Little Sitkin island is an Aleutian calc-alkalic volcanic center that has erupted a suite of lavas ranging from andesite through rhyodacite. Whole-rock chemistry of these lavas indicates contrasting evolutionary processes; major-oxide silica variation diagrams exhibit linear trends that are suggestive of magma-mixing while trace-element trends are largely controlled by accessory-phase fractionation.

Plagioclase, the dominant phenocryst phase in all lavas, commonly occurs in two distinct populations with markedly different compositions and textures. Both normal and reverse zonation is noted in the plagioclase and clinopyroxene of several samples. In addition, clinopyroxene is found as rims on orthopyroxene grains and as cores with orthopyroxene rims in one sample. These inhomogeneities and indications of disequilibrium are supportive of mixing.

The phase chemistry of the Little Sitkin samples indicates that several andesites of intermediate composition formed as a result of mixing. There is considerable overlap of phase compositions in the intermediate andesites and other samples, however the most complete overlap occurs with a rhyodacite. This suggests that the intermediate andesites formed as a result of mixing between a silicic rhyodacite and a more primitive

low-silica andesite. The andesitic endmember has not been sampled, although its bulk-rock major-element chemistry has been estimated.

Least-squares modelling of four whole-rock mixes shows close agreement between observed and calculated andesite compositions. The sum of the squares of the residuals for these calculations are all less than one. The best match is given by a mixing pair of rhyodacite and the estimated andesite composition, for which the sum of the squares of the residuals is approximately 0.02.

Comparison of the petrography and whole-rock chemistry of a sample previously described as a basalt suggests that addition of approximately 35 to 45 weight percent clinopyroxene to an andesite resulted in the observed composition. Least-squares analysis of the Little Sitkin samples indicates that incorporation of a smaller proportion of clinopyroxene, approximately 34 weight percent, plus lesser olivine, plagioclase and magnetite by an andesitic liquid formed the "basalt". These phases are possibly cumulate and were incorporated into the andesitic liquid when a fresh pulse of parental magma carried them up to a shallow crustal magma chamber from lower crustal depths. This indicates that andesite, not basalt, is the most primitive composition sampled on the island, and therefore the composition of the parental magma must be inferred. Amphibole compositions indicate that the most

reasonable composition of the parent is that of high-alumina basalt (HAB).

A model is proposed in which partial melting of mantle peridotite yields an olivine tholeiite liquid. High-pressure fractionation of this liquid at the base of the crust produces the HAB parent magma. The HAB magma then undergoes low-pressure fractionation at upper crustal depths. This process, along with mixing between fresh HAB and more evolved compositions yields the suite of rocks found on the island. Late stage mixing of magmas intermediate between HAB and the silicic component is recorded by intermediate andesite compositions.

ACKNOWLEDGMENTS

I am deeply indebted to many people for their help in the writing of this thesis. No doubt if I were to list them all the result would be a volume almost as thick as this thesis itself! Obviously, a word of thanks must go to the professors and instructors that I have had the privelege to study under: John Delano, Greg Harper, Mark Harrison, Bill Kidd, Win Means, Akiho Miyashiro and George Putman. Steve DeLong deserves an extra word of thanks for enlightening me to the problems of Aleutian petrology and his patience when I seemed extraordinarily unintelligent. It is because of his guidance that I feel as if I am finally starting to understand igneous petrology. Extra thanks to Steve, George and Don Baker for serving as my defense committee. Extra extra thanks to Greg for generously allowing me the use of his computer and associated hardware and software.

In my eight (lord, is it really that many?) years at SUNYA I have been fortunate to have made a great many lasting friendships on campus, in the department and at the New York State Geological Survey. The support of many of them went far in keeping my morale up, especially when times got tough and a completed thesis seemed like a pipe dream. For putting up with me during the duration of this project they deserve thanks.

Special thanks to Ed Landing down at the Survey for

friendship and financial support over the last year and a half of this undertaking. Where else could I have developed a deep appreciation for the fine art of picking conodonts? Additional special thanks to Sandy Bromble down at Lamont for her patience, good humor and thoughtful instruction on microprobe usage and psychology (you have to know how to talk to these machines!).

Of course a large amount of support came from my family, and I can never really thank them enough. My parents, grandparents and brother have all been a great help and have always had an encouraging word. Last, but by no means least, a million thanks and a big hug and kiss to Fuji. Without her support, I never would have finished.

TABLE OF CONTENTS

LIST OF FIGURES

LIST OF TABLES

1 - ALEUTIAN ISLANDS

The Aleutian Islands are located between aproximately 52^{o} and 54^{o} N latitude and between 165^{o} W and 170^{o} E longitude. The islands form a broad arc (figure 1-1), which continues the trend of the Alaskan Peninsula. The arc is associated with active subduction of the northwesterly moving Pacific plate beneath the North American plate. Subduction in the eastern part of the arc and the Alaskan peninsula is virtually orthogonal, while in the western parts of the arc subduction becomes more and more oblique until strike slip motion predominates at the extreme western end (Marsh, 1982).

The Aleutian arc is geologically young. The oldest rocks found in the arc are Eocene an have been dated as about 45 m.y. (Marlow et al., 1973; DeLong et al., 1978). These rocks, termed the early series, are primarily altered marine volcanics and sediments. DeLong et al. (1978) estimated a time of metamorphism for the rocks of the early series at about 30 m.y. based on K-Ar ages.

Deposition of the rocks of the early series was followed by a period of plutonism within the arc. The composition of the plutonics ranges from gabbro to granite, with the majority of the plutons being granodioritic (Scholl et al., 1970; Marlow et al., 1973). Ages for these bodies range from about 11 to 16 m.y. b.p., based on K-Ar analyses, and they intrude the rocks of the early series

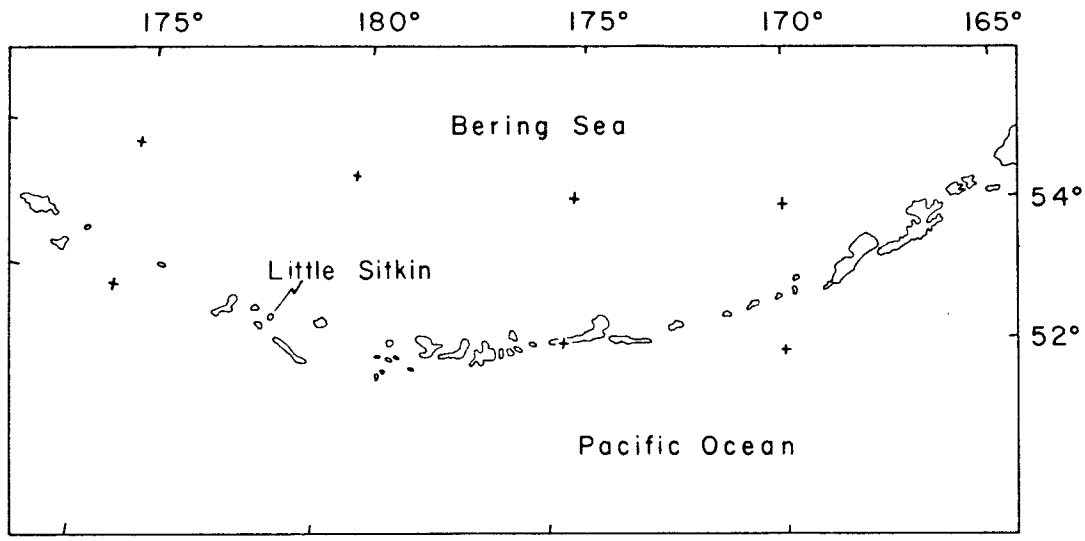

Figure 1-1 Location map for Little Sitkin island in the Aleutian chain.

(Marlow et al., 1973).

The youngest rocks exposed in the arc are collectively termed the late series and consist mostly of lavas and pyroclastic deposits ranging in age from late Tertiary to Quaternary (Marlow et al., 1973). The bulk of the rocks exposed on the islands are products of these Quaternary volcanoes, and volcanic activity continues to the present.

On many of the islands the late series rests unconformably upon rocks of the early series. This unconformity reflects a change from mostly marine to mostly subaerial volcanism (Marlow et al., 1973). This change in the nature of the extrusive environment represents uplift of the Aleutian ridge, although timing of this event is subject to some uncertainty. DeLong et al. (1978) suggested that the emergence of the Aleutian plateau was related to the subduction of the Kula Ridge at the Aleutian trench. Using the rock record and calculated plate motions, DeLong et al. (1978) present a possible model for the subduction of the Kula Ridge and the subsequent uplift of the Aleutian plateau.

The sequence of events as theorized by DeLong et al. (1978) can be summarized as the following: Arc magmatism gradually slowed and finally shut off with the approach of the Kula Ridge. This served to end the period of extrusion and deposition of rocks of the early series. Slowly, the crest of the Aleutian ridge was exposed in the late Eocene

to Oligocene time, and then the greatest uplift and metamorphism occurred at about 30 m.y. ago due to the subduction of the ridge crest beneath the arc. As the remainder of the Kula Ridge was subducted, the arc began to subside in late Oligocene to early Miocene time. Finally, arc magmatism resumed at about middle Miocene time, approximately 15 m.y. ago. This eventually resulted in the formation of the Quaternary volcanoes that are the hallmark of the modern arc.

Volcanism in the Aleutian chain has resulted in the formation of two contrasting sets of volcanic centers, calc-alkalic and tholeiitic. According to Kay et al. (1982) the tholeiitic centers are generally large, basaltic volcanoes, while the calc-alkalic volcanoes are more often small to medium sized and andesitic. The distinction between the two trends is shown best in plots of FeO^*/MgO (where FeO is all iron as Fe^{+2}) versus SiO_2 (Miyashiro, 1974). The tholeiitic centers have FeO^*/MgO ratios that increase greatly with increasing silica, while the calc-alkalic centers have ratios that remain basically constant or increase slightly with increasing silica (Kay et al., 1982). This can be seen in figure 3-1. Although these differences may be hard to distinguish at low silica contents, at higher silica contents they become more pronounced. Indeed, for intermediate to high silica levels, the tholeiitic centers have higher FeO^*, K_2O, Na_2O

and TiO_2, but lower levels of MgO, CaO and Al_2O_3 than the calc-alkalic centers (Kay et al., 1982). Thus the Aleutian tholeiites are distinguished on the basis of iron enrichment with increasing silica, yet show anomalously high concentrations of the alkalis and anomalously low concentrations of CaO when compared with the Aleutian calc-alkalic rocks. Kay et al. (1982) do not explain this curious feature of the Aleutian volcanics.

A question that immediately arises is, "What is the cause or causes for the contrasting trends within the arc?" Kay et al. (1982) presented a possible explanation for the occurrence of the contrasting trends throughout the arc. Specifically, they noted that the Aleutian arc may be broken up into several linear segments whose boundaries correspond to rupture zones of great earthquakes and areas where fracture zones on the northern Pacific plate are being subducted beneath the North American plate. Kay et al. (1982) further showed that there is a correlation between the position of a volcanic center within a segment and the bulk chemical trend displayed by that center. The tholeiitic volcanic centers are generally found at the ends of, or between, segments where, perhaps, magmas can more easily reach the surface, and where shallow closed-system fractionation may be the dominant process. Calc-alkalic centers are found primarily within the segments. Here, movement of magma through the thicker material of the upper

plate is apparently more difficult, thus causing the magmas to undergo differentiation at much greater depths than the magmas beneath the tholeiitic centers (Kay et al., 1982).

Kay and Kay (1985a) further subdivided the Aleutian trends into calc-alkalic classes 1 and 2 and tholeiitic classes 1 and 2. Although this subdivision results in the need for greater detailed knowledge of the different processes responsible for the diversity in rock chemistry, the basic conclusions drawn by these workers support the earlier work of Kay et al. (1982). Specifically, Kay and Kay (1985a) reported that both classes of calc-alkalic rocks indicate deep formational processes were active during their evolution, although specific processes may have been different, and each class may have been subject to further differentiation at different levels within the crust. The two tholeiitic classes indicate, through various petrographic and chemical features, that shallow formational processes were at work, although as in the case of the calc-alkalic classes, the dominant processes responsible for the formation of each class were most likely not the same.

Thus, it appears that variations in volcanic rock chemistry within the arc may be explained largely on the basis of the tectonics of the region, i.e. the breaks that define the segmentation of the arc. However, another possibility exists, and this is that the differing trends

may be explained by the existence of two or more parent magmas within the arc. Kay et al. (1982) and Kay and Kay (1985b) suggest that the parent magmas for both the calc-alkalic and tholeiitic centers within the arc are the same. These workers suggest that this parent magma may be an olivine tholeiitic basalt that is similar, except for K_2O content, to primitive MORB based on major element chemistry, but contains arc lava trace element and isotopic characteristics. However, they do not rule out the possibility of other more primitive magmas within the arc.

The proximity of two volcanoes with contrasting bulk chemistries affords a chance to test the theories of Kay et al. (1982) and Kay and Kay (1985a and 1985b). The object of the present study, Little Sitkin island, is located approximately 65 kilometers to the west of neighboring Semisopochnoi island. Semisopochnoi is a large tholeiitic volcanic center located between the Rat and Adreanof segments of the Aleutian chain and at the intersection of the Bowers Ridge with the Aleutian plateau.

Ach and DeLong (1980) and DeLong et al. (1985) reported that near-surface processes, namely mixing of magmas and fractional crystallization, combined to produce the tholeiitic trend seen on Semisopochnoi island. They further concluded that the parental magma for the island was derived by partial melting of depleted mantle modified by liquids derived from subducted MORB with a small

sediment component. In general, this is in agreement with the results of Kay et al. (1982) and Kay and Kay (1985a) in regards to the formation of the tholeiitic trend within the Aleutian arc as a whole.

In contrast to Semisopochnoi island, Little Sitkin island is a small calc-alkalic volcanic center located within the Rat segment of the Aleutian chain. This is the position that the models of Kay et al. (1982) and Kay and Kay (1985a) predicted for a volcanic center with this type of chemistry, thus providing first order adherence to the models. However, except for cursory petrographic work and a geologic study of the island that is over twenty five years old (Snyder, 1959), nothing has been done with the detailed petrology of the full suite of volcanic rocks, from basalt through rhyodacite, that is found on Little Sitkin. The following study of the petrography and phase chemistry of these rocks will lead to a better understanding of the processes responsible for their formation.

2 - LITTLE SITKIN ISLAND

Little Sitkin island is located in the Rat Islands segment of the Aleutian chain, at approximately longitude 178° 30' E, and latitude 52° N (figure 1-1). It is roughly circular, with a maximum diameter of about eleven kilometers. The highest peak on the island is 1188 meters above sea level, and five other mountains rise more than 400 meters. In addition, sea cliffs, some over 600 meters in height, rise up precipitously around the island (Snyder, 1959).

The rocks of Little Sitkin island are subaerial lavas and pyroclastic deposits, with some shallow water sedimentary deposits derived from the volcanics. This thesis is concerned only with the volcanics. The bulk of this chapter, except where noted, is distilled from the report by Snyder (1959) on the geology of the island.

Eight bedrock units, ranging from late Tertiary (?) to Recent, have been distinguished. The youngest rocks on the island were extruded early in the first half of this century. In order of decreasing age, the units are:

Williwaw Cove formation
Sitkin Point formation
East Point formation
Double Point Dacite
Patterson Point formation
Little Sitkin Dacite
  Pratt Point member
  West Cove member

During latest Tertiary to earliest Quaternary, the first recorded magma extrusion occurred on Little Sitkin. Massive flows, along with great quantities of ash and pyroclastic debris made up the rocks of the Williwaw Cove formation. These rocks range from basalt through andesite and dacite. These outpourings formed a volcano that may have reached a height of 2100 to 2500 meters. Following this eruptive period was a time of erosive activity, possibly related to mid-Pleistocene glaciation.

This relatively quiet period came to an abrupt end with a large eruption that caused part of the mountain to collapse and the formation of a large caldera. The mountain was subsequently lowered, relative to sea level, resulting in the formation of a crater lake and the inundation of the island's margins. Explosive volcanism continued throughout this time, with deposition of tuffs and breccias occurring in offshore basins and the caldera lake. These water-laid pyroclastic deposits are andesitic to dacitic and make up the Sitkin Point formation.

Uplift of the island followed, leading to subaerial erosion of the pyroclastic deposits. Concurrently, a new vent formed on the northeast side of the island, and extrusion of a thick series of basalt and andesite flows resulted. These rocks are termed the East Point formation.

In latest Pleistocene or earliest Holocene, following

the extrusion of the rocks of the East Point formation, a more silicic magma was forming beneath the island. This new magma was to become the source for the Double Point Dacite, and was distinctive in that it contained andesitic inclusions that were texturally distinct from all previously extruded rocks, but were chemically similar to the inferred original magma of the Williwaw Cove formation. These inclusions may represent torn off pieces of the conduit walls. The magma of the Double Point Dacite was relatively volatile-poor, and thus the majority of the material extruded was as flows rather than pyroclastics. These eruptions resulted in the formation of a large central cone within the confines of the caldera created by the Sitkin Point eruptions.

As in the past, an erosive period followed the construction of the Double Point cone. Pressure built up beneath the surface, and a new magma formed, possibly mixing, to a greater or lesser extent, with any remaining magma of the Double Point Dacite. A huge explosive eruption followed, causing the formation of a second caldera, and blanketing the island with a thick pile of ash. This unit is the Patterson Point formation, and the ash that comprises it ranges from andesite to dacite. Some of the volcanic bombs lying within the dacite matrix show contrasting layers of black and white banding, the so-called "marble-cake" texture, which may be evidence of

pre- to syneruptive mixing of magmas.

After formation of the second caldera, and the eruptions associated with it, lava eruptions of the Little Sitkin Dacite occurred on the southern flank of the remainder of the Double Point cone. Due to the low volatile content of the magma, only flows were extruded, again of andesitic to dacitic compositions. The Little Sitkin Dacite contains two separately mapped members. The Pratt Point member is a rhyodacite obsidian. Where in contact with the andesite of the Little Sitkin Dacite, complex interfingering of andesite and rhyodacite is common. Contemporaneous extrusion from a single vent was suggested by Snyder (1959). The West Cove member of the Little Sitkin Dacite consists of a blocky aa flow of black, glassy dacite. These flows are considered to be the result of the last extrusive episode on the island, early in this century.

It is the intended purpose of this study to determine the magmatic history of Little Sitkin island. The following chapters will explore the petrography, petrology and geochemistry of the rocks of Little Sitkin island in order to suggest a reasonable magmatic history for the island. The end result will be a more complete picture of the evolutionary processes responsible for the formation of this volcano.

3 - BULK ROCK CHEMISTRY

The whole-rock chemistry of the rocks of Little Sitkin island offers some insight into the processes responsible for the range of rock compositions. Based on a simple chemical classification scheme, the analyses reported by Snyder (1959) include one basalt (53% SiO_2), seven andesites (55% - 60% SiO_2), one dacite (65% SiO_2) and two rhyodacites (69% - 70% SiO_2). Average compositions for these rocks are given in table 3-1.

Major Element Chemistry

The rocks of Little Sitkin belong to the calc-alkalic series as defined by the discriminant diagram of Miyashiro (1974) and the AFM plot of Irvine and Baragar (1971), figures 3-1 and 3-2 respectively. Sample 491 falls in the tholeiitic field on the AFM plot of figure 3-2, but this sample contains what appears to be a large proportion of xenocrystic clinopyroxene. The addition of this pyroxene would tend to change the bulk chemistry of the rock, thus making the whole-rock point somewhat suspect for classification purposes.

Figure 3-3 is a composite silica variation diagram for all of the major oxides. The most striking feature of this diagram is the linearity of the trends. For all of the oxides, the variation diagrams show a virtually linear trend from the basic to silicic end-members, with the

TABLE 3-1

Whole Rock Major Oxide Averages*

	Basalt	Andesite	Dacite	Rhyodacite
SiO2	52.74	57.59	64.74	69.11
TiO2	0.57	0.80	0.53	0.36
Al2O3	11.99	17.33	16.25	15.09
Fe2O3	1.90	3.36	1.72	1.43
FeO	6.72	4.26	3.17	2.13
MnO	0.17	0.15	0.13	0.12
MgO	11.02	3.50	1.97	1.04
CaO	12.49	7.64	5.07	3.43
Na2O	1.78	3.34	4.13	4.38
K2O	0.64	1.21	1.71	2.03
P2O5	0.11	0.16	0.15	0.12
TOTAL	100.13	99.34	99.57	99.22

* - Averages of analyses reported by Snyder (1959).

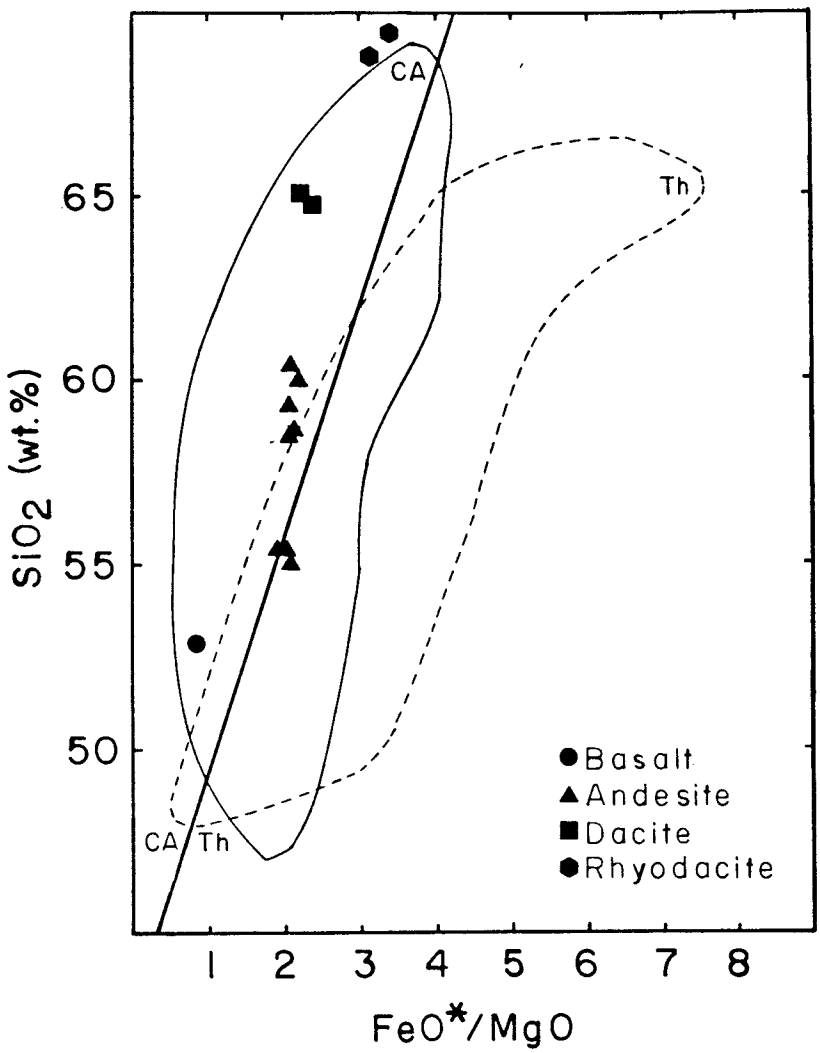

Figure 3-1 FeO^* (total Fe as FeO)/MgO ratio versus SiO_2 in rocks of Little Sitkin island. The calc-alkaline - tholeiitic discriminant line is from Miyashiro (1974). The fields enclosed by the solid and dashed lines are for Aleutian calc-alkaline and tholeiitic volcanic centers respectively. After Kay et al. (1982).

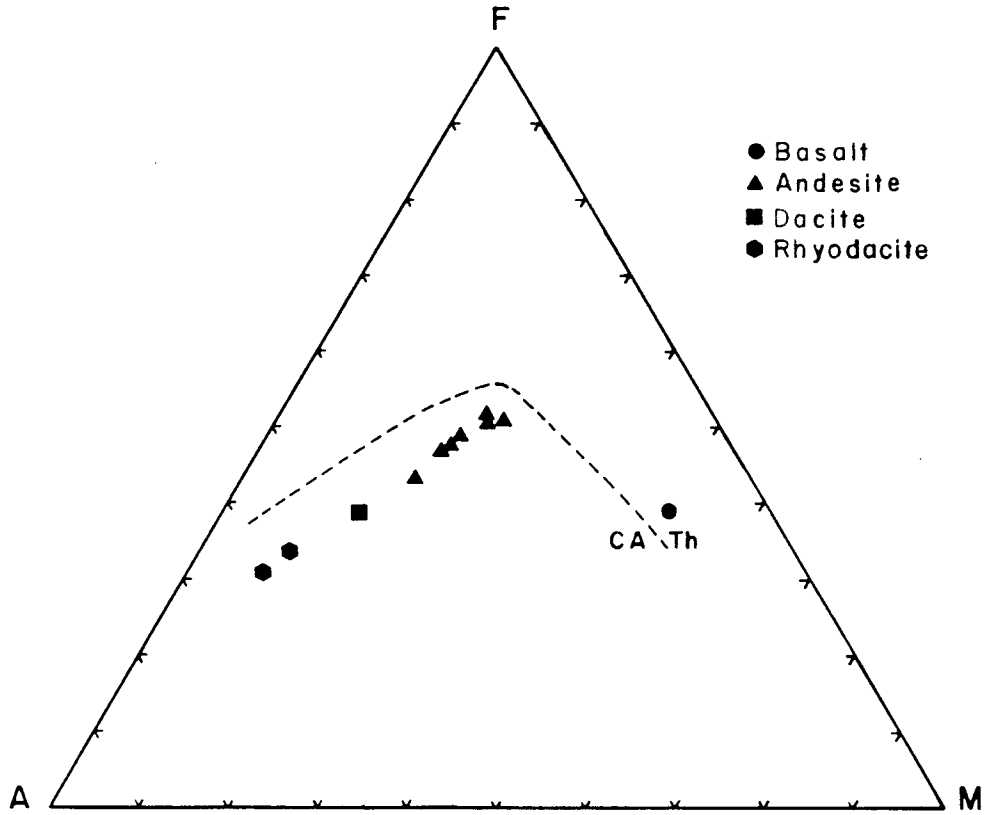

Figure 3-2 AFM plot of the rocks of Little Sitkin island. Dashed line separates fields of tholeiitic and calc-alkalic rocks. After Irvine and Baragar (1971).

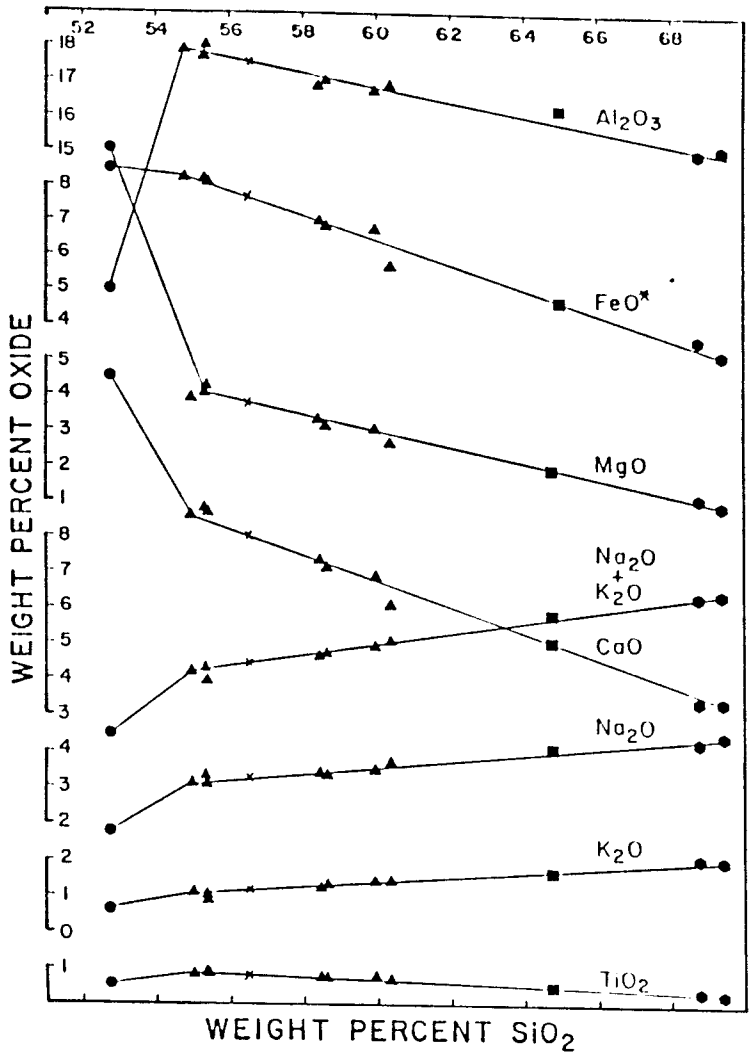

Figure 3-3 Composite silica variation diagram for all of the major oxides of the rocks of Little Sitkin island. Note the linearity of the trends. (From Snyder, 1959).

exception of basalt sample 491. The effects of possible pyroxene accumulation on this sample will be dealt with more fully in subsequent chapters.

Linear trends, such as those shown in figure 3-3, may arise in several ways. Simple crystal fractionation may be responsible; however, for this to occur certain criteria must first be met. The rocks must get progressively more siliceous as they get younger. This increase in silica is due to the removal from the magma of mafic phases that have remained constant in composition or have varied systematically. These mafic phases must also be removed continuously, from the beginning to the end of the entire rock series. No other phases may be removed at any point within the series (Snyder, 1959).

The trends for Little Sitkin island do not correlate well with simple crystal fractionation, based on observed mineral assemblages, and thus this process acting alone may not be sufficient to explain the observed trends. Another process that may give rise to linear trends is the mixing of two discreet magmatic endmembers in varying proportions. Variations on this theme are the incorporation and dissolution of mafic inclusions in silicic melts, or silicic inclusions in melts of mafic composition.

Trace Element Chemistry

Whole-rock trace element analyses were performed by Snyder (1959) on five samples of the series using spectrochemical methods. Perfit and DeLong (unpublished data) have analyzed the entire suite for the following trace elements: Rb, Sr, Cs, Zr, Nb, Ba, Hf, Pb, U, Th, Y, V, Cr, Ni, Co, Cu and Zn. In addition, six of the samples - the basalt, three andesites, the dacite and a rhyodacite were analyzed for the rare earth elements.

Figure 3-4 is a plot of Zr versus silica for the rocks of Little Sitkin island. Whereas the major oxides vary linearly with silica for whole-rock abundances, zirconium does not, but instead appears to become saturated in a Zr-bearing phase at 60-65 weight percent SiO_2. The obvious conclusion that may be drawn is that zircon has become a fractionating phase in the more siliceous members of the series. This difference between major oxide silica variation diagrams and that for zirconium is profound. It implies that different processes are affecting these rocks with respect to their major and trace element behavior.

Zirconium is not the only trace element to exhibit this behavior. Figure 3-5, a plot of Zr versus TiO_2, shows that, as in the case of zirconium, TiO_2 also increases in concentration almost linearly at first, but then the concentration of TiO_2 begins to fall and the trend turns

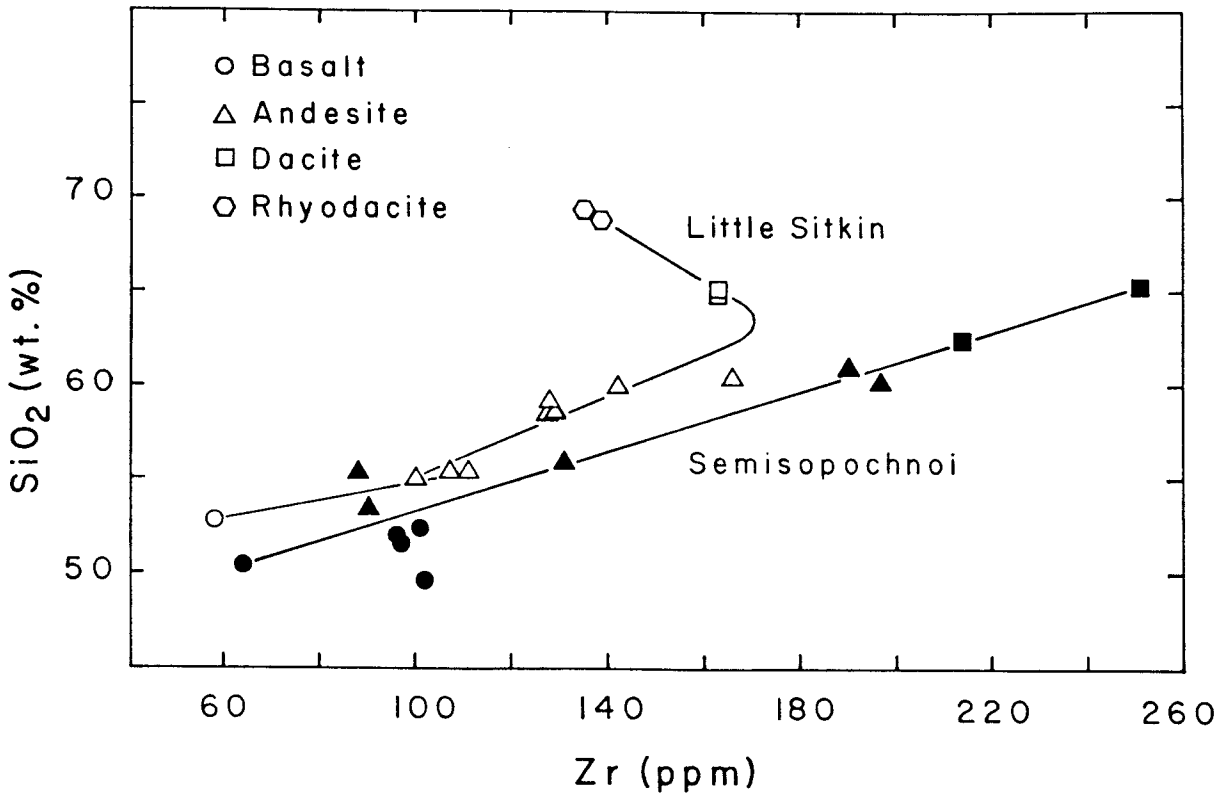

Figure 3-4 Plot of silica versus Zr for the rocks of Little Sitkin island and neighboring Semisopochnoi island. Silica data for Little Sitkin and Semisopochnoi from Snyder (1959) and Coats (1959) respectively. Zr data for Little Sitkin and Semisopochnoi from DeLong (unpublished data) and DeLong et al. (1985) respectively.

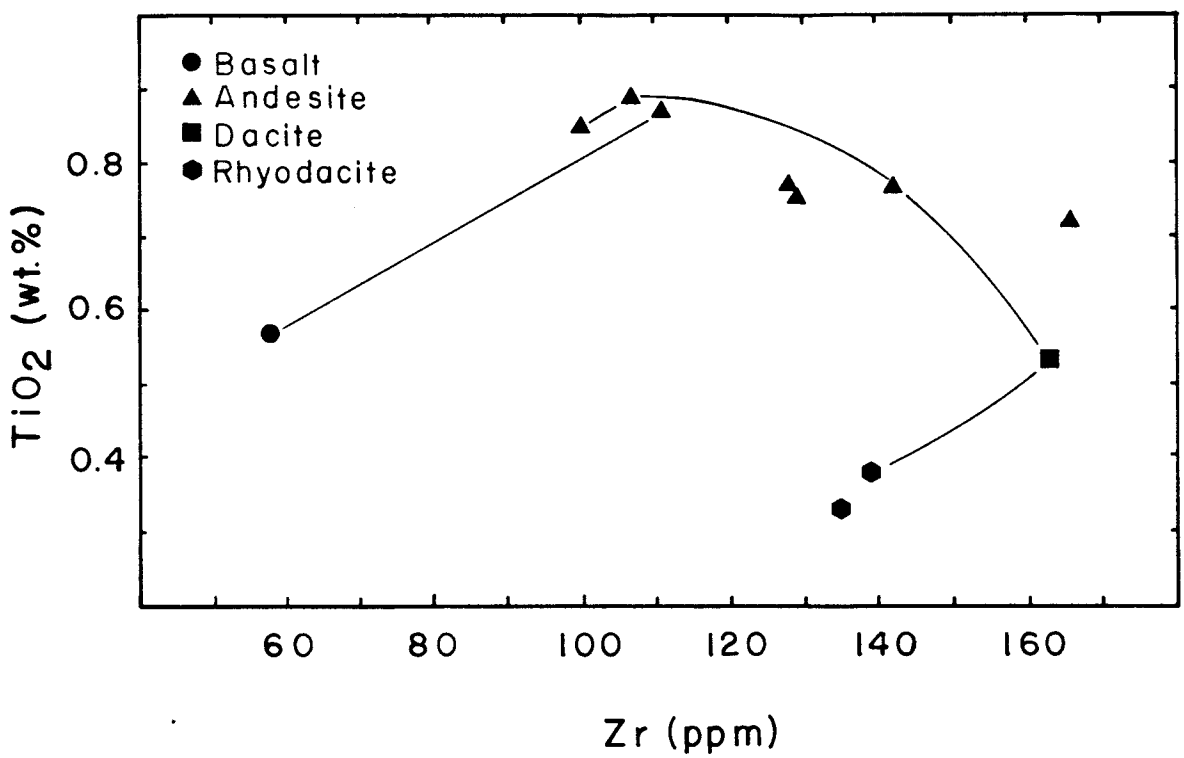

Figure 3-5 Plot of TiO_2 versus Zr for the rocks of Little Sitkin island. Although Ti is not a trace element, this plot serves as a generalization of the behavior of trace elements as a group for these rocks. Line suggests one possible evolutionary path. TiO2 (unpublished data).

back on itself when the more siliceous members are plotted. Thus, not only is zirconium concentration being controlled by fractionation of zircon, but the concentration of titanium is controlled by fractionation of titanomagnetite or ilmenite. The concentrations of many of the trace- and rare-earth elements appear to be controlled by the fractionation of accessory phases. Indeed plots of these elements invariably yield doubly curving trends.

4 - PETROGRAPHY

Introduction

Previous petrographic studies of the rocks of Little Sitkin Island have been limited to the very brief reviews given by Snyder (1959). A summary of Snyder's comments is given below, with detailed petrographic descriptions of these rocks based on the present study to follow. Snyder's work was used as a base on which to build a detailed petrographic picture of these rocks, so it is important to understand what Snyder himself recognized.

In both Snyder's original study, as well as in this present one, only one basalt sample was studied. Snyder described it as a light reddish grey holocrystalline porphyritic basalt. Phenocryst minerals are greenish-black augite and plagioclase. Minor quantities of olivine and magnetite were also said to occur, and the groundmass is a microcrystalline aggregate of each of these minerals.

Snyder studied eight andesite samples that ranged from about 55 to 60 weight percent silica. It should be noted that Snyder termed andesites with 58 to 60 weight percent silica "low-silica dacites"; however based on current convention, these rocks are termed andesites, and this will be the terminology used throughout the present study. In general, these andesites are greyish, hypocrystalline porphyritic rocks. Phenocryst phases present include

plagioclase, clinopyroxene, orthopyroxene and magnetite. Olivine and hornblende may also occur. Groundmass usually consists of glass and microlites of plagioclase, with or without any of the other phases.

Two rocks which Snyder termed "high-silica dacites", but which will be referred to here as simply dacites, have been described. They are both grey, hypocrystalline porphyritic rocks with plagioclase as the dominant phenocryst phase. Orthopyroxene, clinopyroxene, magnetite, hornblende and tridymite are also said to occur. The groundmass consists of glass and the ubiquitous microlites of plagioclase, with some minor pyroxene and magnetite.

The rhyodacites are the most evolved rocks found on Little Sitkin island. The two samples studied by Snyder were said to be yellowish-grey hypocrystalline, vesicular, porphyritic rocks. Plagioclase and hornblende are the major phenocryst phases, with orthopyroxene, magnetite and quartz present in lesser amounts. The groundmass of each sample consists of a clear, pinkish glass containing many vesicles.

Included here are detailed petrographic descriptions of one basalt (sample 491), seven andesites (samples 500, 492, 493, 494, 496, 497 and 499), one dacite (sample 501) and two rhyodacites (samples 495 and 489). Textural terminology used by Snyder (1959) (e.g. hypocrystalline, etc.) has been retained in the present study. Volume

TABLE 4-1

Volume Modal Analysis of Samples*

(Present Study)

	491	500	492	493	494	496
Groundmass	13.9	30.1	58.8	33.6	48.7	56.6
Phenocrysts						
Plagioclase	50.0	32.4	28.7	49.3	22.3	23.2
Clinopyroxene	33.2	3.6	6.8	7.4	7.2	3.2
Orthopyroxene	0.0	3.7	1.3	2.1	2.8	3.1
Olivine	0.5	0.0	0.7	1.1	0.0	0.0
Quartz	0.0	0.0	0.0	0.0	0.0	0.0
Tridymite	0.0	0.0	0.0	0.0	1.4	0.0
Hornblende	0.0	6.6	0.0	0.0	0.2	0.1
Magnetite	2.1	4.0	3.7	5.5	3.1	1.5
Xenoliths**	0.0	0.3	0.0	0.0	11.6***	3.2
Vesicles	0.3	19.3	0.0	1.0	3.0	9.0
Total	100.0	100.0	100.0	100.0	100.0	100.0

* - Samples listed in order of increasing silica content.
** - Totals are for all types found within each sample.
*** - Area of clear "dyke" material is included in total.

TABLE 4-1 (continued)

	497	499	501	495	489
Groundmass	48.6	61.3	56.3	71.1	58.1
Phenocrysts					
Plagioclase	30.0	20.3	23.7	15.2	14.6
Clinopyroxene	5.9	2.8	2.4	1.1	0.1
Orthopyroxene	2.3	2.8	2.6	2.4	0.6
Olivine	0.5	0.0	0.0	0.0	0.0
Quartz	0.0	0.0	0.0	2.5	1.2
Tridymite	0.0	0.0	0.0	0.0	0.0
Hornblende	0.0	0.0	0.8	0.5	1.6
Magnetite	3.1	1.9	1.6	0.7	0.4
Xenoliths**	0.0	0.0	5.3	0.0	18.2
Vesicles	9.6	10.9	7.3	6.5	5.2
Total	100.0	100.0	100.0	100.0	100.0

modal analyses for all samples as determined by the present study (1000 points per sample) are given in table 4-1.

Basalt

The basalt studied was taken from the oldest recorded formation on Little Sitkin island, the Williwaw Cove formation. It is a light reddish-grey holocrystalline porphyritic rock. The phenocrysts include plagioclase, clinopyroxene, olivine and magnetite. All these phases, plus apatite, are also found in the groundmass.

Plagioclase phenocrysts occur as subhedral to euhedral elongate section up to 1.5 mm in length (figure 4-1a). Complex twinning and zoning is common. Although some grains are almost inclusion free, it is much more common to find crystals containing small needles of apatite, magnetite or glass as included phases. These inclusions may be concentrated in the crystal cores or they may parallel the crystal outlines as rings. A few of the larger grains scattered throughout the section contain extremely fritted interiors with thin, clear rims.

Clinopyroxene occurs as large, colorless megacrysts which may have a cumulate or xenocrystic origin (see chapters 5 through 8). These crystals usually occur in aggregates and are up to about 6 mm long (figure 4-1a). Twinning and zoning is very common in these subhedral to euhedral grains. Some of the grains have rounded outlines,

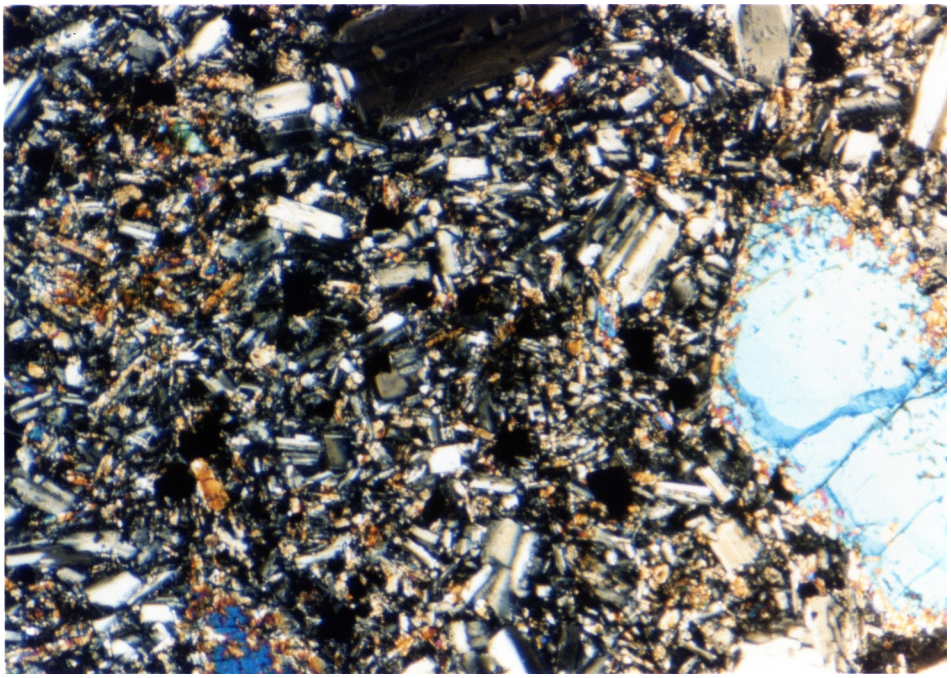

Figure 4-1a Basalt 491 showing groundmass texture, typical plagioclase phenocryst at top center and partially resorbed clinopyroxene at right. Field of view is approximately 3.65 mm in the long direction in this and all subsequent photographs.

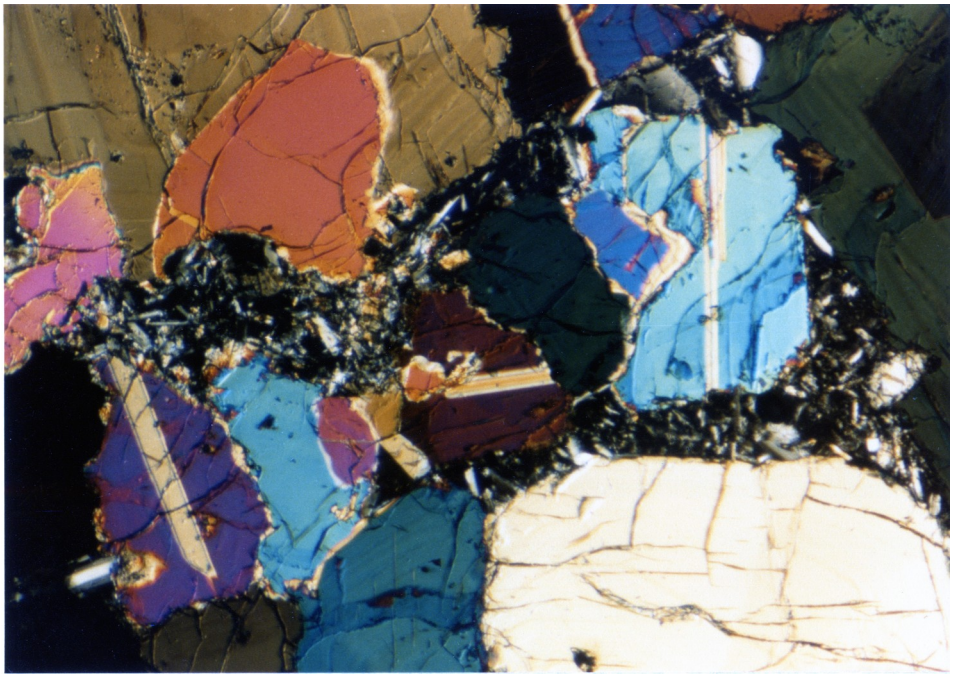

Figure 4-1b Clinopyroxene megacryst clot in basalt 491. Note twins and zonation.

and many have single or multiple rings of inclusions paralleling the crystal outlines. Included phases appear to be apatite and glass. Some of the crystals show limited exsolution of orthopyroxene as well.

The olivine grains that occur in this rock are colorless, clear anhedral to subhedral and relatively small, usually no larger than about 0.5 mm, although one large grain with a length approaching that of the clinopyroxene megacrysts does occur. This too may have a xenocrystic or cumulate origin. A few crystals show brownish discoloration along cracks within the grain. Magnetite appears to be the only included phase in this mineral. Isolated grains appear to have somewhat resorbed margins.

Magnetite occurs as small, opaque anhedrons up to about 0.25 mm. It is also found as inclusions in the other phenocryst phases. A brownish red coloration surrounds many of these larger magnetite grains, possibly the cause of the rocks reddish tint. In reflected light, limited magnetite-ilmenite exsolution is observed.

Andesites

The formations from which the seven andesites studied were taken are: Williwaw cove formation, Double Point Dacite, Patterson Point formation and the Little Sitkin Dacite. The andesites range from light to dark grey, with

intersertal to holocrystalline texture. All are porphyritic. Phenocryst phases include plagioclase, clinopyroxene, orthopyroxene and magnetite. Olivine occurs in three samples, 492, 493 and 497, while hornblende occurs in three others, 500, 494 and 496. The two phases never occur together.

Plagioclase phenocrysts generally occur as colorless, subhedral to euhedral sections up to about 4 mm long. Some samples appear to show two optically distinct populations of plagioclase crystals. One population contains small relatively clear grains (figure 4-2a), while the other contains large grains with fritted cores or rings following the crystal outlines (figure 4-2b). Twinning and zoning are common in both populations. While inclusion-free grains do occur, most grains contain inclusions of apatite, pyroxene (?), magnetite and glass. The inclusions may be concentrated in either the crystal core or in rings following the crystal outlines. Grains that have fritted interiors may or may not have a thin, clear rim that is optically continuous with the rest of the crystal. Some grains show resorbed crystal margins.

Clinopyroxene occurs as colorless to pink-green pleochroic subhedral to euhedral grains up to about 2 mm long. Twinning and zoning occur as does exsolution of orthopyroxene in some of the grains. Hourglass zonation was noted in a few crystals in sample 492 (figure 4-2b).

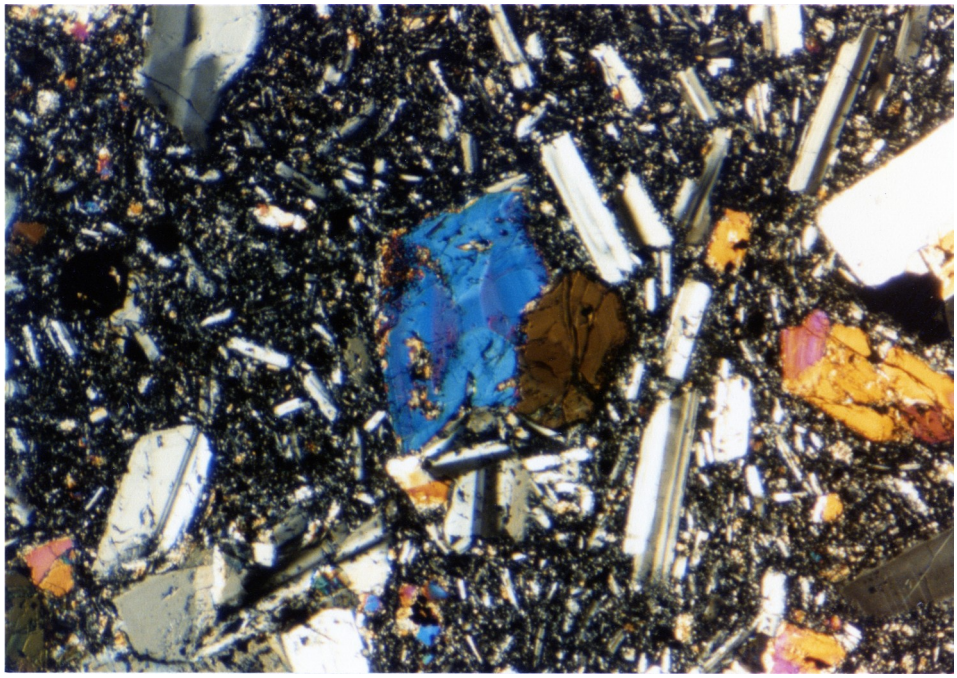

Figure 4-2a Andesite sample 492 showing typical rock texture. Plagioclase phenocrysts in this view are small, relatively clear grains. Note also the clinopyroxene grain in center with well developed hourglass zonation.

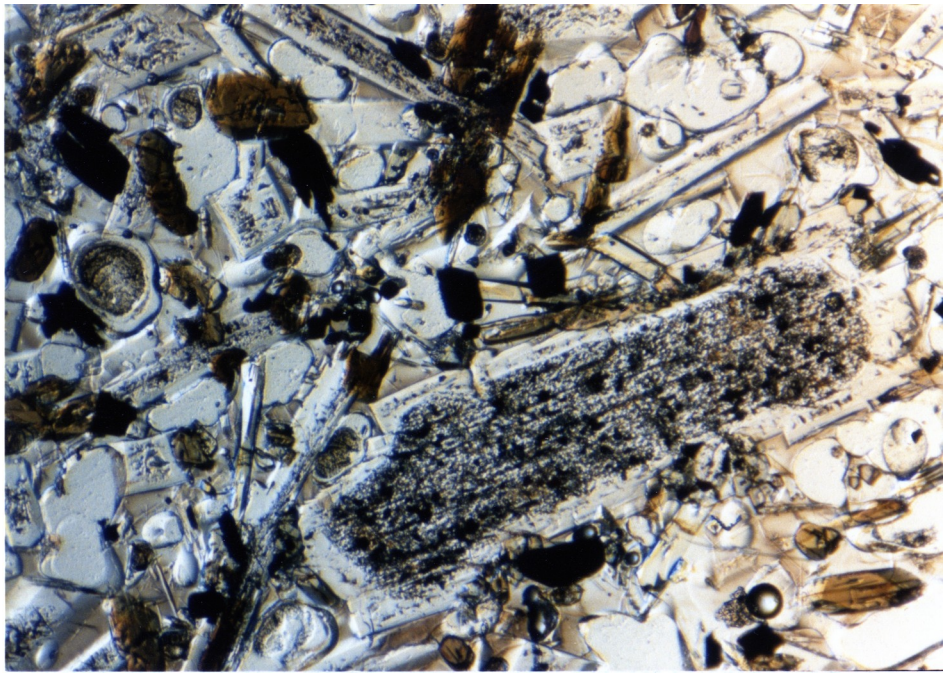

Figure 4-2b Plane polarized photo of andesite sample 500. Plagioclase grain in center is typical of the large grains with "dirty" interiors. Smaller clear plagioclase grains also occur in this view along with glass and hornblende.

Clinopyroxene may occur as cores to orthopyroxene or as rims around an orthopyroxene core, with both occurrences in sample 497 (figures 4-3a, 4-3b). Grains in a few of the samples show resorbed outlines. Inclusions are fairly common, with apatite, plagioclase, glass and magnetite being the most abundant.

Orthopyroxene, as subhedral to euhedral sections up to about 2 mm long is found in all of the andesite samples. The crystals range from colorless to a pale pink to green pleochroism. In sample 500, the orthopyroxene occurs as needles with length:width ratios approaching 50:1, in addition to crystals with more regular form. Clinopyroxene may be found as both cores and rims to orthopyroxene. Common included phases are apatite, plagioclase, magnetite and glass. Some of the orthopyroxene is partially to almost wholly resorbed. In addition, isolated grains in some of the sections show a brownish discoloration along cracks in the crystal.

The last phenocryst mineral common to all the andesite samples is magnetite. It may occur as anhedrons, as small subhedral to euhedral sections or as needles. In sample 500 these needles of magnetite are of similar size, shape and length:width ratio as the needles of orthopyroxene found in the same section. Size varies, but may be anywhere from 0.25 mm up to about 1.5 mm. Magnetite is also found as an included phase within other phenocryst

minerals. Under reflected light, weak to strong magnetite-ilmenite exsolution may be noted.

Olivine occurs in three of the sections studied, samples 492, 493 and 497. Abundance is limited in each of these samples, and the grains are usually small, rarely more than 0.4 mm long. Crystals are colorless anhedral to subhedral sections containing few inclusions (figure 4-3a). Many crystals have resorbed margins.

Hornblende is a fairly common phenocryst in two of the three slides that contain it. It is usually found as dark to light brown or tan pleochroic laths or subhedral to euhedral cross-sections (figure 4-2a). Crystals may be up to 2-3 mm long. Inclusions are present but, aside from magnetite, their identification is difficult. Some grains have opaque replacement on their edges, and others have hollow cores. Sample 496 contains just two crystals of hornblende. One of these grains is being replaced by pyroxene, plagioclase and opaques (figure 4-4), while the other grain is subhedral, with plagioclase inclusions, and is just slightly resorbed. These grains appear to be xenocrysts.

Tridymite occurs as an important accessory phase in sample 494. This sample is unique, not only due to the occurrence of the tridymite, but also because of the large amount of hematite contained within it, giving this specimen a reddish color.

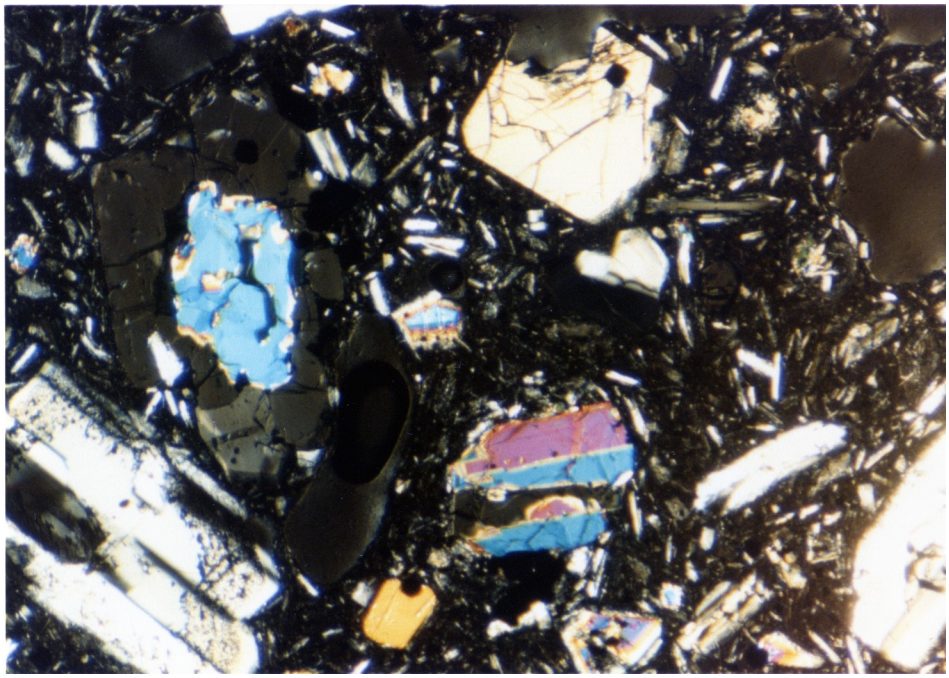

Figure 4-3a Andesite sample 497 with orthopyroxene surrounding a clinopyroxene core. Olivine grain is at top center.

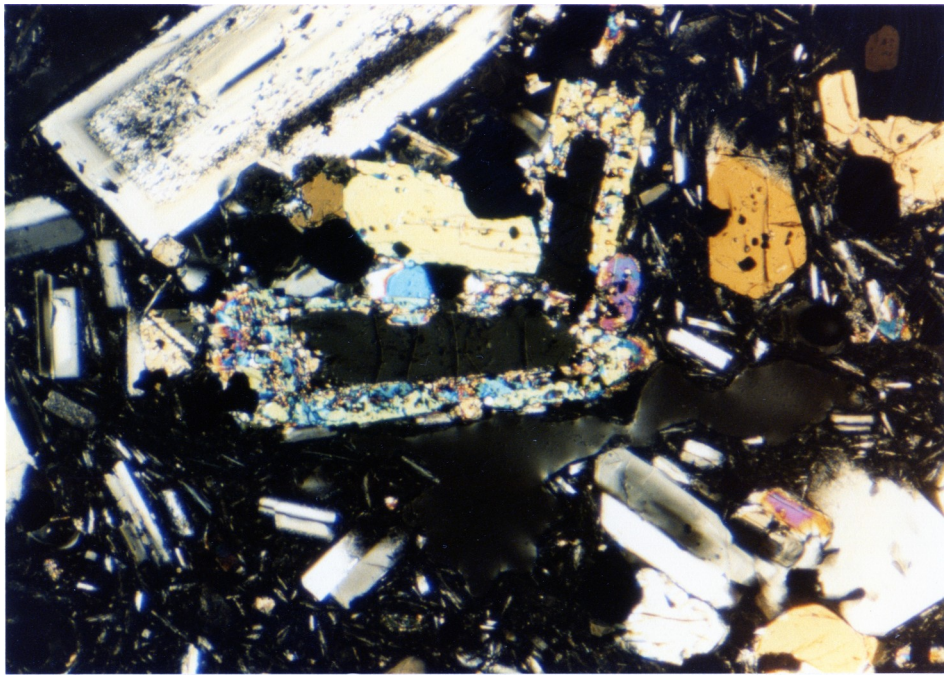

Figure 4-3b Andesite sample 497 a few mm from view in figure 4-3a, showing orthopyroxene core to clinopyroxene. Olivine grains are at lower right. Note large "dirty" plagioclase and orthopyroxene grain with opaque inclusions.

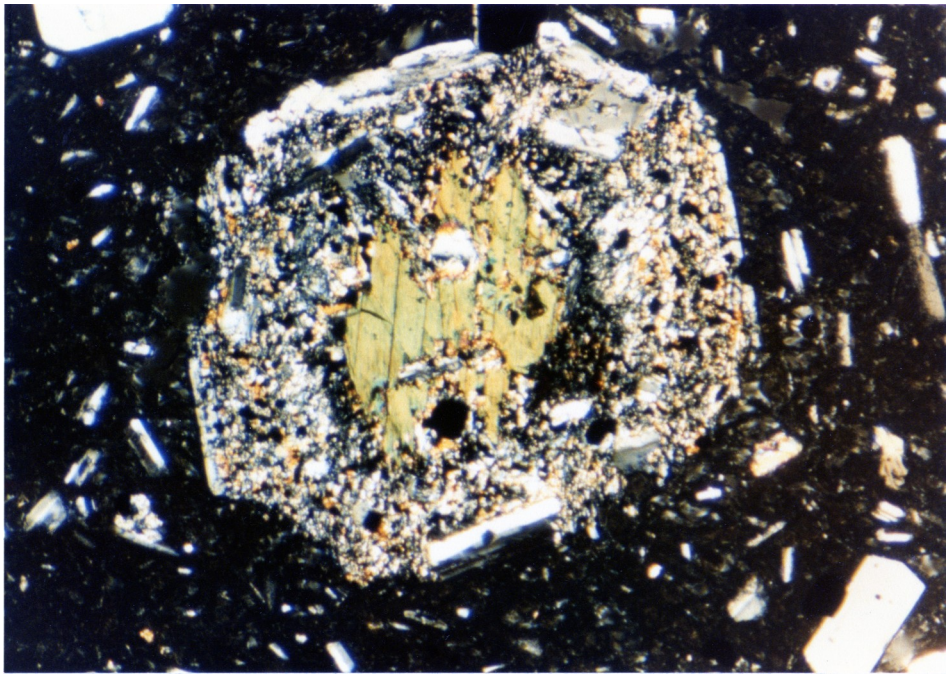

Figure 4-4 Large hornblende xenocryst (?) found in andesite 496. Note replacement by pyroxene, plagioclase and opaques.

Four of the seven andesites contain crystal clots composed of all of the phenocryst phases found in each individual sample (figure 4-5). The grains in these clots appear to be optically identical to the grains found throughout the rest of each slide. Some of the clots contain an interstitial brown glass between the mineral grains; however this glass is similar in appearance to the glass found within the rest of the sample. These crystal clots are easily distinguished from the xenoliths also found in some of the samples, and appear to be the result of mechanical segregation.

The groundmass of these rocks consists predominantly of plagioclase and magnetite with minor amounts of orthopyroxene, clinopyroxene, apatite and, possibly, zircon in some of the samples. These groundmass minerals may be set in a brownish glass which may or may not be vesicular. In a few of the samples, little or no glass is seen in the groundmass.

Xenoliths are found in a few of the andesites studied, and probably represent torn off pieces of conduit walls. The xenoliths of sample 494 contain inclusion-free plagioclase, clinopyroxene, orthopyroxene and magnetite. The crystals contained within these xenoliths are all fairly small. Sample 494 is further distinguished by the occurrence of a small dike or vein of clear, colorless glass running across one corner of the section (figure

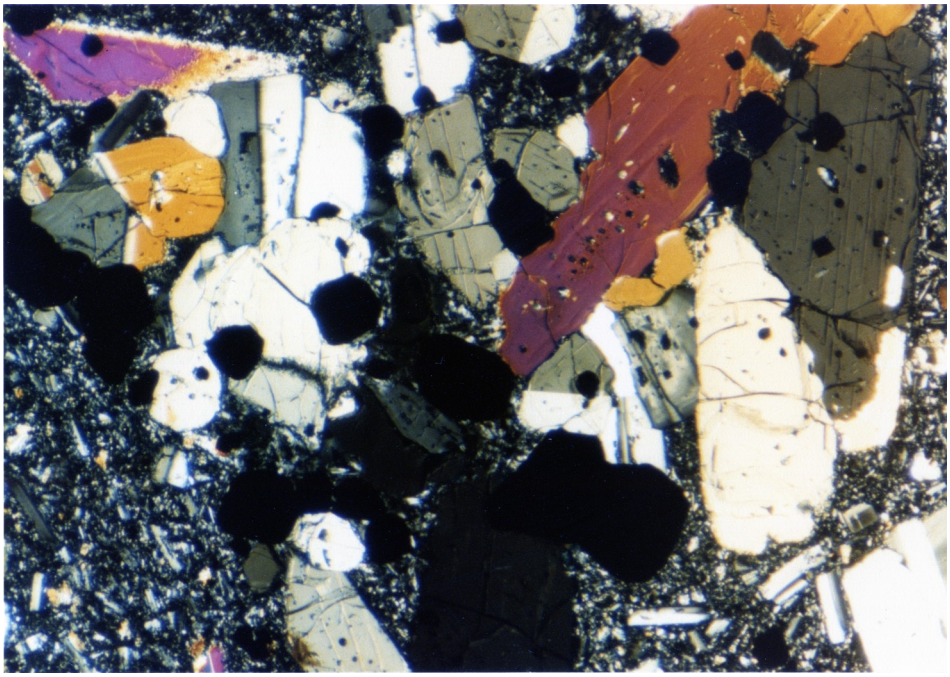

Figure 4-5 Crystal clot in andesite sample 492. These clots are a common feature of the andesites, and contain the same phases as are found within the rest of the sample.

4-6a). This area contains plagioclase, orthopyroxene and hornblende phenocrysts, with the hornblende being much more abundant than in the rest of the sample. In addition, this part of the section contains a significant proportion of partially resorbed quartz crystals (figure 4-6b). Hematite is virtually absent from this portion of the slide, being found only along the dike or vein margins. Contained within this zone are small pieces of rock typical of the rest of the section, which may have been torn up by the intrusion of this clear dike.

Sample 496 contains two distinct sets of xenoliths, here labeled type 1 and type 2. Type 1 xenoliths contain small euhedral zoned and twinned plagioclase. These grains are clear and inclusion-free for the most part. Small grains of orthopyroxene and clinopyroxene are also found in these areas. The crystals are set in a clear brown glass (figure 4-7). Type 2 xenoliths contain much larger plagioclase crystals than those found in type 1 xenoliths. These grains may be as large as those found in the host rock. Twinning and zoning are common, and the crystals give a very dirty appearance. These inclusion-rich grains contain much glass, and are mantled by thin, clear rims. Clinopyroxene grains, much larger than those found in type 1 xenoliths, are also seen, as are opaques and scattered orthopyroxene crystals. A small amount of brown glass was also noted in these grains.

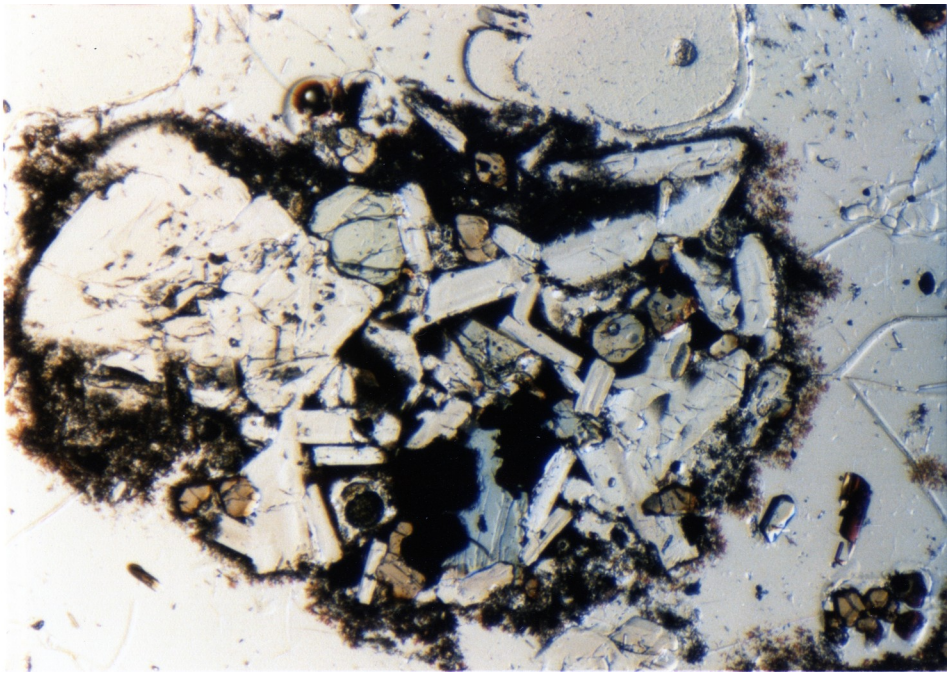

Figure 4-6a "Xenolith" of host rock found within clear dike of sample 494. Note textural contrasts between the two areas, and the large amount of hematite in the groundmass of the host. Plane polars.

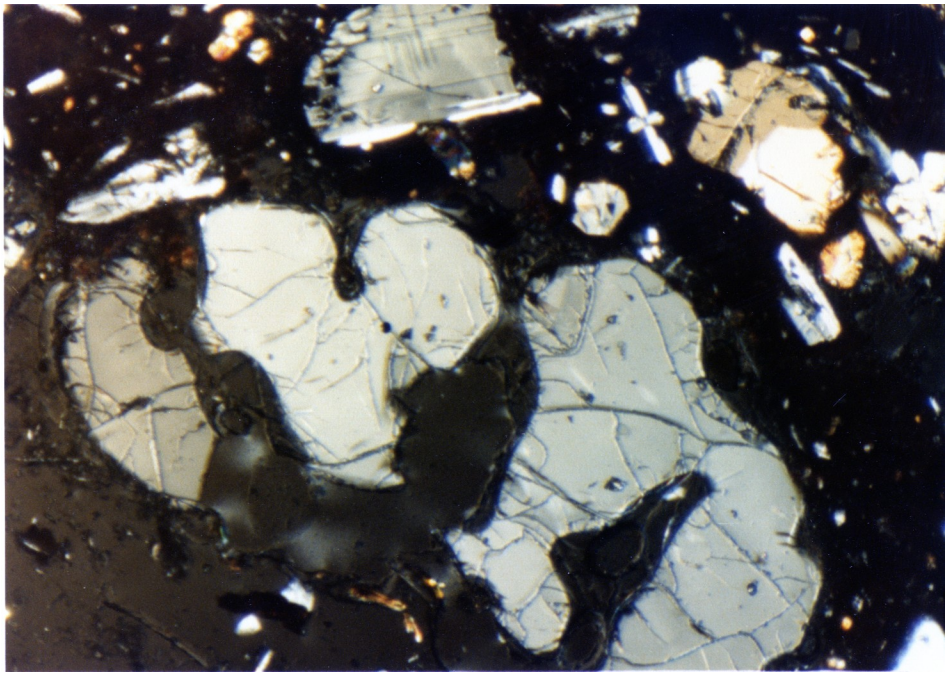

Figure 4-6b Partially resorbed quartz along dike margins in sample 494.

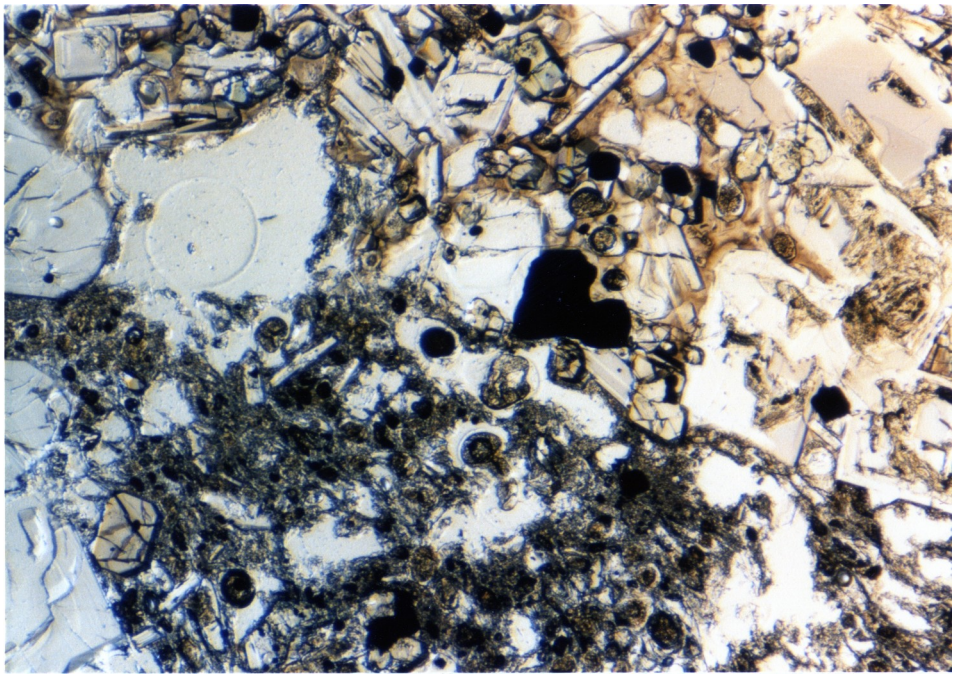

Figure 4-7 Type 1 xenolith in andesite sample 496. Xenolith is at upper right. Note textural differences between xenolith and host rock. Compare with figure 4-5 to note differences between xenoliths and crystal clots.

Dacites

The only dacite studied is a light grey, hypocrystalline porphyritic rock taken from the Double Point Dacite formation. Phenocryst minerals are plagioclase, orthopyroxene, clinopyroxene, magnetite and oxyhornblende. Tridymite occurs as an accessory phase.

Plagioclase occurs as small to large, subhedral to euhedral crystals. Complex twinning and zoning is common, as are inclusions of apatite and glass that form rings paralleling the crystal outlines. Some grains show partial resorption around the edges. Monominerallic clots of plagioclase grains are also common in this sample.

Pale green sections of orthopyroxene are very common in this dacite. Most of the crystals are euhedral, and some contain inclusions, but these are not at all common. Apatite and plagioclase appear to be the included phases. A few crystals show resorption features to varying degrees, and a few skeletal crystals were noted as well.

Clinopyroxene occurs as colorless, anhedral to subhedral sections up to about 1.5 mm long. Twinning is common and some crystals show limited zonation. Most crystals show resorption features to a greater or lesser extent, and all are inclusion-rich. Some have clear rims. This phase is usually found in close association with the orthopyroxene.

Magnetite occurs as fairly abundant anhedral to euhedral grains, either as phenocrysts and microphenocrysts, or as inclusions in other phases. These grains may show weak magnetite-ilmenite exsolution under reflected light.

Oxyhornblende crystals are mostly euhedral, but some are anhedral to subhedral. Dark brown to light tan pleochroism is noted in these grains. Small clear inclusions occur in most of the grains and appear to be either apatite or plagioclase. In at least two cases the hornblende appears to be forming at the expense of clinopyroxene.

A few scattered crystal clots occur in this sample and consist of plagioclase, both pyroxenes and magnetite. In all cases the crystals appear optically identical to those found throughout the rest of the section.

The groundmass of this rock consists of feldspar microlites with a semi-trachytic texture, magnetite and orthopyroxene. Some devitrified glass is also present, along with minor amounts of tridymite, which also occurs as rare, larger grains scattered throughout the section. In addition to the feldspar microlites, small square crystals of feldspar also occur scattered about the groundmass. They are clear, inclusion-free and show no twinning or zoning.

Xenoliths of a fairly coarse grained rock are found

throughout the section. Minerals that make up these xenoliths are plagioclase, highly corroded clinopyroxene, orthopyroxene and some magnetite. Brown glass, some of which appears to be devitrified, and tridymite also occur. Small inclusions of apatite and what appears to be zircon are contained within grains of the major mineral phases. These xenoliths are easily distinguished from the scattered crystal clots.

Rhyodacites

The two rhyodacites studied come from the Pratt Point member of the little Sitkin Dacite. They are light to medium grey, hypocrystalline, porphyritic and highly vesicular. Phenocryst phases include plagioclase, hornblende, quartz and magnetite. Clinopyroxene occus in one sample.

The plagioclase that occurs in the rhyodacites is usually found as anhedral to subhedral crystals up to about 4 mm long. Inclusions are common, and consist of apatite, orthopyroxene needles, hornblende, magnetite and glass. The included glass appears to have a pinkish color. The inclusions may form rings following the crystal outlines, or, in a few cases, the inclusions may be concentrated in the cores of crystals with clear rims. As in previously described samples, complex twinning and zoning are common. Intergrown crystals and clumps of plagioclase crystals are

common, but the features of the crystals found in these clumps are similar to those of the crystals in the rest of the sample.

Orthopyroxene occurs as fairly common, anhedral to euhedral crystals up to about 2 mm in length. They are clear and colorless, but many contain abundant inclusions of apatite, magnetite, plagioclase and glass (figure 4-8). Needles of orthopyroxene with length:width ratios approaching 10:1 also occur. Some crystals show slight resorption features along grain margins.

Hornblende, as anhedral to euhedral crystals up to 1.5 mm long, with dark brown to olive green to tan pleochroism, is a common phenocryst phase in these rocks. A few of these crystals have rims that appear to be slightly more pleochroic than their cores. Slight resorption features were noted along the crystal margins of some grains. Inclusions of orthopyroxene needles, plagioclase and magnetite occur in some of the grains.

Quartz becomes an important phenocryst mineral in these samples. It occurs as large (up to 2-3 mm) anhedral, rounded crystals with conchoidal fracture. Inclusions are present, but appear to be limited to apatite and a clear, pinkish glass.

Magnetite occurs as anhedral to euhedral grains up to about 0.5 mm long, and also as inclusions in the other phases. Under reflected light, very fine scale

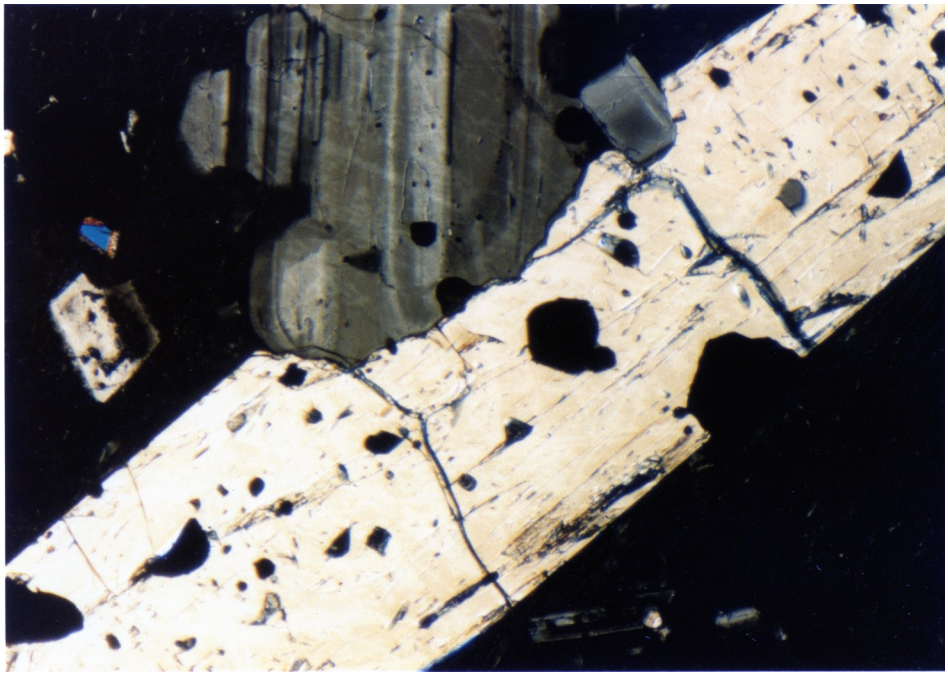

Figure 4-8 Large orthopyroxene phenocryst in rhyodacite 495. Note large plagioclase phenocryst above it, and abundance of inclusions in these phases.

magnetite-ilmenite exsolution can be seen.

Clinopyroxene occurs as a phenocryst mineral in one of the rhyodacites, sample 495 (figure 4-9). It is found both as large, clear, colorless, anhedral to euhedral grains, and smaller, anhedral microphenocrysts. The larger grains are "free-floating" within the rock, while the smaller grains are usually found in association with orthopyroxene and hornblende. Both phenocrysts and microphenocrysts contain inclusions, but what these may be is not clear. Apatite and zircon are two possibilities. Zoning and twinning are also fairly common in these grains.

Crystal clots in these two samples contain the same mineral phases found within the rest of each section. Optically, the phenocrysts in these clots are virtually indistinguishable from those found in the rest of the rock. A few of these clots contain only plagioclase with some magnetite, but again, these grains are optically identical to those found in the rest of the sample.

The groundmass of these samples consists mostly of brown, vesicular glass with feldspar microlites, orthopyroxene needles, magnetite and possibly a small amount of quartz and hornblende. Small amounts of apatite and zircon also occur. The glass seems to show some sort of flow structure, as seen in the patterns of the vesicles and feldspar microlites.

Only one of the rhyodacite samples, sample 489,

Figure 4-9 Large clinopyroxene in rhyodacite 495 containing abundant inclusions of glass, opx (?) and opaques. Clinopyroxene does not occur in rhyodacite sample 489 as a phenocryst phase but rather as grains within the xenoliths in that sample.

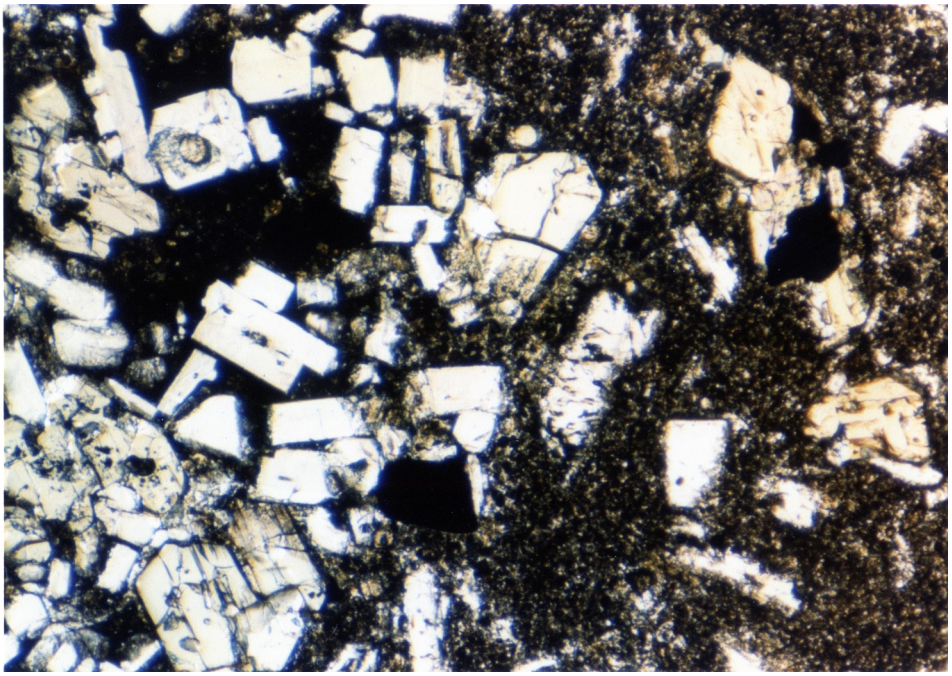

Figure 4-10 Composite xenolith in rhyodacite sample 489 showing the two contrasting textures in this xenolith. Note the sharp dividing line between the highly porphyritic side to the left and the sparsely porphyritic side to the right.

contains any xenolithic material. This sample contains a very large xenolith, about 1 cm in diameter. One half of the xenolith is composed of a light brown, sparsely porphyritic rock, while the other side is composed of a much darker brown, much more heavily porphyritic rock. The dividing line between the two sides is extremely sharp under the microscope (figure 4-10).

The sparsely porphyritic side of the xenolith contains plagioclase, clinopyroxene, orthopyroxene, and magnetite. All of the non-opaque phases show varying signs of resorption and are fairly inclusion-rich. Inclusions are orthopyroxene, apatite, magnetite and glass. Both the plagioclase and clinopyroxene show complex twinning and zoning.

The highly porphyritic side contains the same mineral assemblage as the sparsely porphyritic one, however the phenocryst/groundmass ratio is much higher. The clinopyroxene:plagioclase ratio also appears to be much higher on this side. Most of the phases contain inclusions and show signs of resorption. The pyroxenes in this part of the xenolith are pleochroic from pale pink to pale green.

The groundmass of each side of this composite xenolith is composed of a clear, brownish glass with magnetite and small amounts of each of the other mineral phases.

5 - PETROLOGY AND MIXING

Bowen (1928) elegantly outlined the possibility of producing evolved volcanic rocks from a basaltic parent magma by the process of fractional crystallization. Fractional crystallization has played an important role in the formation of a large portion of evolved volcanic rocks (Ringwood, 1974; Marsh, 1976; O'Hara, 1977; Garcia, 1979; Kushiro, 1979; Gill, 1981; Gust and Johnson, 1981; Gust and Perfit, in press). This process may be wholly responsible for the formation of these rocks, or may act in conjunction with some other formational process such as mixing or assimilation (McBirney, 1980; Gill, 1981 p. 298). However, variation in properties such as pressure, temperature, oxygen fugacity and the initial composition of the melt may drastically alter the composition of the final product and even the trend itself.

Fractional crystallization, although very important, is not the only method of producing volcanic rock series. Bowen (1928) himself pointed this out in his chapter on the role of assimilation in the evolution of igneous rocks. Many workers have shown, both theoretically and experimentally, that the mixing of two or more components of differing compositions may produce rocks with hybrid characteristics (Anderson, 1976; Shibata, 1979; McGarvie, 1984). These components may be magmatic (Dungan and Rhodes, 1978; Gerlach and Grove, 1982; Grove et al., 1982a and b;

Grove and Baker, 1984) or they may be magma and solid (Watson, 1983). Thus, under the heading of mixing, those processes that involve true magma-magma mixing as well as assimilation of pre-existing rock may be included. Distinguishing the results of these two different types of processes, however, is not always easy. Variations in isotopic ratios (Sr for instance) may help to differentiate between them.

A third method for producing volcanic rocks is by partial melting. Most primitive parental magmas are produced by partial melting of a source rock, either in the mantle, along a subducting slab or in the lower crust (Tuttle and Bowen, 1958; Perfit et al., 1980; Tatsumi et al., 1983; Meyers et al., 1986; Nye and Reid, 1986). Cases in which highly evolved melts have been produced by partial melting in the crust have been noted, e.g. rhyolite rift volcanism associated with coeval basalt volcanism or the formation of granitoid masses (Yoder, 1973; Wyllie, 1979). Factors such as the source rock composition or whether melting occurs as equilibrium or fractional fusion determine the role partial melting may play. That partial melting is responsible for the formation of some igneous rocks is without doubt, whether this process can form voluminous volcanic suites is uncertain.

Identifiying the different processes that may have been at work during the formation of a particular volcanic rock

or suite of rocks is, at best, difficult. Lines of evidence that are used in order to help pick out specific processes include the petrographic features of the sample, as well as a detailed study of the sample's phase chemistry.

Curious petrographic features or mineral assemblages that are unusual may point towards a particular evolutionary process. Examples of this sort of petrographic evidence include disequilibrium mineral assemblages such as quartz and magnesian olivine, or more subtle features such as the occurrence of two distinct populations of a phenocryst phase such as plagioclase (Sakuyama, 1979, 1981). Obvious features such as banded lavas or pumice may immediately suggest one particular process, i.e. magma mixing (MacDonald and Katsura, 1965; Eichelberger, 1975) or at least co-extrusion of two separate magmas through the same vent. The more subtle features of the rock, such as the composition of inclusions and xenoliths within the magma, may be just as important as the obvious ones (Conrad et al., 1983; Conrad and Kay, 1984). In fact, these features may be even more important because they require further detailed study and do not allow for an immediate or simple conclusion to be drawn.

Chemical studies of the bulk rock samples, the phases that comprise them and any inclusions found within these phases yield important information that may help define the processes active during the formation of the rock. The

smallest scale of study involves the analysis of the inclusions found within the phenocryst phases of the rock. These inclusions may be glass, or they may be another mineral phase. Analysis of these inclusions may serve to point out certain inconsistencies within the rock (Dungan and Rhodes, 1978). An obvious example is the occurrence of glass inclusions of rhyolitic composition trapped within a plagioclase phenocryst in an andesite. This case may be extreme, but several cases of just this type have been noted (Dungan and Rhodes, 1978). The composition of included mineral phases may serve to call notice to certain peculiarities within a sample. Hornblende inclusions within a plagioclase phenocryst in a basalt suggest that this particular crystal may not have formed in this environment. It may either be xenocrystic or may have been incorporated into the rock while it was molten as the result of a mixing event. A less severe case might be the occurrence of plagioclase that was either too sodic or calcic to have formed in the rock in which it was found, based on the bulk chemistry of that rock.

The chemistry of the phenocrysts found within any particular rock sample is also important when trying to distinguish between evolutionary processes. Maybe the most obvious and simplest case is that of two distinct populations of a particular phenocryst phase occurring in a sample (Sakuyama, 1979). In the same manner, although some

disequilibrium mineral assemblages may be quite obvious during a detailed inspection of the petrography of a sample, others may only be distinguished once the chemistries of the phases are known. Sakuyama (1979) cites experimental work done by Matsui and Nishizawa (1974) involving the partitioning of iron and magnesium between orthopyroxene and olivine at various pressures and temperatures. By using the results of this work and comparing it to data obtained from orthopyroxene and olivine pairs from rocks that he was studying, Sakuyama (1979) was able to show that there was considerable disequilibrium between these two phases during the formation of the rocks in which they were found. He concluded that the two phases were formed in two totally separate environments and then mixed together.

Zonation profiles across phenocryst phases are another example of the application of chemical studies in order to obtain knowledge of the rock's formational history. Normal zonation profiles for a given phase in a particular rock type may indicate that crystallization occurred in an orderly fashion and that fractional crystallization was most likely the formational process responsible for the sample's final composition. However, cases have been noted where both normal and reverse zonation of a particular phenocryst phase within a sample has occurred (MacDonald and Katsura, 1965; Sakuyama, 1979; Gerlach and Grove, 1982). This, of course, could imply that crystals of this particular phase

grew in two or more different environments, and were mixed together and cooled before they had a chance to re-equilibrate with the new composition of the melt. Processes other than mixing could form reversely zoned crystals, loss of volatiles for example (G. Putman, pers. comm.), but if this were the case all phenocryst phases might be expected to show reverse zoning. If only some of the phases do, mixing becomes a stronger candidate.

The bulk rock chemistry of a sample is the third area of study that may provide some insight into the formational processes responsible for the chemical and mineralogical composition of the rock. This area of study is especially important when an entire suite of rocks from a single volcano is studied. The knowledge of how the chemistry of the rocks varied with time may allow a picture of that particular volcano's evolutionary history to be drawn. Chemical trends may become apparent both in the major and trace elements that point towards one particular evolutionary process. However, sometimes the trends for the major elements may point towards one process, while the trends for the trace elements point towards another, as may be the case for Little Sitkin island (see chapter 3).

In an attempt to investigate possible formational processes at work during the formation of the Little Sitkin island rocks, the known bulk rock major oxide concentrations (Snyder, 1959) were used to plot each rock on a ternary

diagram that is a projection of the tetrahedron plagioclase-olivine-diopside-silica into two dimensions. Onto these diagrams were added lines representing the liquid line of descent of a crystallizing magma. Boundaries dividing the different phase volumes were constructed, in each case, from electron microprobe analyses of experimental glasses. Points plotted on these diagrams should, theoretically, fall in the field that matches the petrography as seen in the sample, providing one important criterion is met. The only way this can happen is if the bulk rock composition is the same as the melt composition. If this is not so then the points plotted will not match with the petrography of the sample. As a suite of rocks gets more silicic, and the criteria discussed above are met, the points should plot closer and closer to the quartz vertex of the ternary diagram.

The bulk rock analyses of the samples from Little Sitkin island, as given in Snyder (1959) and found in Appendix I, were plotted on two different diagrams. Both are basically modifications of a diagram first presented by O'Hara (1968a). One of the diagrams was first presented in Grove et al. (1982) with revisions in Grove et al. (1983) and Grove and Baker (1984). The other diagram was presented in Walker et al. (1979). For simplicity the diagrams will be referred to as Grove or Walker diagrams respectively. The formulae for plotting points on these diagrams and a

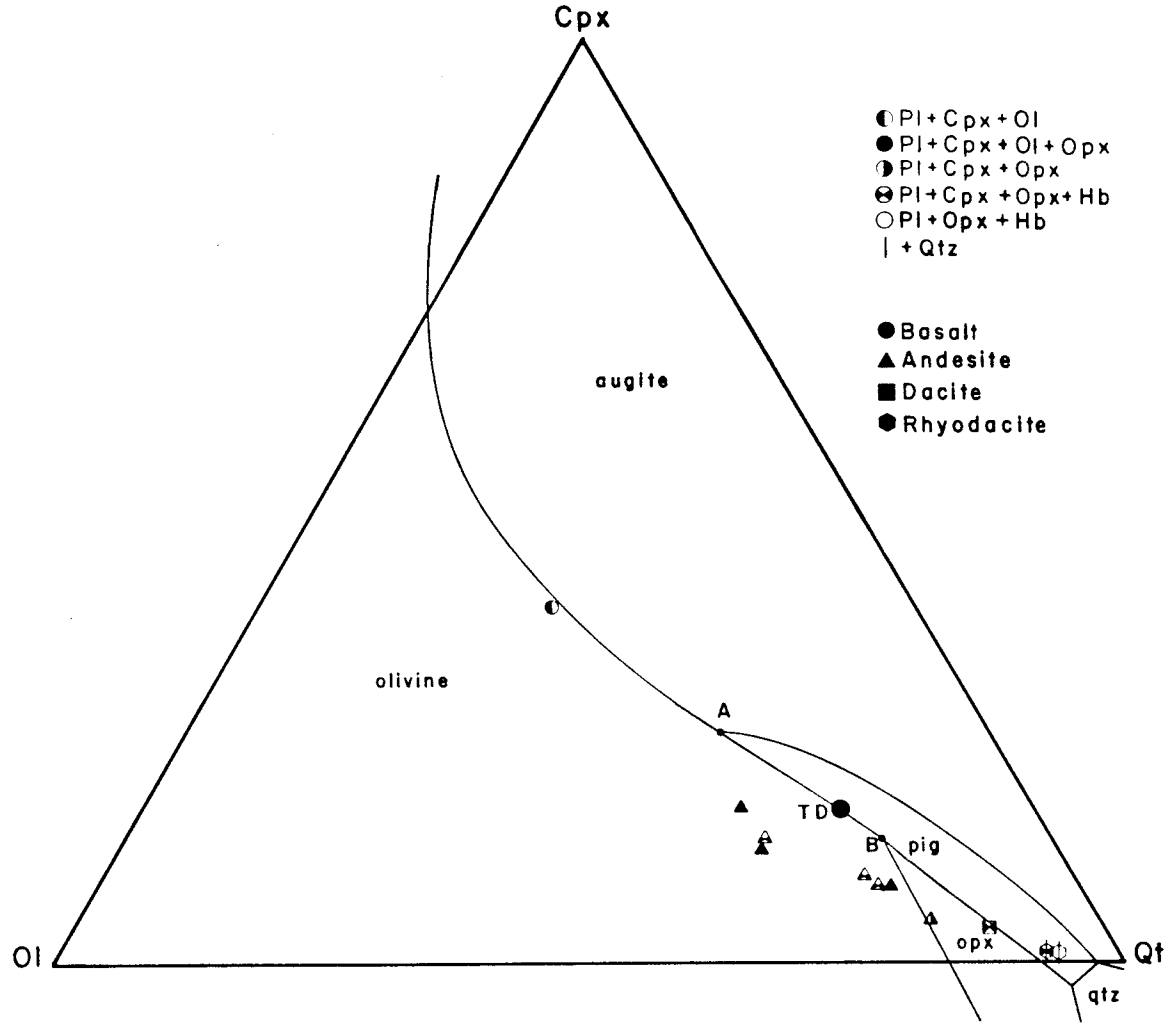

Figure 5-1 1 atmosphere Grove diagram with points plotted for the rocks of Little Sitkin island. Points A and B are reaction points terminal to the coexistance of olivine and liquid. TD is a thermal divide on the ol-pig-plag reaction curve. All phase volumes include plagioclase. After Grove et al. (1982, 1983).

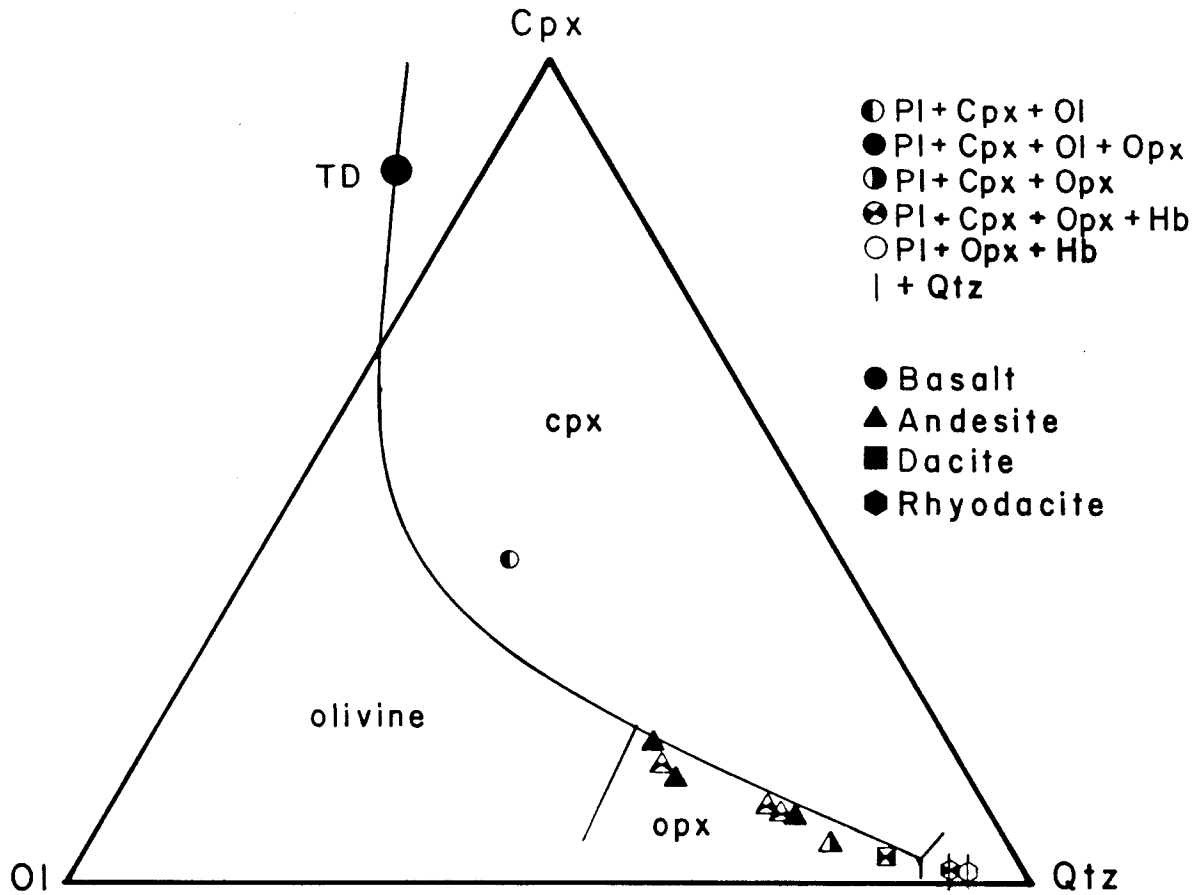

Figure 5-2 Low pressure Walker diagram with points plotted for the rocks of Little Sitkin island. TD is a thermal divide. All phase volumes include plagioclase. After Walker et al. (1979).

summary of the theory behind them is given in Appendix III.

A comparison of figures 5-1 and 5-2 shows that, although they are similar, there are significant differences between the Grove and Walker diagrams with respect to the liquid line of descent, the phase boundaries and the phase volumes themselves. Both diagrams represent one atmosphere, anhydrous conditions. Grove and Baker (1984) state that an increase in total pressure will expand the pyroxene phase volumes, while water saturation will create the opposite effect and enlarge the olivine phase volume at the expense of the pyroxenes. It can be seen that due to the differences in the diagrams, rocks will plot differently on each. Thus it is interesting to see which of these diagrams better represents the actual compositions of the rocks from Little Sitkin island, and whether or not the samples follow the path of the liquid line of descent. If they do follow the line, then a formational process of fractional crystallization is strongly suggested, although other possibilities cannot be ruled out entirely. This is especially true at higher levels of SiO_2, where the phase volumes are relatively small and distinguishing between processes can be difficult. If the samples do not follow the line of descent, then other processes may become important in deciphering the evolutionary history of the samples.

A comparison of the two diagrams, shows that, in

general, the samples from Little Sitkin island show a better fit to the Walker diagram than the Grove diagram. When plotted on the Walker diagram, the samples from Little Sitkin island plot in the phase volumes that agree fairly closely with the observed petrography. One or two exceptions do exist and may indicate that fractional crystallization did not act alone in the formation of these rocks. In contrast, the Grove diagram plots agree much less closely with the observed petrography. In fact, there is not a single point that plots within the field that theory would predict it should. In both diagrams points do not follow exactly the plotted liquid line of descent, but fall relatively close to it.

The detailed study of the phase chemistries of these rocks that follows in chapter 6, and the modelling of these results in chapter 7, should help to better define what the formational processes responsible for the rocks of Little Sitkin island were.

6 - Phase Chemistry

Introduction

Chemical analysis of all phases contained within the rocks of Little Sitkin island was performed at Lamont Doherty Geological Observatory on a Cameca Camebax electron microprobe using four wavelength dispersive spectrometers. All specimens were analyzed at an accelerating voltage of 15KV. A beam current of 50nA was used for the ferro-magnesian minerals and opaques. A 5nA beam current was used for sodium and potassium in both plagioclase and glass in order to minimize volitization of these elements. A 25nA beam current was used for the remaining elements in both plagioclase and glass. Full ZAF correction was used.

Phenocryst compositions comprise the majority of the approximately 500 analyses. Most of these grains were analyzed at both the core and rim. Those phases that showed zonation had a representative grain analyzed along a core to rim traverse. These traverses were run along as straight a line as the mineral surface and inclusions would allow. Hourglass zoned clinopyroxenes were traversed in two directions at right angles. Where the size of the grains allowed, analyses were also performed on the groundmass phases.

For a review of the petrography of these samples, see Chapter 4 and Appendix II. Representative chemical analyses

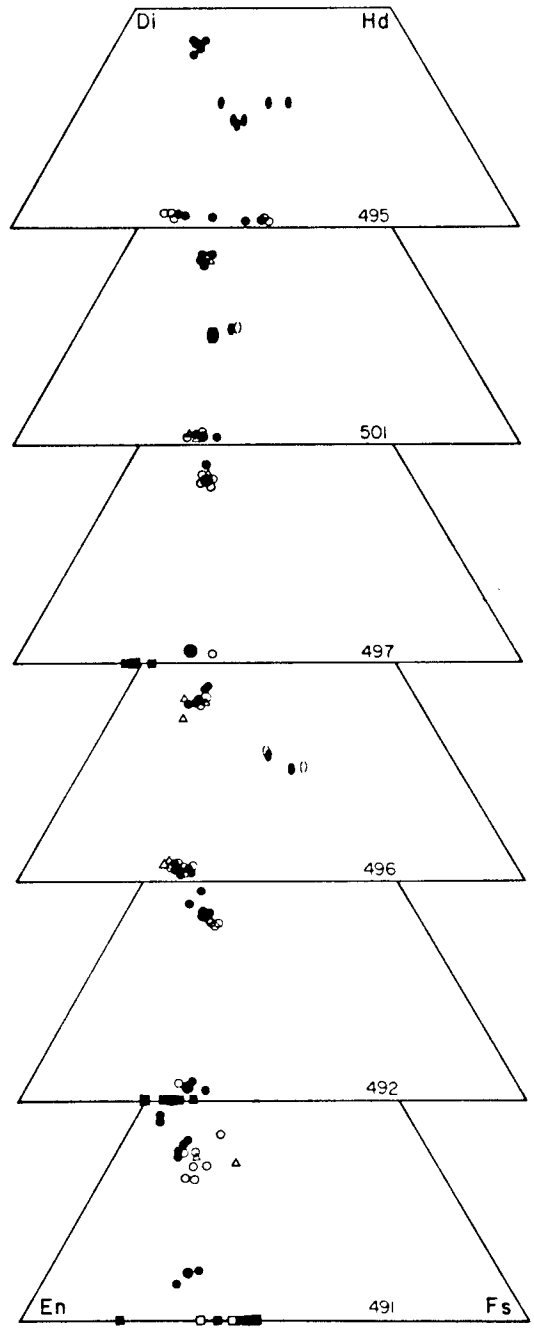

Figure 6-1 Analyses of pyroxene (small filled circles), olivine (small filled squares) and hornblendes (small filled elipses) in Little Sitkin lavas. Open symbols represent phenocryst rims, and triangles are groundmass compositions. Symbols of relatively larger size represent two or more closely coincident analyses.

are listed by weight percent and molar proportions in Appendix IV.

Olivine

Olivine was found and analyzed in three samples (figure 6-1). Basalt 491 contained a single megacryst with a composition of Fo_{81}, but the many smaller grains range from Fo_{64} to Fo_{54} and average Fo_{56}. Crystals from andesite 492 range from Fo_{75} to Fo_{66} and have an average composition of Fo_{71}, while the three olivine grains found in andesite 497 range from Fo_{77} to Fo_{73} and average Fo_{76}. There is a clear, although unusual, trend of increasing magnesium in olivine with increasing silica in the bulk rock.

Clinopyroxene

Clinopyroxene compositions are virtually identical in all of the samples studied (figure 6-1). The overwhelming majority of phenocrysts are augitic. Overgrowths of clinopyroxene on orthopyroxene and clinopyroxene grains with orthopyroxene rims have compositions similar to the phenocrysts.

Basalt 491 contains phenocrysts of augite with average core compositions of $Wo_{43}En_{48}Fs_{9}$. Rims average $Wo_{35}En_{48}Fs_{17}$. The megacrystic clinopyroxene contained in this sample has an average composition of $Wo_{42}En_{48}Fs_{10}$ in the core and $Wo_{34}En_{42}Fs_{24}$ at the crystal margins. A few of

TABLE 6-1

Average Clinopyroxene Compositions

Sample	Core	Rim	Groundmass
491	$Wo_{42}En_{49}Fs_{9}$	$Wo_{35}En_{48}Fs_{17}$	N.A.
492	$Wo_{43}En_{42}Fs_{15}$	$Wo_{41}En_{41}Fs_{18}$	N.A.
496	$Wo_{43}En_{42}Fs_{15}$	$Wo_{42}En_{42}Fs_{16}$	$Wo_{40}En_{45}Fs_{15}$
497	$Wo_{43}En_{41}Fs_{16}$	$Wo_{42}En_{41}Fs_{17}$	$Wo_{43}En_{41}Fs_{16}$
501	$Wo_{43}En_{40}Fs_{17}$	$Wo_{43}En_{41}Fs_{16}$	$Wo_{43}En_{40}Fs_{17}$
495	$Wo_{42}En_{42}Fs_{16}$	$Wo_{42}En_{42}Fs_{16}$	N.A.

these crystals have cores of diopside. Groundmass augite averages $Wo_{37}En_{43}Fs_{20}$.

The andesites, dacite and rhyodacite all have augites with very similar compositions. Averages range from $Wo_{43}En_{42}Fs_{15}$ to $Wo_{43}En_{40}Fs_{17}$ in the cores and $Wo_{43}En_{41}Fs_{16}$ to $Wo_{41}En_{41}Fs_{18}$ at the rims. Groundmass composition averages range from $Wo_{40}En_{45}Fs_{15}$ to $Wo_{43}En_{40}Fs_{17}$. Sample 492 contains crystals exhibiting hourglass zonation. These crystals have salite cores ($Wo_{47}En_{40}Fs_{13}$) and augite rims ($Wo_{33}En_{47}Fs_{20}$). Xenolith clinopyroxene compositions are almost all augite. The lone exception is a very calcium-rich salite xenocryst in dacite 501. Average clinopyroxene compositions are summarized in table 6-1.

Pigeonite

Pigeonite is found in only one sample, basalt 491, and it is clearly a groundmass phase (figure 6-1). The average composition is $Wo_{10}En_{62}Fs_{28}$, and is more correctly termed magnesian pigeonite according to the nomenclature of Deer, Howie and Zussman (1966).

Orthopyroxene

Orthopyroxene is present in every sample except 491 (figure 6-1). Compositions all lie within the hypersthene field, but show a progressive increase in iron content with increasing bulk rock silica content. Average compositions

fall between $Wo_2En_{68}Fs_{32}$ and $Wo_2En_{60}Fs_{38}$, and compositions in any given sample show a very limited range. An exception is rhyodacite 495 which contains some relatively iron-rich crystals. Groundmass compositions average $Wo_4En_{68}Fs_{28}$ in andesite 496 and $Wo_2En_{63}Fs_{35}$ in dacite 501.

Amphiboles

Amphibole is contained in three samples. Although there is a wide range in crystal composition, all grains fall in the hornblende field. Crystals in andesite 496 appear to be xenocrystic (see chapter 4) but fall within the field defined by compositions contained within rhyodacite 495. These compositions are chemically distinct from those found in dacite 501. The hornblende compositions have been recalculated in terms of the pyroxene quadrilateral components and plotted on figure 6-1. Average compositions are $Wo_{26}En_{34}Fs_{40}$ for 495 and $Wo_{25}En_{48}Fs_{27}$ for 501.

Plagioclase

Plagioclase is the dominant phase in all samples. There is considerable variation in plagioclase composition within each sample and, consequently, there is a large degree of overlap in compositions among samples (figure 6-2). Most crystals are zoned, and this is manifested most notably by an increase in sodium and potassium and decrease

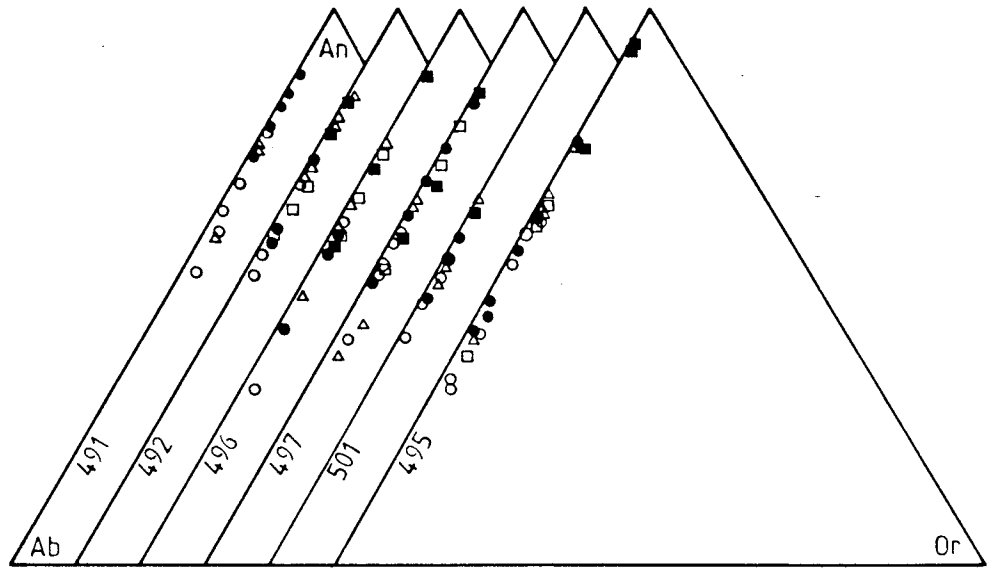

Figure 6-2 Analyses of plagioclase cores (filled circles) and rims (open circles), "dirty" plagioclase cores (filled squares) and rims (open squares) and groundmass compositions (triangles).

in calcium toward the crystal margin. Some crystals in a few samples show reverse zonation. In addition to the clear, relatively inclusion-free plagioclase crystals, several samples contain grains that have severely fritted and/or inclusion-rich interiors. These grains will be referred to as "dirty" plagioclase.

In general, most samples contain an abundance of grains of bytownite with labradorite rims. This is true for basalt 491 and several of the andesite samples. Crystals of labradorite composition are also quite common in these slides. Crystals of andesine are relatively rare, but do occur in andesite 496, dacite 501 and rhyodacite 495. The grains of andesine in samples 496 and 495 are very similar in composition, and are the most sodium-rich grains seen in the entire suite. Crystal margins on these grains approach oligoclase compositions. Most plagioclase grains exhibit normal zonation, although several crystals do show the reverse. These crystals generally range from labradorite in the core to bytownite at the rim.

Dirty plagioclase grains are usually more calcic than the clean plagioclase crystals in the same sample. The most calcic compositions observed were found in dirty plagioclase cores. Core compositions range from anorthite to labradorite, and rim compositions may extend from bytownite to labradorite. As is the case with the clean plagioclase crystals, several samples contain reversely

TABLE 6-2

Average Plagioclase Compositions

Sample	Core	Rim	DPCore	DPRim	Groundmass
491	$An_{80}Ab_{19}Or_1$	$An_{69}Ab_{29}Or_2$	N.A.	N.A.	$An_{70}Ab_{29}Or_1$
492	$An_{66}Ab_{33}Or_1$	$An_{53}Ab_{45}Or_2$	$An_{81}Ab_{19}Or_0$	$An_{62}Ab_{37}Or_1$	$An_{72}Ab_{27}Or_1$
496	$An_{62}Ab_{37}Or_1$ $An_{43}Ab_{56}Or_1$	$An_{67}Ab_{32}Or_1$ $An_{32}Ab_{66}Or_2$	$An_{71}Ab_{29}Or_0$ $An_{56}Ab_{43}Or_1$	$An_{60}Ab_{39}Or_1$ $An_{70}Ab_{29}Or_1$	$An_{62}Ab_{37}Or_1$
497	$An_{75}Ab_{24}Or_1$	$An_{56}Ab_{43}Or_1$	$An_{58}Ab_{41}Or_1$	$An_{75}Ab_{24}Or_1$	$An_{65}Ab_{34}Or_1$
501	$An_{54}Ab_{45}Or_1$	$An_{48}Ab_{51}Or_1$	N.A.	N.A.	$An_{54}Ab_{45}Or_1$
495	$An_{67}Ab_{32}Or_1$ $An_{47}Ab_{51}Or_2$	$An_{60}Ab_{39}Or_1$ $An_{40}Ab_{58}Or_2$	$An_{84}Ab_{16}Or_0$	$An_{54}Ab_{45}Or_1$	$An_{67}Ab_{32}Or_1$ $An_{40}Ab_{58}Or_2$

zoned crystals of dirty plagioclase. Cores are usually labradorite and rims of bytownite composition.

Groundmass plagioclase ranges from sodic bytownite in 491 and 492 to labradorite in the remaining samples. Andesite 497 and rhyodacite 495 contain a few groundmass grains of andesine composition. Most xenolith plagioclase compositions are in the bytownite-labradorite field. Average plagioclase compositions are listed in table 6-2.

Opaques

Two opaque minerals are contained within the rocks of Little Sitkin island (figure 6-3). Most grains are of titanomagnetite compositions, a few are ilmenite. This holds true for the included opaques as well as the phenocrystic and groundmass grains. Magnetite-ilmenite exsolution was noted in several samples, most notably, basalt 491.

Glasses

Groundmass glasses show a very wide range of compositions in those samples in which they exist (figure 6-4). A general trend of decreasing Mg # with increasing silica is observed when these parameters are plotted for both whole-rock compositions as well as the groundmass glasses. This may indicate a possible fractionation trend, at least for the groundmass glasses. Sample 497 is a bit

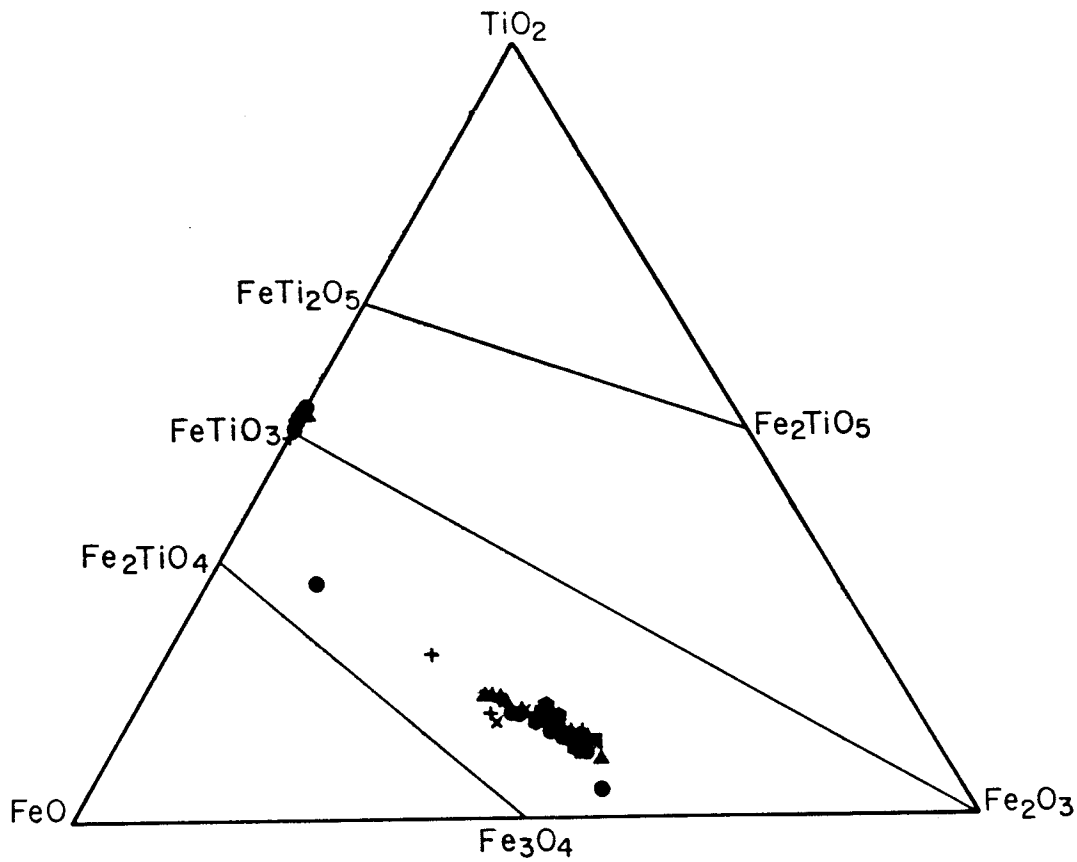

Figure 6-3 Opaque phase compositions plotted on the ternary $FeO-Fe_2O_3-TiO_2$. Circles represent basalt, triangles andesite, squares dacite, hexagons rhyodacite, crosses inclusions and x's xenolith opaque compositions. Solid lines connect the major solid solution series (from the bottom up) magnetite-ulvospinel, hematite-ilmenite and pseudobrookite-ferropseudobrookite.

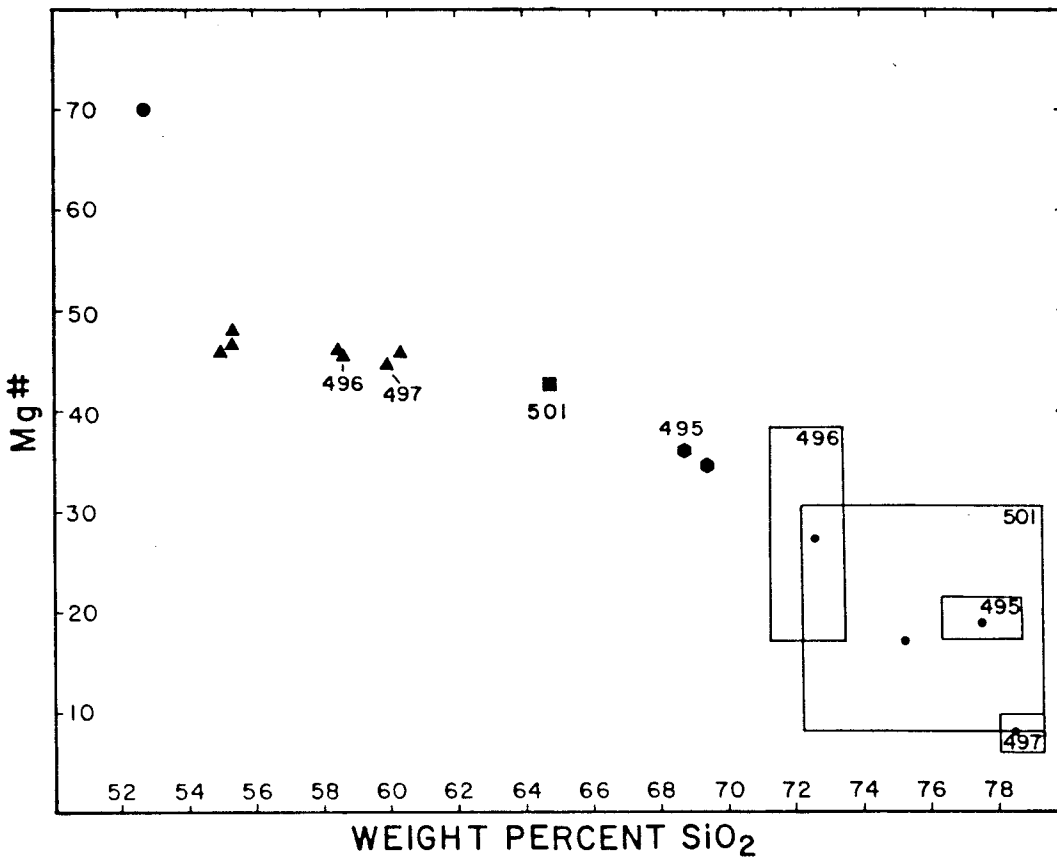

Figure 6-4 Plot of Mg # versus silica for the rocks of Little Sitkin island (solid symbols as defined previously) and groundmass glasses of four labeled samples. Boxes define range in groundmass glass compositions and dots represent average compositions.

of an oddity, as it would be expected to plot in a much more primitive position, but this may be a result of a mixing event associated with the formation of this sample (see Chapters 7 and 8).

Glasses included within mineral phases were rather difficult to analyze. The few analyses that were obtained suggest that glasses trapped within plagioclase are more primitive than those in the groundmass of the same sample. Glasses trapped within clinopyroxene in sample 497 are much more primitive than the groundmass glasses in that sample, yet the clinopyroxene glasses in sample 496 are more evolved than the groundmass. Orthopyroxene glasses were analyzed in samples 497, 501 and 495 and show no obvious relationship with the groundmass glasses. In sample 497 these glasses are lower in silica and Mg # than the clinopyroxene glasses in the same sample, but have a higher Mg # than the plagioclase and groundmass glasses. In sample 501 the orthopyroxene glass composition is lower in silica and Mg # than the average groundmass glass composition in that sample, but falls within the field defined by the range of groundmass glass compositions. Finally, orthopyroxene glass compositions in 495 are much lower in both silica and Mg # than the groundmass glasses.

7 - LEAST-SQUARES MODELS

Introduction

The phase chemistry data obtained for the six rock samples (chapter 6 and appendix IV) were used, together with the bulk-rock major-element chemistries of these rocks (appendix I), to model the possible magmatic relations of the suite of rocks found on Little Sitkin island. These six samples were chosen based on their plotted position on the TiO_2 vs. Zr diagram (figure 3-5).

Least-Squares Mixing

The least-squares approximation of Bryan et al. (1969) is an algebraic calculation that may be used to estimate a given sample composition provided the chemistries of the included phases and the true composition of the sample are known. This method is useful as a means of testing hypotheses involving magma mixing and, as will be shown subsequently, it may also effectively approximate crystal fractionation.

Algebraically, this calculation may be summarized as the linear equation:

$$XB = Y \qquad \text{(eq. 7-1)}$$

where X is a matrix of n rows of oxides and k columns of phases, B is a column vector containing k terms, each representing the estimated amount of a given phase and Y is

a column vector of n terms each representing the estimated amount of a given oxide. Algebraic manipulation yields a unique solution:

$$B' = [X^T X]^{-1} X^T Y \qquad \text{(eq. 7-2)}$$

where X^T is the transpose of the matrix X. Equation 7-2 may be substituted for B in equation 7-1 and the multiplication performed. A vector Y' is obtained which is the least-squares approximation of Y, the actual chemical composition of the sample.

The least-squares calculation yields an estimated amount of each phase needed to approximate the desired composition and an estimated amount of each oxide in this composition. An assesment of the validity of the proposed mixture may be made based on the sum of the squares of the residuals. The residuals are the differences between the observed and estimated compositions for each oxide in the sample.

A consequence of this type of calculation is that the more variables (phases, rock compositions) that are included in the calculation, the closer the resemblance between the observed and calculated compositons and, hence, the lower the sum of the squares of the residuals. This is a result solely of the algebra and may not accurately reflect the petrology of the sample. Thus it is necessary to keep variables to a minimum.

Basalt 491 Formation

The least-squares method of Bryan et al. (1969) was used to assess the possibility of forming basalt 491 by the addition of cumulate clinopyroxene, for which there is petrographic and chemical evidence (see chapters 3 and 4). From the geologic history of Little Sitkin island, and a review of the TiO_2 vs. Zr diagram (figure 3-5), it appears that the composition of this sample prior to clinopyroxene accumulation may have been similar to that of andesite 493.

To assess the validity of this hypothesis, two calculations were performed. The first calculation, termed the clinopyroxene subtraction calculation, can be generalized by the reaction:

$$Y + CPX = 491 \quad \text{(eq. 7-3)}$$

where Y is the original composition.

This may be tested by the use of the equation:

$$X^{Y}C^{Y}_{TiO2} + X^{CPX}C^{CPX}_{TiO2} = C^{491}_{TiO2} \quad \text{(eq. 7-4a)}$$

and

$$X^{Y}C^{Y}_{Zr} + X^{CPX}C^{CPX}_{Zr} = C^{491}_{Zr} \quad \text{(eq. 7-4b)}$$

where: X = Weight Fraction of given phase
C = Concentration of element or oxide in given phase

This may be restated as:

$$(1-X^{CPX})C^{Y}_{TiO2} + X^{CPX}C^{CPX}_{TiO2} = C^{491}_{TiO2} \quad \text{(eq. 7-5a)}$$

and

$$(1-X^{CPX})C^{Y}_{Zr} + X^{CPX}C^{CPX}_{Zr} = C^{491}_{Zr} \quad \text{(eq. 7-5b)}$$

Since $X^{CPX} + X^{Y} = 1$, X^{CPX} may be rewritten as:

$$X^{CPX} = \rho^{CPX}V^{CPX}/[\rho^{Y}V^{Y} + \rho^{CPX}V^{CPX}] \quad \text{(eq. 7-6)}$$

where: ρ = given phase density
V = volume percent of given phase

The calculated value for X^{CPX} is substituted into equation 7-5a along with the other known values, and the equation is solved for C^{Y}_{TiO2}. For the determined modal values (table 4-1), equation 7-6 yields $X^{CPX} = 0.45$. Because of possible petrographic heterogeneity, the effects of variation in X^{CPX} was explored.

Since Zr was not analyzed in the mineral phases, C^{CPX}_{Zr} is unknown. However, since:

$$C^{CPX}_{Zr}/C^{Y}_{Zr} = D^{CPX/l}_{Zr} \quad \text{(eq. 7-7)}$$

where $D^{CPX/l}_{Zr}$ is the crystal/liquid distribution coefficient for Zr, we can divide both sides of equation 7-5b by C^{Y}_{Zr} to yield:

$$(1-X^{CPX}) + X^{CPX}D^{CPX/l}_{Zr} = C^{491}_{Zr}/C^{Y}_{Zr} \quad \text{(eq. 7-8)}$$

which may then be solved for the unknown, C^{Y}_{Zr}.

The results of these calculations (figure 7-1) show that for various values of X^{CPX}, and $D^{CPX/l}_{Zr} = 0.1$ (Pearce and Norry, 1979), the composition of 491 moves essentially linearly toward that of 493, and that a value between 0.50 and 0.55 would probably match exactly for these two elements (TiO_2 and Zr). Changing the value of $D^{CPX/l}_{Zr}$ by ten percent in either direction will not significantly alter the value of Y. This range in value is represented by

the diameter of the symbol for Y (figure 7-1). It is important to note that the linearity of the points for clinopyroxene, 491 and Y is to be expected. It is a result of the calculation. The fact that 493 is also colinear with these points, however, is not a result of the calculation and is taken as evidence that the sample may have indeed formed by the addition of cumulate clinopyroxene to a composition similar to 493.

As a further test of the original hypothesis, a least-squares calculation was performed using the bulk-rock composition of 493 and various mineral phases in an attempt to match the bulk composition of 491. The results of this calculation are given in appendix V, and summarized as follows: A simple mixture of 493 and cumulate clinopyroxene does not adequately match the bulk chemistry of 491. However, 491 does contain what appears to be a megacryst of cumulate olivine and some anorthite-rich plagioclase (appendix IV). If these phases are added to the mixture, quite a good match is obtained. Iron is the only element that shows a considerable difference between observed and calculated values. Addition of magnetite takes care of this discrepancy. The composition of 491 can be derived by the addition of cumulate clinopyroxene, cumulate olivine, high-anorthite plagioclase and magnetite to the bulk chemical composition of sample 493 in the proportions (weight percent) 34:7:3:1:55.

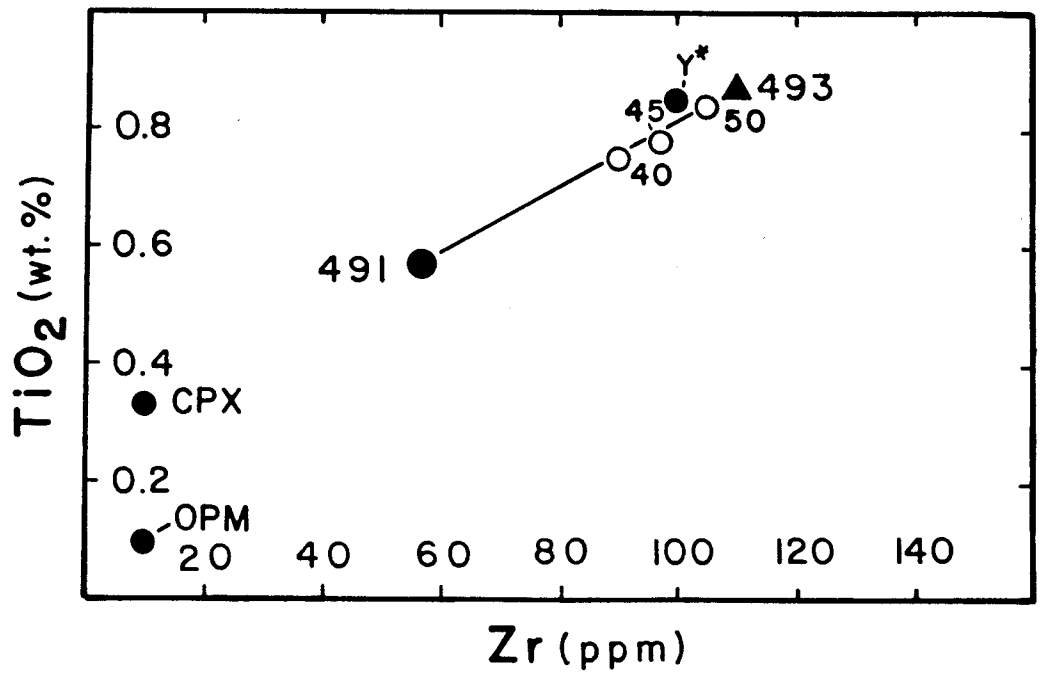

Figure 7-1 TiO_2 versus Zr diagram for samples 491 and 493. Points labelled 40, 45 and 50 represent composition Y corresponding to X^{CPX} of 40, 45 and 50 respectively in the clinopyroxene subtraction calculation. Point labeled OPM represents composition of the weighted sum of olivine, plagioclase and magnetite. See text for discussion.

The results of the two calculations are in general agreement. They show that formation of 491 resulted from the mixture of cumulate clinopyroxene and other mineral phases with a liquid having a bulk composition similar to that of sample 493. The differences between the results of the two calculations may be explained by the following: (1) Only mineral core compositions were used in the least-squares calculation. Use of the whole-grain average mineral chemistry may bring the results of the two calculations into better agreement. (2) The mode is based on a single thin section in an obviously heterogeneous rock. (3) The results of the clinopyroxene subtraction calculation are based upon just two parameters, TiO_2 and Zr. Perhaps the use of other parameters would show the need for small amounts of other phases to be subtracted from the composition of 491 to truly approach that of sample 493.

As a test of this last possibility, the clinopyroxene subtraction calculation was performed with additional terms added to take into account the weight fractions of olivine, plagioclase and magnetite (OPM) and the concentrations of TiO_2 and Zr in these phases. Weight fractions used are from the results of the least-squares mixing calculation. The concentration of Zr in these phases is considered to be negligible, while TiO_2 concentration is negligible in olivine and plagioclase and 10 weight percent in magnetite. The result of this calculation is point Y^* in

figure 7-1. The addition of the other phases to the clinopyroxene subtraction calculation shifts the position of Y slightly. Sample 491 should plot within the triangle defined by the points CPX, OPM and Y^*, and this is indeed the case. This calculation provides additional support to the hypothesis that sample 491 formed by the addition of clinopyroxene, with a minor quantity of other phases, to a composition similar to 493.

Whole Rock Mixes

Mixing of magmas has been proposed as a method to generate the suite of rocks on Little Sitkin island, based on the bulk-rock major element chemistries. Trace element plots, such as the TiO_2 vs. Zr diagram (figure 3-5) suggest a fractionation mechanism at work. However, several samples of the suite (494, 496) do not plot along a proposed fractionation trend. The position of these samples suggests mixing as a possible method of achieving their chemistries. Using the least-squares method of Bryan et al. (1969), results of several hypothetical but possible whole-rock mixes to create these samples can be tested.

Possible mixtures that could produce these samples are shown in figure 7-2 by the dashed tie-lines:

Basalt 491 + Andesite 497
Andesite 492 + Dacite 501

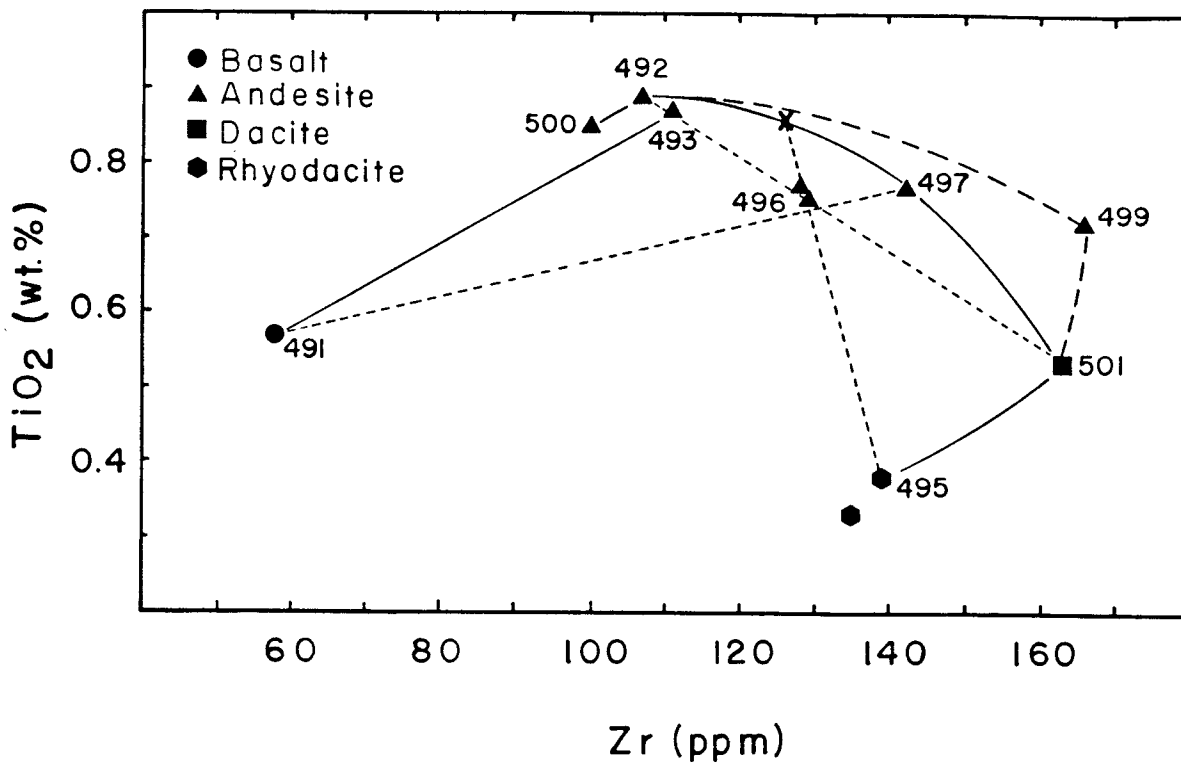

Figure 7-2 TiO_2 versus Zr plot of chapter 3 with tie-lines of possible mixing pairs (small dashes) and a second possible mixing trend (large dashes) shown. See text for discussion.

Andesite 493 + Dacite 501
Rhyodacite 495 + Andesite "X"

Andesite "X" is a hypothetical composition for a magma that may have existed, but was either totally used up in a mixing event or not sampled by Snyder in his study of the island. It is therefore important to determine a possible composition for "X" in order to determine the feasibility of this possible mixing pair.

Before a summary of the results of the mixing models can be given, it is important to understand how the composition of "X" was calculated. Using the TiO_2 vs. Zr diagram (figure 3-5), a line was drawn through the points for samples 496 and 495. The point at which this line intersected the postulated fractionation curve (solid line) was labelled "X" and the concentration of Zr noted. A vertical line was then drawn on the plot of SiO_2 vs. Zr (figure 3-4) at this zirconium concentration. Where this line intersected a line connecting the points for samples 495 and 496 a horizontal line was drawn and the concentration of SiO_2 for the sample noted. With the knowledge of the silica concentration, and assuming the bulk-rock compositions to equal liquid compositions, the remaining major oxide concentrations were read off figure 3-3, the whole-rock composite silica-variation diagram. The composition of "X" is given in table 7-1.

The composition of the endmembers of the proposed mixing pairs were used in a least-squares mixing program

TABLE 7-1

Composition of "X"

SiO2	57.00
TiO2	0.80
Al2O3	17.40
FeO*	7.50
MnO	0.15
MgO	3.70
CaO	7.90
Na2O	3.30
K2O	1.20
P2O5	0.18
TOTAL	99.13

and an attempt was made to match the composition of sample 496. Sample 496 was used rather than sample 494 because of the availability of trace-element data for this sample.

All of the possible mixes give good results, with the sum of the squares of the residuals for each under 1. However, the proposed mixture of sample 495 and "X" to account for the formation of 496 gives the best match between observed and calculated compositions. In addition, the sum of the squares of the residuals for this mixing pair is about twenty times smaller than the others. An argument may be made that it would be expected for this to be the best fit simply because the composition of "X" was derived using 496 and 495 in the first place. For other reasons, which will be discussed in the following chapter, this mixture still appears to be the best.

Fractionation Trend

The nature of the least-squares method of Bryan et al. (1969) allows representation of fractionation as "unmixing" of a rock and its phases to yield a new composition, if the bulk-rock composition is assumed to equal the liquid composition. This method should not be confused with true Rayleigh fractionation, as it yields only qualitative results and says nothing about the parititioning of elements between phases and melt. However, this method allows us to start with a particular

bulk-rock composition and the chemistries of the phases that comprise it and attempt to generate the composition of a more evolved sample by subtracting various amounts of the different phases.

This was attempted for six of the samples lying along the proposed fractionation trend of the TiO_2 vs. Zr diagram (figure 7-2), in order to determine the possibility of producing this trend by fractionation. Starting with sample 492, an attempt was made to generate the bulk compositions of "X", 497, and 499. In addition, an attempt was made to generate the bulk compositions of 501 from 497 and 495 from 501. Andesite 499 is included because the true position of the fractionation trend for this suite is not accurately known. It may actually pass through the point for sample 499 rather than 497 (figure 7-2), a subject that will be discussed in greater detail subsequently. Results of these models are given in appendix V.

It is difficult to assess the plausibility of the results of these models. The sum of the squares of the residuals are all low, most are 0.1 or less. However, to achieve this, and to get subtraction of all the phases used, orthopyroxene, as well as the "dirty" plagioclase must be neglected as a phase in most samples. It is obviously unsatisfactory to have to neglect a phase such as orthopyroxene that is clearly phenocrystic (see chapter 4). This results in the failure to achieve mass-balance in the

least-squares calculation that is petrologically accurate. Perhaps there is another, unseen, phase whose chemistry would affect the calculation. Alternately, orthopyroxene may not truly be a phenocryst phase in these samples regardless of what other lines of evidences suggest. Both these possibilities seem remote. In the absence of any other evidence this must remain a mystery, and it appears as if fractionation alone cannot explain the observed trend.

Other Mixes

Because of the uncertainty in the position of the fractionation trend in the TiO_2 vs. Zr plot, it may be that sample 497 is also a mixture of two or more compositions. Indeed, the petrography of this sample tends to support such an idea. Several whole-rock mixes were modelled along the lines discussed for sample 496 in order to account for the chemistry of 497, but none of these gave very good results (appendix V). Many of the possible mixing endmembers are hornblende bearing, while sample 497 contains olivine. Although 497 may have evolved from a more primitive sample (492, "X") by fractionation, the petrography suggests otherwise. The mixing models, in general, do not give a good fit in accounting for the bulk composition of this sample. However, the mix involving composition "X" yields a sum of the squares of the

residuals that is about four to five times lower than that given by any of the other postulated mixing pairs. This reinforces the possibility of the existence of a composition similar to "X". It may be that a combination of these two factors, mixing and fractionation, led to the formation of this sample.

8 - DISCUSSION OF RESULTS

Fractionation and Mixing

The results of the study of the rocks of Little Sitkin island indicate both crystal fractionation and magma mixing as evolutionary processes important during the formation of the suite.

The postulated fractionation trend seen in the plot of bulk rock TiO_2 vs. Zr is in general agreement with the results of least-squares calculations. It appears as if crystal fractionation has played a role in the formation of the Little Sitkin suite. However, crystal fractionation alone cannot explain the formation of several of the samples in the suite (andesite samples 496, 494 and possibly 497) nor can it explain the linear whole-rock major element trends (figure 3-3).

Least-squares mixing models strongly suggest that sample 496, and by inference sample 494, was formed by magma mixing. The best possibilities for mixing pair endmembers are rhyodacite 495 and a hypothetical andesite composition, "X". The sum of the squares of the residuals of this proposed mixture is very low (appendix V). In addition, it is important to note that variables in this mixing calculation were kept to an absolute minimum.

Both the petrography and phase chemistry support a mixing process during the formation of these rocks.

Evidence from phase chemistry that suggests samples 496 and 495 may be related by a mixing process includes the similarity of mafic and plagioclase phase compositions. Although there is considerable overlap in phase compositions in all of the analyzed samples, it is only in samples 496 and 495 that these similarities are so complete. Samples 496 and 495 are the only two samples that contain plagioclase phenocrysts with core compositions as sodic as andesine - An_{40}. Plagioclase core compositions in all other samples are much more calcic. Table 8-1 summarizes the observed range of core compositions in the four hypothesized mixing pairs and sample 496.

Hornblende compositions of the two xenocrysts in sample 496 plot within the field defined by the compositions of hornblende phenocrysts in sample 495. These compositions are distinctly different from the hornblende phenocryst compositions from dacite 501, and tends to exclude sample 501 as a feasible mixing pair endmember in the formation of 496.

Petrographic evidence for mixing is readily apparent in many of the thin sections. Two distinct populations of plagioclase were distinguished in these rocks. One population contains relatively small grains (1-2 mm in length) that are inclusion-free. The other population's grains are larger and contain abundant inclusions. These inclusions may occur either as rings paralleling the

TABLE 8-1

Range of Core Compositions

Mixing Pairs	OL	CPX		OPX		HB	PLAG
	Mg#	Mg#	Wo En Fs	Mg#	Wo En Fs	Mg#	An Wt.%
491	58-53*	92-79	46-40 49-47 8-13	***		None	89-74
&							
497	79-73	73-71	46-42 39-41 15-17	68-66	3- 3 65-63 32-34	None	84-51
493**	58-53	92-79	46-40 49-47 8-13	****		None	84-51
&							
501	None	72-69	44-43 40-39 16-18	66-61	2- 2 63-59 35-39	67-62	59-48
492	76-66	80-72	44-42 44-41 12-17	69-64	3- 2 66-62 31-36	None	73-59
&							
501	None	72-69	44-43 40-39 16-18	66-61	2- 2 63-59 35-39	67-62	59-48
495	None	73-71	40-43 44-40 16-17	69-52	3- 2 66-49 31-49	62-43	76-42
&							
"X"	?	?		?		?	?
496	None	78-72	41-44 46-40 13-16	70-67	3- 2 67-65 30-33	64-55	60-43

TABLE 8-1 (continued)

* - Only olivine in groundmass.
** - Assumed compositions (see text, chapter 7).
*** - No opx in this sample, just groundmass pigeonite.
**** - Orthopyroxene compositions not known and cannot be assumed from 491 compositions. May be similar to opx compositions in 492.

crystal margins or concentrated in crystal cores. Subsequent phase chemical analysis of these thin sections confirmed the existence of these two populations of plagioclase phenocrysts. The inclusion-rich or "dirty" plagioclase are consistently higher in calcium and lower sodium and potassium than the inclusion-free or "clean" plagioclase. In addition, when least-squares mixing models were performed, the inclusion of the "dirty" plagioclase as a possible fractionating phase gave very poor results. In these cases the model suggested addition of this phase to the parent rock, rather than subtraction. Since addition implies mixing or contamination rather than fractionation, this negative result in "dirty" plagioclase fractionation can be regarded as further evidence for mixing.

Further petrographic evidence for mixing is found in the occurrence of both normal and reverse zoned phenocrysts of a number of different phases in the same thin section. This is most obvious in the case of plagioclase, but is also seen in clinopyroxene.

Additional support for a mixing mechanism active in the formation of the Little Sitkin rocks comes from observations by Snyder (1959). He noted banded pumice within the Patterson Point formation and interfingering of andesitic and rhyodacite lavas in the Little Sitkin dacite. Banded pumice has been taken as evidence of mixing (MacDonald and Katsura, 1965), and the interfingering of

the two lava types was explained by Snyder as contemporaneous extrusion from a single vent. What Snyder does not state and presumably does not know, is when and where the mixing of these two rock types took place. This incomplete mixing may have taken place in a shallow magma chamber with eruption following, or perhaps caused by, the mixing (Sparks et al., 1977). Alternately, mixing may have taken place between two separate magmas in a common conduit just prior to, or during, extrusion.

Samples 496 and 495 were collected within a half meter of each other at the contact between the Little Sitkin dacite and the Pratt Point member, near the zone of interfingering lavas. Based on the field evidence alone, it seems likely that some sort of mixing event affected these rocks. Unfortunately, there is no evidence of the proposed mixing pair endmember, andesite "X". This may be a result of the complete exhaustion of the supply of "X" during mixing. If this is the case, the existence of "X" may never be proven, it may only be inferred from the data. Another possibility, however, is that composition "X" was not sampled. Only two samples were collected in the zone of mixing of andesite and rhyodacite lavas. Perhaps a more thorough sampling of this area would uncover samples with compositions similar to the inferred composition of "X". Indeed further sampling might show an entire range of mixed compositions from "X" through 496 to

495.

Sample 494 is inferred to have formed in a similar manner to 496. Both their major and trace-element compositions are similar, and they come from the same formation, although different flows. Sample 494 contains a clear "dike" of what may be one of the endmembers of a possible mixing pair.

Andesite 497 is another case of a possible mixing product. While the results are not as satisfactory as those for sample 496, least-squares analysis of this composition suggests mixing as a feasible process to account for its formation. This is supported by both the phase chemistry and petrography of the sample. If 497 is a mixture, then the proposed fractionation trend of figure 3-5 is incorrect. One possible alternative is shown in figure 7-2 and suggests that andesite 499 lies along the fractionation path rather than 497. Although 499 has an eruptive age that is older than sample 492, which theoretically fractionated to form 499, this age may not give an accurate representation of the processes occurring at depth.

Mixing of another sort appears to have been responsible for the production of "basalt" 491. Least-squares and clinopyroxene subtraction calculations (see chapter 7) suggest that cumulate clinopyroxene, along with lesser amounts of olivine, plagioclase and magnetite,

was mixed with, or added to, a liquid having a bulk composition similar to that of andesite 493. These rocks are from the oldest unit on the island, and may have no strong relationship to the other samples.

Parent Magma

Whole rock and phase chemistry of the Little Sitkin island samples allows some inferences to be made with regards to parent magma composition.

The suite of rocks on Little Sitkin island falls within the Aleutian transitional calc-alkalic (TCA) field of Kay and Kay (1985a). Transitional calc-alkalic rocks are the result of differentiation of a high-alumina basalt (HAB) at mid to lower crustal depths. Subsequent shallow level processes produce further differentiation. The HAB magma has an olivine tholeiite parent that is produced by partial melting of mantle peridotite (Tatsumi et al., 1983). According to Kay and Kay (1985a) this olivine tholeiite is primary to all the magmas of the Aleutian arc, both calc-alkalic and tholeiitic. The depth at which differentiation processes takes place is the primary control on the rock series produced (Kay et al., 1982).

Kay and Kay (1985a) suggest that high-alumina amphiboles contained within some aleutian TCA lavas record crystallization from mafic magmas at relatively high pressures suggestive of deep crustal magma chambers. These

TCA lavas may also contain low-alumina amphiboles that are taken to indicate crystallization pressures that are lower than those indicated by the high-alumina amphiboles. These lower pressures suggest fractionation in shallow level magma chambers, possibly those directly underlying the volcanoes.

Amphibole bearing lavas from Little Sitkin island contain both high- and low-alumina amphiboles with compositions similar to those reported by Kay and Kay (1985a) (table 8-2). This suggests that there were both deep- and shallow-level differentiation processes at work during the formation of these rocks. None of the primary HAB magmas are seen as lavas because of these two levels of magma chambers. The shallow level chambers serve as sites of subsequent differentiation and mixing prior to extrusion (Conrad et al., 1983)

Summary of Magmatic Evolution

It is suggested that a primary olivine tholeiite, parental to all the magmas in the arc, is produced by partial melting of mantle peridotite (Kay et al., 1982; Tatsumi et al., 1983). Subsequent fractionation of this olivine tholeiite at deeper crustal depths produces the parent magma of the calc-alkalic trend, a high-alumina basalt (Gust and Perfit, in press). This deep crustal fractionation is evidenced by high-alumina amphiboles

TABLE 8-2

	HIGH-ALUMINA AMPHIBOLES		LOW-ALUMINA AMPHIBOLES	
	Bul1Ca*	495AMP1	MOF3b*	495AMP4
SiO2	43.74	43.49	46.86	47.78
TiO2	1.26	2.06	1.73	1.16
Al2O3	13.65	11.39	8.10	6.49
FeO*	11.08	14.07	13.19	17.46
MnO	0.04	0.33	0.45	0.71
MgO	14.79	12.80	14.54	12.24
CaO	11.88	11.35	11.22	10.02
Na2O	1.95	2.18	1.55	1.35
K2O	0.40	0.28	0.41	0.23
TOTAL	98.79	97.95	98.05	97.44

* - From Kay and Kay (1985a)

contained within some lavas. Eventually, the HAB magma may reach a shallow crustal magma chamber where it undergoes further differentiation. This stage of magmatic evolution is recorded in the fractionation of low-alumina amphiboles (Kay and Kay, 1985a).

This scenario is in general agreement with one proposed by Baker and Eggler (1983) for the rocks of Atka. They suggest that fractionation of HAB magmas at shallow depths leads to the formation of andesitic liquids. These relatively dry magmas will become concentrated in water as anhydrous phases crystallize. When the water concentration in the magma reaches approximately 5 weight percent, crystallization of low-pressure amphiboles occurs. In contrast with Kay and Kay (1985a), Baker and Eggler suggest that HAB magmas form at moderate pressures (8 Kbar) and low water contents. This precludes the crystallization of high pressure amphiboles as seen in the Little Sitkin lavas, and noted by Kay and Kay (1985a) for other Aleutian volcanic centers. Thus parental HAB magmas at Little Sitkin must have had higher initial water contents than those of Atka. This water may be derived from the subducted slab.

Gust and Perfit (in press) suggest that clinopyroxene fractionation is the primary control on the evolution of primary magmas at depth. Thus it is possible that the cumulate clinopyroxene trapped within sample 491 is further evidence of the deep crustal differentiation of the olivine

tholeiite to form the HAB magma. Indeed these clinopyroxene crystals have compositions very similar to cumulate clinopyroxene that Conrad and Kay (1984) suggest are the first fractionates of mantle-derived melts (table 8-3). These crystals may have been brought up to the shallow level magma chamber directly underlying the volcano with a pulse of HAB magma. This HAB magma then mixed with previously fractionated HAB that had a composition similar to sample 493, with formation of a magma with the composition of 491 the result. Eruption of this magma emptied the shallow level chamber while forming the bulk of Little Sitkin island. New HAB then migrated to this shallow level chamber and underwent further fractionation and periodic eruption.

Figure 8-1 is a representation of the whole-rock major-oxide silica variation diagram with the positions of three Aleutian HAB lavas plotted. These compositions fall on or near the extension of the linear whole-rock trends at lower silica concentrations. This suggests that the parental HAB magma may have ultimately been one endmember in various mixing events, and that occasional mixing of this composition with more evolved magmas led to the formation of the Little Sitkin suite. Zonation profiles in plagioclase and clinopyroxene phenocrysts may record times of replenishment of the shallow level magma chamber by hotter, more mafic HAB magma. Plagioclase phenocrysts in

TABLE 8-3

	CLINOPYROXENES		OLIVINES	
	MM75C-2b*	491MCPX2c	MM7743-1*	491OL1c
SiO2	53.97	53.66	39.21	39.53
TiO2	0.12	0.12	0.01	0.01
Al2O3	1.15	1.26	0.02	0.02
Cr2O3	0.30	0.47	N.A.	N.A.
FeO*	2.81	3.55	16.89	17.84
MnO	0.12	0.09	0.43	0.25
MgO	18.21	17.95	43.21	42.14
CaO	23.65	22.42	0.10	0.19
Na2O	0.30	0.19	N.A.	N.A.
TOTAL	100.63	99.72	99.87	99.97

* - From Conrad and Kay (1984)

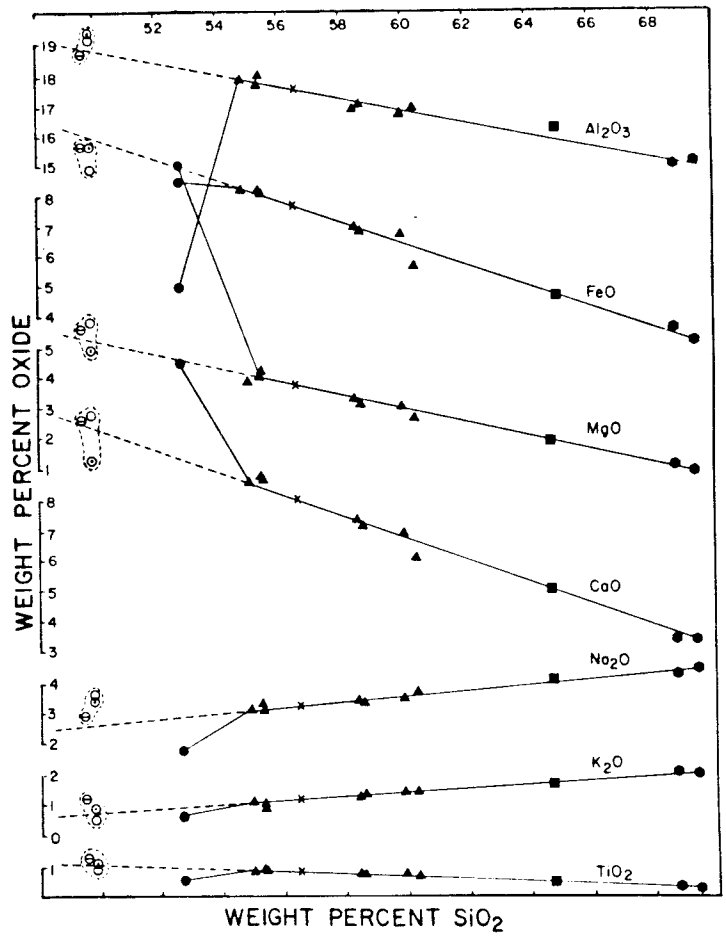

Figure 8-1 Little Sitkin whole-rock major-oxide silica variation diagram with linear trends extended to lower silica concentrations. Three representative Aleutian HAB compositions plot on or near this linear trend (open circle with bar from Kay et al., 1982; open circle from Baker and Eggler, 1983; open circle with dot from Nye and Reid, 1986). See text for discussion.

dacite 501 show this fairly well. The compositions of three adjacent zones situated between the core and rim of the crystal range from An_{48} to An_{85} to An_{52}, suggesting influx of a mafic magma.

Late stage mixing is recorded primarily by the rocks of the Little Sitkin dacite, and appears to involve a highly fractionated rhyolite or rhyodacite composition and a less evolved andesite.

9 - CONCLUSIONS

The results of this study lead to the following conclusions:

1. The lavas of Little Sitkin island constitute a calc-alkaline suite. Andesite is the dominant rock type, but dacite and rhyodacite also occur in significant quantities. Plagioclase is the dominant phenocryst phase and occurs along with clinopyroxene, orthopyroxene and magnetite in all samples. Olivine or hornblende occur in some samples, but never together.
2. Major- and trace-element whole-rock trends suggest contrasting evolutionary processes for the suite. Major elements plot as linear trends on silica variation diagrams that suggest magma-mixing. Curving trace-element trends indicate accessory-phase fractionation.
3. Petrographic and phase chemical analyses of thin sections of these rocks provide further evidence for mixing, and support inferences made by Snyder (1959) based on field relations.
4. Least-squares analysis of the whole-rock and phase chemistry of these samples suggests that magma-mixing produced andesite 496, and by inference sample 494.

One endmember in this mix was a rhyodacite whose bulk composition was similar to that of rhyodacite 495. The other endmember of this mixing pair has not been found, its composition can only be estimated.

5. Basalt 491 was produced by addition of clinopyroxene, olivine, plagioclase and magnetite to a fractionated liquid similar in composition to andesite 493. These added crystals were probably brought, from depth, to a shallow magma chamber with a pulse of more mafic parent magma.
6. The proposed parental magma is a high-alumina basalt produced by high-pressure fractionation of an olivine tholeiite. Subsequent fractionation at lower pressures produces andesitic liquids. This HAB magma is a possible endmember in numerous mixing events that led to the formation of the suite.

BIBLIOGRAPHY

Ach, J., and DeLong, S.E., 1980. Magmatic Evolution of Little Sitkin and Semisopochnoi Volcanoes, Alaska. EOS, 61: 1170.

Anderson, A.T., 1976. Magma Mixing: Petrological Process and Volcanological Tool. Jour. Volc. Geotherm. Res., 1: 3-33.

Baker, D.R., and Eggler, D.H., 1983. Fractionation Paths of Atka (Aleutians) High-Alumina Basalts: Constraints from Phase Relations. Jour. Volc. Geotherm. Res., 18: 387-404.

Bowen, N.L., 1928. The Evolution of the Igneous Rocks. Princeton University Press, Princeton, 334pp.

Bryan, W.B., Finger, L.W., and Chayes, F., 1969. Estimating Proportions in Petrographic Mixing Equations by Least Squares Approximation. Science, 163: 926-927.

Coats, R.R., 1959. Geologic Reconnaissance of Semisopochnoi Island, Western Aleutian Islands, Alaska. U.S. Geol. Surv. Bull. 1028-0: 477-519.

Conrad, W.K., Kay, S.M., and Kay, R.W., 1983. Magma Mixing in the Aleutian Arc: Evidence from Cognate Inclusions and Composite Xenoliths. Jour. Volc. Geotherm. Res., 18: 279-295.

Conrad, W.K., and Kay, R.W., 1984. Ultramafic and Mafic Inclusions from Adak Island: Crystallization History and Implications for the Nature of Primary Magmas and Crustal Evolution in the Aleutian Arc. J. Petrol., 25: 88-125.

Deer, W.A., Howie, R.A., and Zussman, J., 1966. An Introduction to the Rock-Forming Minerals. Longman, Burnt Mill, 528pp.

DeLong, S.E., Fox, P.J., and McDowell, F.W., 1978. Subduction of the Kula Ridge at the Aleutian Trench. Geol. Soc. Am. Bull., 89: 83-95.

DeLong, S.E., Perfit, M.R., McCulloch, M.T., and Ach, J., 1985. Magmatic Evolution of Semisopochnoi Island, Alaska: Trace-Element and Isotopic Constraints. J. Geol., 93: 609-618.

Dungan, M.A., and Rhodes, J.M., 1978. Residual Glasses and Melt Inclusions in Basalts from DSDP Legs 45 and 46: Evidence for Magma Mixing. Contrib. Min. Pet., 67: 417-431.

Eichelberger, J.C., 1975. Origin of Andesite and Dacite: Evidence of Mixing at Glass Mountin in California and at Other Circum-Pacific Volcanoes. Geol. Soc. Am. Bull., 86: 1381-1391.

Garcia, M.O., and Jacobson, S.S., 1979. Crystal Clots, Amphibole Fractionation and the Evolution of Calc-Alkaline Magmas. Contrib. Min. Petrol., 69: 319-327.

Gerlach, D.C., and Grove, T.L., 1982. Petrology of Medicine Lake Highland Volcanics: Characterization of Endmembers of Magma Mixing. Contrib. Min. Pet., 80:147-159.

Gill, J.B., 1981. Orogenic Andesites and Plate Tectonics. Springer-Verlag, Berlin, 390pp.

Grove, T.L., Gerlach, D.C., and Sando, T.W., 1982. Origin of Calc-Alkaline Series Lavas at Medicine Lake Volcano by Fractionation, Assimilation and Mixing. Contrib. Min. Pet., 80: 160-182.

Grove, T.L., Gerlach, D.C., Sando, T.W., and Baker, M.B., 1983. Origin of Calc-Alkaline Series Lavas at Medicine Lake Volcano by Fractionation, Assimilation and Mixing: Corrections and Clarifications. Contrib. Min. Pet., 82: 407-408.

Grove, T.L., and Baker, M.B., 1984. Phase Equilibrium Controls on the Tholeiitic Versus Calc-Alkaline Differentiation Trends. J. Geophys. Res., 89, No. B5: 3253-3274.

Gust, D.A., and Johnson, R.W., 1981. Amphibole-Bearing Inclusions from Boisa Island, Papua New Guinea: Evaluation of the Role of Fractional Crystallization in an Andesitic Volcano. J. Geol., 89: 219-232.

Gust, D.A., and Perfit, M.R., In Press. Phase Relations of a High-Mg Basalt from the Aleutian Island Arc: Implications for Primary Arc Basalts and High-Al Basalts. Contrib. Min. Pet.

Irvine, T.N., and Baragar, W.R.A., 1971. A Guide to the Chemical Classification of the Common Volcanic Rocks. Can. J. Earth Sci. 8: 523-548.

Kay, S.M., Kay, R.W., and Citron, G.P., 1982. Tectonic Controls on Tholeiitic and Calc-Alkaline Magmatism in the Aleutian Arc. J. Geophys. Res., 87, No. B5: 4051-4072.

Kay, S.M., and Kay, R.W., 1985a. Aleutian Tholeiitic and Calc-Alkaline Magma Series I: The Mafic Phenocrysts. Contrib. Min. Pet., 90: 276-290.

Kay, S.M., and Kay, R.W., 1985b. Role of Crystal Cumulates and the Oceanic Crust in the Formation of the Lower Crust of the Aleutian Arc. Geology, 13: 461-464.

Kushiro, I., 1979. Fractional Crystallization of Basaltic Magma. In Yoder, H.S., Jr. (ed.) The Evolution of the Igneous Rocks: Fiftieth Anniversary Perspectives. Princeton University Press, Princeton. 588pp.

MacDonald, G.A., Katsura, T., 1965. Eruption of Lassen Peak, Cascade Range, California, in 1915: Example of Mixed Magmas. Geol. Soc. Am. Bull., 76: 475-482.

Marlow, M.S., Scholl, D.W., Buffington, E.C., Alpha, T.R., 1973. Tectonic History of the Central Aleutian Arc. Geol. Soc. Am. Bull., 84: 1555-1574.

Marsh, B.D., 1976. Some Aleutian Andesites: Their Nature and Source. J. Geol., 84: 27-45.

Marsh, B.D., 1982. The Aleutians. In Thorpe, R.S. (ed.) Andesites: Orogenic Andesites and Related Rocks. John Wiley & Sons, New York, 724pp.

Matsui, Y., and Nishizawa, O., 1974. Iron(II)-Magnesium Exchange Olivine and Calcium-Free Pyroxene Over a Temperature Range 800°C to 1300°C. Bull. Fr. Mineral. Crystallogr., 97: 122-130.

McBirney, A.R., 1980. Mixing and Unmixing of Magmas. J. Volc. Geotherm. Res., 7: 357-371.

McGarvie, D.W., 1984. Torfajokull: A Volcano Dominated by Magma Mixing. Geology, 12: 685-688.

Miyashiro, A., 1975a. Island Arc Volcanic Rock Series: A Critical Review. Petrologie, t. I, No. 3: 177-187.

Miyashiro, A., 1975b. Volcanic Rock Series and Tectonic Setting. An. Rev. Earth Planet. Sci., 3: 251-269.

Myers, J.D., Frost, C.D., and Angevine, C.L., 1986. A Test of a Quartz Eclogite Source for Parental Aleutian Magmas: A Mass Balance Approach. J. Geol., 94: 811-828.

Nye, C.J., and Reid, M.R., 1986. Geochemistry of Primary and Least Fractionated Lavas from Okmok Volcano, Central Aleutians: Implications for Arc Magmagenesis. J. Geophys. Res., 91, B10: 10,271-10,287.

O'Hara, M.J., 1968a. The Bearing of Phase Equilibria Studies in Synthetic and Natural Systems on the Origin and Evolution of Basic and Ultrabasic Rocks. Earth-Sci. Rev., 4: 69-133.

O'Hara, M.J., 1977. Geochemical Evolution During Fractional Crystallization of a Periodically Refilled Magma Chamber. Nature, 266: 503-507.

Pearce, J.A. and Norry, M.J., 1979. Petrogenetic Implications of Ti, Zr, Y and Nb Variation in Volcanic Rocks. Contrib. Min. Pet., 69: 33-47.

Perfit, M.R., Gust, D.A., Bence, A.E., Arculus, R.J., and Taylor, S.R., 1980. Chemical Characteristics of Island-Arc Basalts: Implications for Mantle Sources. Chem. Geol., 30: 227-256.

Ringwood, A.E., 1974. The petrological Evolution of Island Arc Systems. J. Geol. Soc. Lond., 130: 183-204.

Sakuyama, M., 1979. Evidence of Magma Mixing: Petrological Study of Shirouma-Oike Calc-Alkaline Andesite Volcano, Japan. J. Volc. Geotherm. Res., 5: 179-208.

Sakuyama, M., 1981. Petrological Study of the Myoko and Kurohime Volcanoes, Japan: Crystallization Sequence and Evidence for Magma Mixing. J. Petrol., 22, Part 4: 553-583.

Scholl, D.W., Greene, H.G., and Marlow, M.S., 1970. Eocene Age of the Adak 'Paleozoic(?)' Rocks, Aleutian Islands, Alaska. Geol. Soc. Am. Bull., 81: 3583-3592.

Shibata, T., DeLong, S.E., and Walker, D., 1979. Abyssal Thoeiites from the Oceonographer Fracture Zone. Contrib. Min. Petrol., 70: 89-102.

Sparks, S.R.J., Sigurdsson, H., and Wilson, L., 1977. Magma Mixing: A Mechanism for Triggering Acid Explosive Eruptions. Nature, 267: 315-318.

Snyder, G.L., 1959. Geology of Little Sitkin Island, Alaska. U.S. Geol. Surv. Bull., 1028-H: 169-207.

Tatsumi, Y., Sakuyama, M., Fukuyama, H., and Kusiro, I., 1983. Generation of Arc Basalt Magmas and Thermal Structure of the Mantle Wedge in Subduction Zones. J. Geophys. Res., 88, B7: 5815-5825.

Tuttle, O.F., and Bowen, N.L., 1958. Origin of Granite in the light of Experimental Studies in the System $NaAlSi_3O_8$-$KAlSi_3O_8$-SiO_2-H_2O. Geol. Soc. Am. Mem., 74.

Walker, D., Shibata, T., DeLong, S.E., 1979. Abyssal Tholeiites from the Oceanographer Fracture Zone. Contrib. Min. Petrol., 70: 111-125.

Watson, E.B., 1982. Basalt Contamination by Continental Crust: Some Experiments and Models. Contrib. Min. Petrol. 80: 73-87.

Wyllie, P.J., 1979. Petrogenesis and the Physics of the Earth. In Yoder, H.S., Jr. (ed.) The Evolution of the Igneous Rocks: Fiftieth Anniversary Perspectives. Princeton University Press, Princeton. 588pp.

Yoder, H.S., Jr., 1973. Contemporaneous Basaltic and Rhyolitic Magmas. Am. Min., 58: 153-171.

APPENDIX I

BULK ROCK MAJOR OXIDE CHEMISTRY

AND

NORMATIVE MINERALOGY

FROM SNYDER (1959)

BULK ROCK MAJOR OXIDE CHEMISTRY

	491	500	492	493	494	496
SiO2	52.74	55.02	55.35	55.37	58.47	58.63
TiO2	0.57	0.85	0.89	0.87	0.77	0.75
Al2O3	11.99	17.91	17.72	18.02	16.91	17.04
Fe2O3	1.90	4.45	3.04	2.91	5.71	2.60
FeO	6.72	4.23	5.45	5.53	1.89	4.50
MnO	0.17	0.15	0.17	0.16	0.15	0.15
MgO	11.02	3.92	4.03	4.24	3.37	3.19
CaO	12.49	8.58	8.77	8.70	7.32	7.15
Na2O	1.78	3.11	3.28	3.03	3.40	3.37
K2O	0.64	1.09	1.00	0.91	1.23	1.33
P2O5	0.11	0.15	0.17	0.16	0.19	0.15
CO2	0.00	0.00	0.00	0.01	0.01	0.01
H2O-	0.01	0.05	0.07	0.06	0.17	0.23
H2O+	0.09	0.41	0.15	0.05	0.37	0.71
TOTAL	100.23	99.92	100.09	100.02	99.96	99.81

NORMATIVE MINERALOGY

Q	0.84	9.66	7.62	8.64	15.48	13.56
or	3.34	6.67	6.12	5.56	7.23	7.78
ab	15.20	26.20	27.77	25.68	28.82	28.30
an	23.07	31.41	30.58	32.53	27.24	27.52
wo	15.89	4.41	4.99	4.06	3.36	3.02
en	10.70	3.10	2.90	2.40	2.90	1.70
fs	3.96	0.92	1.85	1.45	0.00	1.19
en	16.90	6.70	7.20	8.20	5.50	6.30
fs	6.07	1.98	4.49	5.15	0.00	3.96
mt	2.78	6.50	4.41	4.18	4.18	3.71
il	1.06	1.67	1.67	1.67	1.52	1.52
ap	0.34	0.34	0.34	0.34	0.34	0.34
TOTAL	100.15	99.56	99.94	99.86	99.45*	98.90

BULK ROCK MAJOR OXIDE CHEMISTRY (continued)

	497	499	501	495	489
SiO2	59.94	60.36	64.74	68.79	69.43
TiO2	0.77	0.72	0.53	0.38	0.33
Al2O3	16.79	16.93	16.25	15.00	15.17
Fe2O3	2.25	2.53	1.72	1.52	1.34
FeO	4.77	3.42	3.17	2.27	1.99
MnO	0.15	0.13	0.13	0.12	0.11
MgO	3.07	2.70	1.97	1.15	0.94
CaO	6.89	6.08	5.07	3.44	3.41
Na2O	3.49	3.72	4.13	4.30	4.46
K2O	1.46	1.42	1.71	2.05	2.00
P2O5	0.15	0.16	0.15	0.11	0.13
CO2	0.00	0.01	0.00	0.01	0.00
H2O-	0.05	0.17	0.03	0.08	0.00
H2O+	0.17	1.39	0.31	0.64	0.52
TOTAL	99.95	99.74	99.91	99.86	99.83

NORMATIVE MINERALOGY

Q	13.98	16.02	19.80	26.28	26.64
or	8.90	8.34	10.01	12.23	11.68
ab	29.34	31.44	35.11	36.15	37.73
an	25.85	25.30	20.85	15.57	15.57
wo	3.13	1.74	1.39	0.35	0.23
en	1.70	1.10	0.80	0.20	0.10
fs	1.32	0.53	0.53	0.13	0.13
en	6.00	5.70	4.10	2.70	2.30
fs	4.49	2.64	3.17	2.38	2.11
mt	3.25	3.71	2.55	2.09	1.86
il	1.52	1.37	1.06	0.76	0.61
ap	0.34	0.34	0.34	0.34	0.34
TOTAL	99.82	98.23	99.71	99.18	99.30

APPENDIX II

PETROGRAPHY OF THE INDIVIDUAL SAMPLES

(PRESENT STUDY)

WITH PHOTOGRAPHS

BASALT

SAMPLE No. 491

Color and Texture

Light reddish-grey. Porphyritic and holocrystalline texture.

Phenocryst Phases

Plagioclase - subhedral to euhedral elongate sections up to 1.5 mm long. Highly twinned, and most show complex zonation as well. Both inclusion-rich and inclusion-free crystals occur, with apatite, glass, magnetite and possible clinopyroxene as the included phases. A few scattered grains have extremely fritted interiors with thin, clear rims.

Clinopyroxene - large megacrysts occurring in crystal aggregates that may reach a size of 5 to 6 mm. Most are subhedral, and are complexly zoned and twinned. Some crystals show exsolution of orthopyroxene. Rings of inclusions paralleling the crystal outlines are common. Included phases are apatite and glass.

Olivine - anhedral to subhedral grains scattered throughout the sample are usually no larger than about 0.5 mm. Some crystals show a brownish coloration along cracks. Magnetite inclusions are common.

Magnetite - small anhedrons up to 0.25 mm. A brownish-red coloration surrounds many of these grains. Some magnetite-ilmenite exsolution occurs in these

crystals.

Groundmass

Plagioclase is the dominant groundmass phase along with significant quantities of clinopyroxene. Olivine, magnetite, pigeonite and apatite also occur.

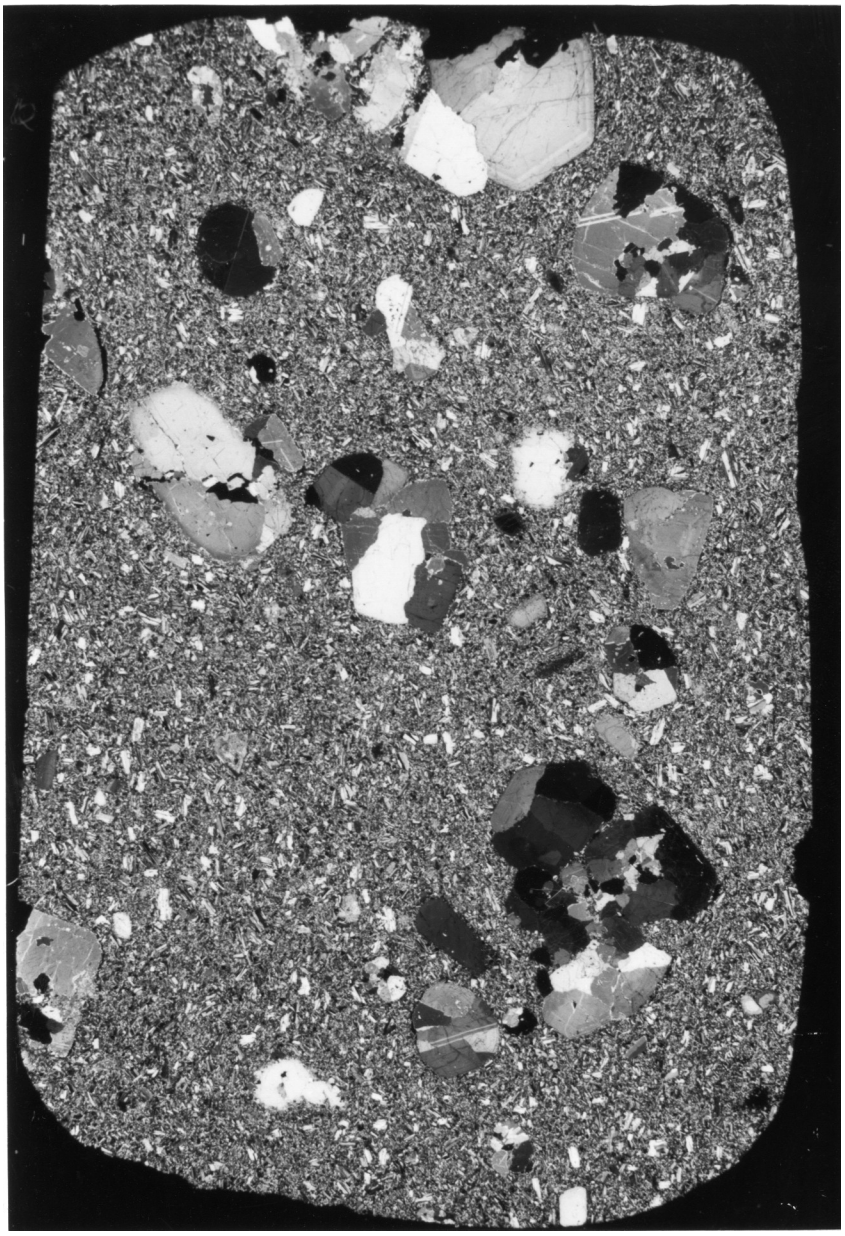

Figure A-1 Basalt sample 491. Note large clinopyroxene megacrysts.

ANDESITE

SAMPLE No. 500

Color and Texture

Medium-dark grey, intersertal texture.

Phenocryst Phases

Plagioclase - mostly small laths up to 1 to 2 mm long, however some larger crystals up to 3 to 4 mm long also occur. Twinning and zoning are common in both types of crystals, but appear to be more complex in the larger ones. Inclusions are common in both, and may be apatite, magnetite, glass and, possibly, orthopyroxene. The larger crystals generally have fritted cores, while the smaller ones are fairly clear.

Hornblende - subhedral to euhedral cross-sections or laths up to 2 to 3 mm long. These crystals are pleochroic from dark to light brown. A few crystals have hollow cores, and all contain inclusions. These may be magnetite or small, clear, colorless needles and squares of some unidentified minerals, possibly apatite and plagioclase.

Clinopyroxene - euhedral to subhedral grains up to 2 to 2.5 mm long. Some grains are zoned and others are twinned. Some cross-section show exsolution of orthopyroxene. Inclusions of apatite, magnetite, orthopyroxene and plagioclase are common.

Orthopyroxene - euhedral to subhedral crystals up to 2 mm long, together with needle-like crystals having length:width ratios of up to 40:1. Crystals may show a brownish discoloration along cracks, and some exhibit exsolution of clinopyroxene. Plagioclase, magnetite and apatite are found as inclusions.

Magnetite - small anhedrons up to 0.25 mm and needles similar in size and length:width ratio to the orthopyroxene. Limited magnetite-ilmenite exsolution occurs as well.

Groundmass

Scattered small plagioclase crystals and orthopyroxene needles along with a small amount of magnetite are set in a clear, brownish glass. In some small patches the glass appears to be slightly devitrified. Cavities within the sample are common.

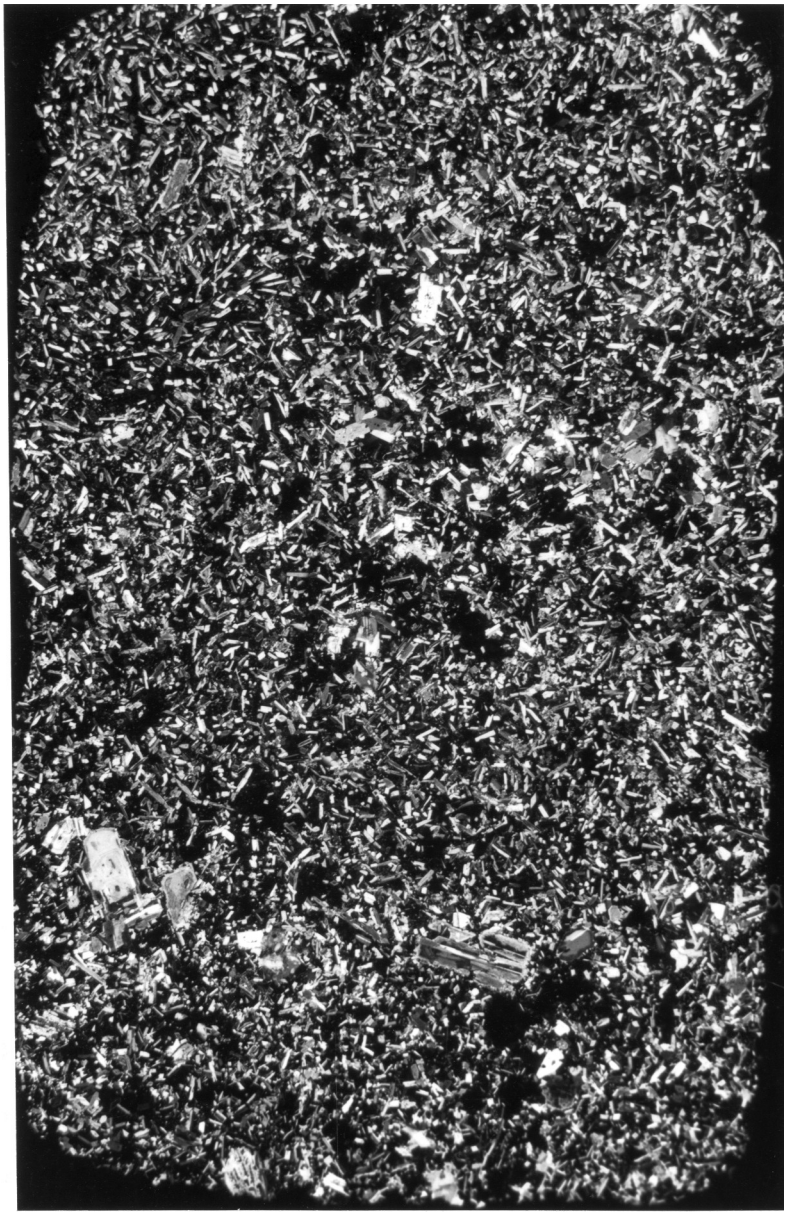

Figure A-2 Andesite sample No. 500.

ANDESITE

SAMPLE No. 492

Color and Texture

Light grey with porphyritic hypocrystalline or intersertal texture.

Phenocryst Phases

Plagioclase - subhedral to euhedral crystals up to 3 mm long, with complex twinning and zoning. Some crystals are neither twinned nor zoned, but these crystals are few. Resorption features are seen in some grains, and many have rings of inclusions that parallel the crystal outline. Crystals with inclusion-rich cores and thin, clear rims also occur. Inclusions are apatite and glass. Some fragmental crystals were also noted.

Clinopyroxene - subhedral crystals up to 2 mm long commonly show twinning. Hourglass zonation was noted in at least three crystals. Partial to almost complete resorption of some crystals was seen. Inclusions of apatite and glass are fairly common.

Olivine - small crystals up to 1 mm long are subhedral and contain very few inclusions. No zonation of these grains was noted.

Magnetite - found as anhedrons and subhedral phenocrysts and microphenocrysts up to about 0.25 mm. Some fine scale magnetite-ilmenite exsolution may occur.

Orthopyroxene - found as cores to several clinopyroxene grains and also as solitary crystals. Grains are subhedral and up to 1.5 mm long. Inclusions are apatite, magnetite and glass.

Groundmass

The groundmass consists of plagioclase needles and magnetite dust, along with minor amounts of clinopyroxene and orthopyroxene. Possible flow structures may be present.

Other Observations

Scattered throughout the thin section are glomerocrysts that consist of plagioclase, clinopyroxene, olivine and magnetite grains. These crystals appear to be identical to those found within the rest of the slide.

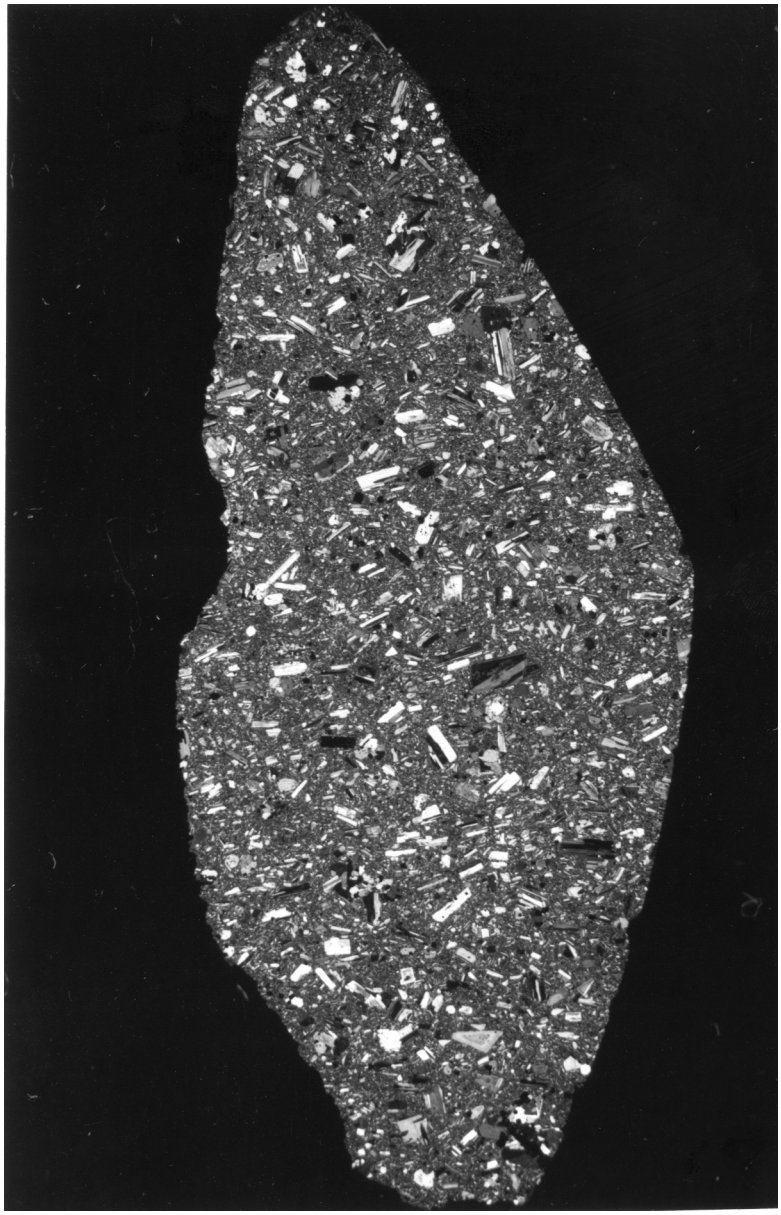

Figure A-3 Andesite sample No. 492.

ANDESITE

SAMPLE No. 493

Color and Texture

Light grey. Porphyritic and holocrystalline.

Phenocryst Phases

Plagioclase - euhedral to subhedral crystals up to about 2 to 3 mm long. Most grains are complexly twinned and zoned. Although clear grains do occur, most have a fritted interior with a clear rim. Many grains show resorption features. Clear grains are inclusion-rich. Glass, apatite, clinopyroxene, magnetite and, possibly, orthopyroxene are the included phases.

Clinopyroxene - subhedral grains up to about 1 mm long ar usually twinned and zoned. Some crystals are intergrown with orthopyroxene, and many are partially resorbed. Inclusions of apatite, orthopyroxene, magnetite, plagioclase and glass are common.

Orthopyroxene - euhedral to subhedral grains up to 1 mm long. some grains have resorbed crystal margins, while others show exsolution of clinopyroxene. Magnetite, plagioclase and glass are contained as inclusions.

Magnetite - anhedral phenocrysts up to 0.7 mm long together with smaller anhedrons show magnetite-ilmenite exsolution in reflected light.

Olivine - rare anhedral grains are up to 0.4 mm long and show a brownish coloration along cracks. Some grains contain unidentifiable inclusions.

Groundmass

The groundmass is composed almost entirely of plagioclase and orthopyroxene needles, along with minor clinopyroxene, olivine and magnetite dust. Some apatite and glass may occur as well.

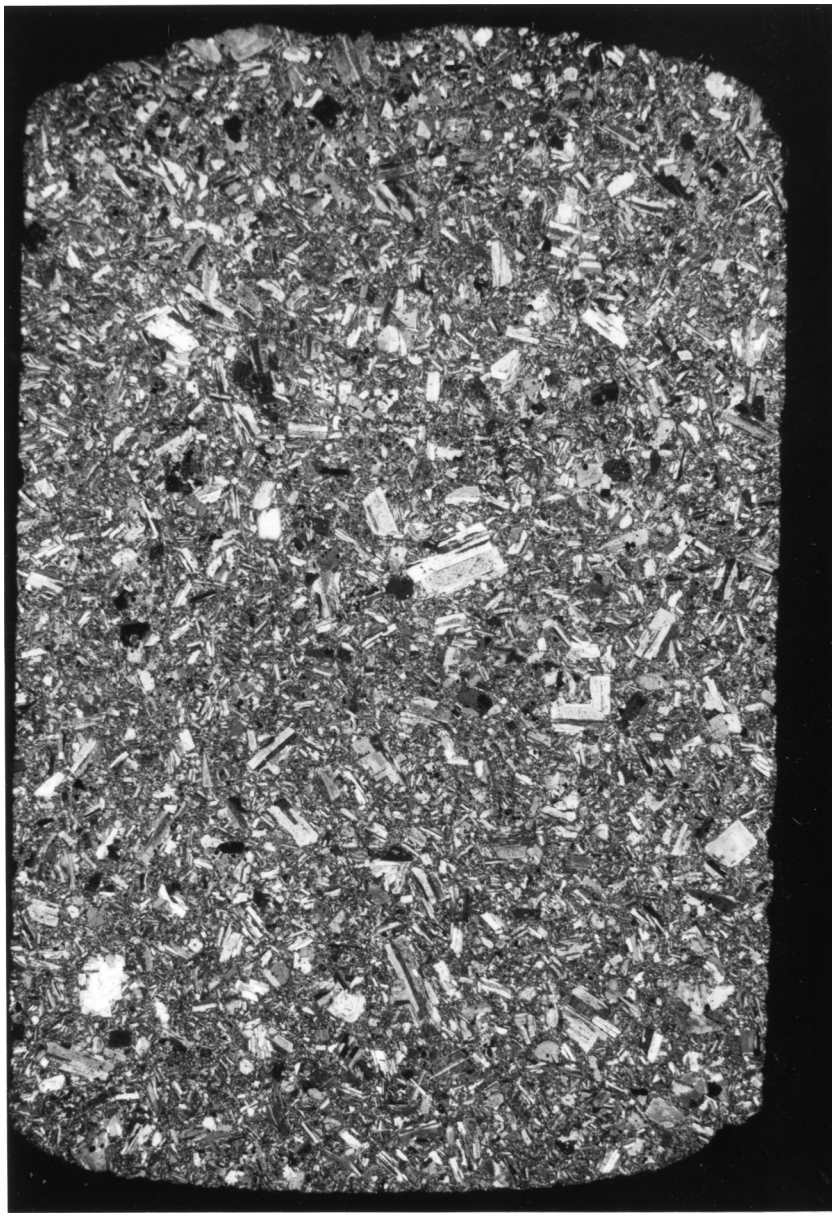

Figure A-4 Andesite sample No. 493.

ANDESITE

SAMPLE No. 494

Color and Texture

Rock has a brownish-red color. Porphyritic and holocrystalline.

Phenocryst Phases

Plagioclase - subhedral to euhedral crystals up to 3 mm long have complex twinning and zoning. Two distinct populations of crystals occur. One consists of clear grains with inclusions of apatite, glass, pyroxene and magnetite. The other contains crystals that have extremely fritted interiors with thin, clear rims. This rim may or may not be optically continuous with the rest of the crystal. Some of these grains have no clear rim at all.

Clinopyroxene - subhedral to euhedral, up to 1.5 mm long. Twinning is common, as are inclusions of apatite, magnetite, plagioclase and glass. Clinopyroxene rims orthopyroxene on three crystals, and orthopyroxene exsolution is seen in several grains. One very large clinopyroxene grain has been almost totally replaced by opaques and plagioclase. The remaining pyroxene suggests an original size of about 6 mm.

Orthopyroxene - subhedral to euhedral with crystals reaching a length of up to 0.75 mm. Limited exsolution of clinopyroxene occurs in some grains.

Plagioclase, apatite, glass and magnetite are found as inclusions.

Magnetite - anhedral phenocrysts and microphenocrysts up to 0.5 mm in size. Well developed magnetite-ilmenite exsolution can be seen in many grains.

Tridymite - small, clear crystals with very low relief occur throughout the sample. May be considered part of the groundmass.

Oxyhornblende - pleochroic tan to deep red-brown crystals that are anhedral to subhedral and up to 0.7 mm long. Inclusions occur, but identification is difficult. Some opaque replacement occurs on crystal margins.

Groundmass

Small plagioclase laths with some minor orthopyroxene, clinopyroxene, magnetite and tridymite comprise the bulk of the groundmass. The reddish color of this sample is probably derived from the large amount of hematite dust that is also contained within the groundmass.

Other Observations

Xenoliths occur in this sample and contain plagioclase, orthopyroxene, clinopyroxene and magnetite. The plagioclase grains appear to be very inclusion-free, as compared to crystals found in the rest of the sample. There is very little hematite dust in these xenoliths. All crystals contained within these areas are fairly small.

A thin "dike" of clear, colorless glass cuts across

one corner of the section. This area contains almost no hematite, but it does contain a much higher proportion of oxyhornblende. In addition, a significant quantity of rounded, partially resorbed quartz occurs in this portion of the sample. Phenocryst phases are plagioclase, orthopyroxene and oxyhornblende. Small amounts of tridymite occur on the margins of this area, but they are probably components of the groundmass of the rest of the slide. "Xenoliths" of rock typical of the rest of the sample are found within this glassy region, possibly ripped up when the "dike" intruded.

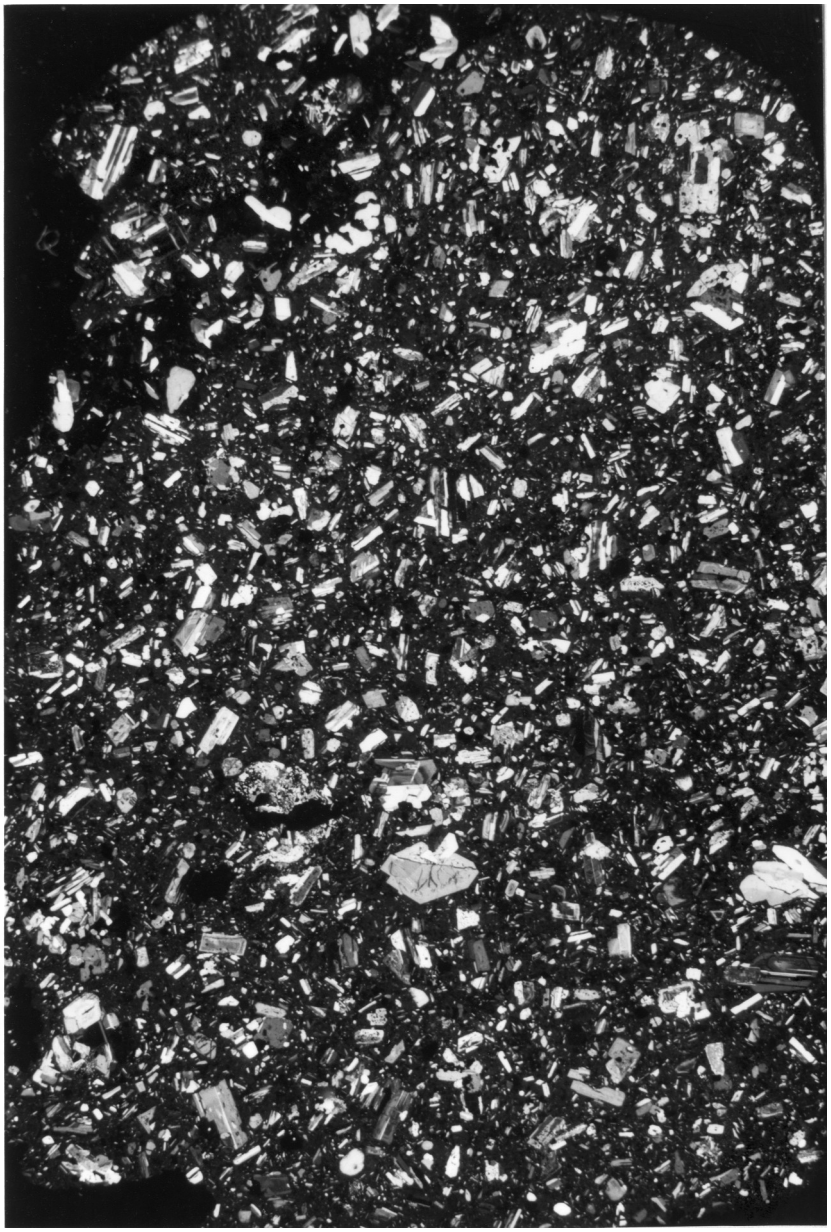

Figure A-5 Andesite sample No. 494. Thin "dike" cuts across lower right corner of photograph.

ANDESITE

SAMPLE No. 496

Color and Texture

Grey to brownish-grey with porphyritic, hypocrystalline texture. Vesicular.

Phenocryst Phases

Plagioclase - complexly twinned and zoned, euhedral to subhedral crystals up to 4 mm long. Rare small, perfectly euhedral crystals show no zoning, twinning or inclusions. The rest of the crystals commonly have fritted cores, or rings of inclusions paralleling the crystal margins. Inclusions are apatite and glass.

Clinopyroxene - euhedral to anhedral grains up to 4 mm long. Some crystals show twinning, and all are pleochroic from pale pink to pale green. inclusions are glass, plagioclase, orthopyroxene and apatite. Some crystals are slightly resorbed. Some grains show exsolution of orthopyroxene, while in some cases clinopyroxene is found as a rim on orthopyroxene grains.

Orthopyroxene - grains are smaller than clinopyroxene, up to 2 to 3 mm at most. They are subhedral to euhedral and are faintly pleochroic from pale pink to pale green. Inclusions are common, and a few of the grains are partially resorbed.

Magnetite - anhedral to euhedral phenocrysts and

microphenocrysts up to 1 mm in length. Very fine scale magnetite-ilmenite exsolution may occur.

Oxyhornblende - occurs as two xenocrysts, both anhedral and both showing resorption features. The crystals are both about 4 mm long and show strong tan to deep brown pleochroism. One grain seems to have been partially replaced along its rim by plagioclase, magnetite, orthopyroxene and clinopyroxene. The other grain contains plagioclase inclusions and is in much better shape.

Groundmass

The groundmass consists of brown glass charged with vesicles, and containing significant quantities of feldspar microlites, opaque grains, orthopyroxene and clinopyroxene.

Other Observations

Crystal clots occur in this sample. They are monominerallic, consisting of plagioclase, and in some cases, a clear brown glass. These plagioclase crystals appear to be optically identical to those found within the rest of the sample.

In addition to the crystal clots two distinct types of xenolith occur, here named type 1 and type 2. Type 1 xenoliths contain small euhedral zoned and twinned plagioclase crystals that are fairly clear and inclusion-free. In addition, orthopyroxene and

clinopyroxene grains are also contained within these xenoliths, and all crystals are set in a clear, brown glass.

Type 2 xenoliths contain larger plagioclase crystals, equal in size to the phenocrysts of the host rock. these crystals are highly zoned and twinned, and are very inclusion-rich. The inclusions appear to be mostly glass. Clinopyroxene grains found in these xenoliths are also much larger than those found within the type 1 xenoliths. Opaques and orthopyroxene grains are also contained in these areas. A very small amount of clear brown glass is contained in some.

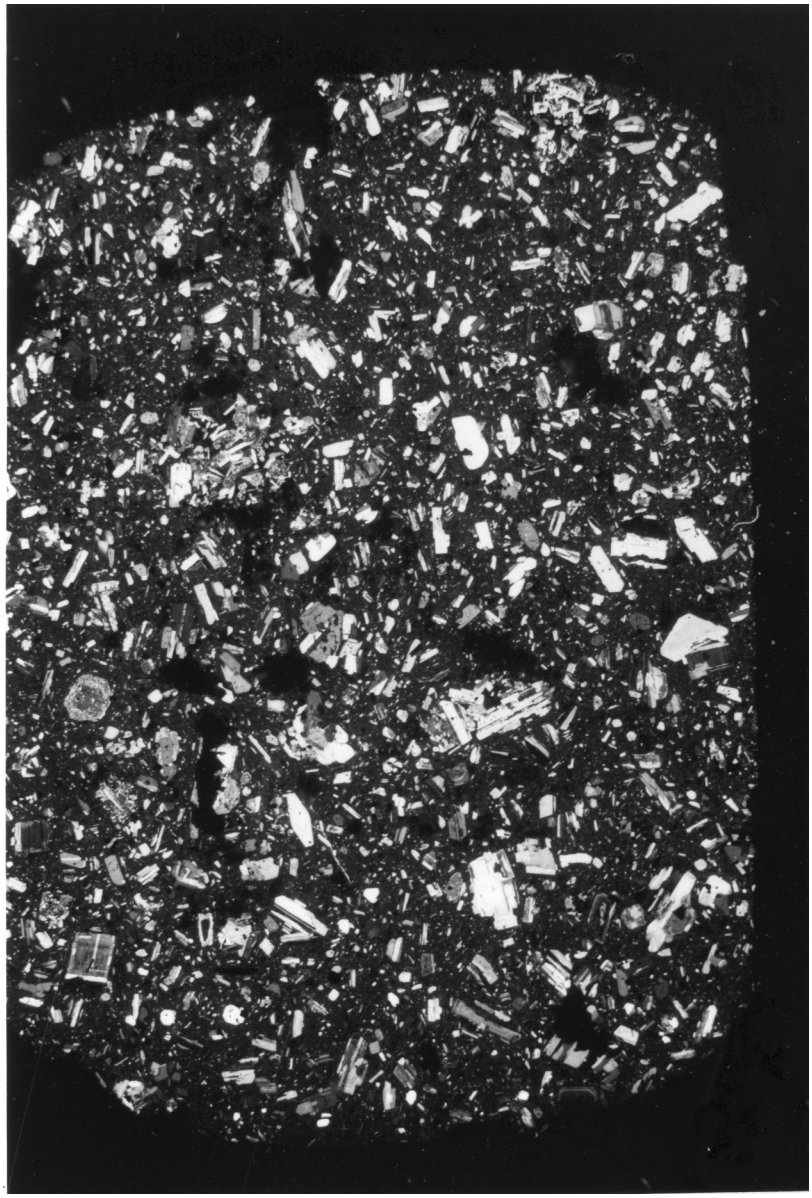

Figure A-6 Andesite sample No. 496. Note xenolith just above and left of center. Large square resorbed crystal at left center is one of two hornblende crystals found in this section.

ANDESITE

SAMPLE No. 497

Color and Texture

Dark grey, porphyritic and hypocrystalline.

Phenocryst Phases

Plagioclase - complexly twinned and zoned, euhedral to subhedral grains up to about 3 mm long. Common inclusions are apatite, glass and magnetite. These are found either concentrated in the crystal cores, or as rings of inclusions following the crystal outlines. Some crystals are partially resorbed.

Clinopyroxene - grains are subhedral to euhedral and up to 2 mm long. Pleochroic from pale pink to pale green. Twinning and zoning common. Inclusions are apatite, glass and possible zircon. Some grains show resorption features.

Orthopyroxene - pale pink to pale green subhedral to euhedral crystals up to about 1.5 mm long. inclusions of apatite and magnetite are present. A few crystals are almost totally resorbed. A few grains have clinopyroxene rims, while some clinopyroxene grains have orthopyroxene rims.

Magnetite - anhedral phenocrysts and microphenocrysts up to 0.4 mm long. slight magnetite-ilmenite exsolution may occur.

Olivine - rare anhedral crystals contain no inclusions, and

commonly show resorption features. Crystals may be up to 1 mm.

Groundmass

The groundmass consists of a brownish glass set with plagioclase microlites and magnetite. In addition, small needles of a clear, colorless mineral with higher relief are also present. These may be orthopyroxene, but identification is difficult. Some of these needles appear to have a greenish tint.

Other Observations

A few scattered crystal clots consisting of plagioclase, magnetite, clinopyroxene and orthopyroxene are found in this sample. The crystals in these clots are optically identical to those in the rest of the sample.

In addition to these clots, there are a few scattered fine grained xenoliths containing plagioclase, clinopyroxene, orthopyroxene and magnetite. At least one rounded quartz grain occurs in this sample, and it is most likely of xenocrystic origin.

Figure A-7 Andesite sample No. 497. Single rounded quartz crystal is located just below and right of center.

ANDESITE

SAMPLE No. 499

Color and Texture

Medium grey, porphyritic and hypocrystalline. Slight flow foliation in the groundmass.

Phenocryst Phases

Plagioclase - most crystals are subhedral to euhedral and up to about 2.5 mm long, with zoning and twinning. These crystals are fairly clear, although inclusions of apatite, orthopyroxene needles, glass and magnetite do occur. Some large grains with severly fritted interiors occur in addition to scattered partially resorbed grains.

Clinopyroxene - subhedral to euhedral crystals up to about 2 mm long are zoned and twinned. Exsolution of orthopyroxene is also seen in some grains. inclusions of apatite, plagioclase, magnetite and, possibly, zircon are also common. Some crystals contain inclusions of glass as well.

Orthopyroxene - subhedral to euhedral grains about the same size as the clinopyroxene. These crystals exhibit a pale pink to pale green pleochroism. Exsolution of clinopyroxene is seen in a few grains, and others have a brownish coloration along cracks. Common inclusions are apatite, plagioclase, magnetite and glass.

Magnetite - anhedral to subhedral phenocrysts and

microphenocrysts up to 0.5 mm long contain small sulphide inclusions. Magnetie-ilmenite exsolution occurs on a very limited basis, and is very fine when it does occur.

Groundmass

A clear, brownish glass loaded with vesicles and magnetite dust makes up the groundmass of this sample. Occasional needles of orthopyroxene are found scattered throughout. A slight flow foliation is also seen.

Other Observations

Crystal clots are scattered throughout this sample and are composed of plagioclase, orthopyroxene, clinopyroxene and magnetite. As with the other samples, crystals in these clots appear to have the same optical characteristics as phenocrysts within the rest of the section.

A few clinopyroxene grains seem to have been almost totally replaced by orthopyroxene, magnetite and plagioclase. These grains occur together in a small area of the section, no bigger than a few millimeters square.

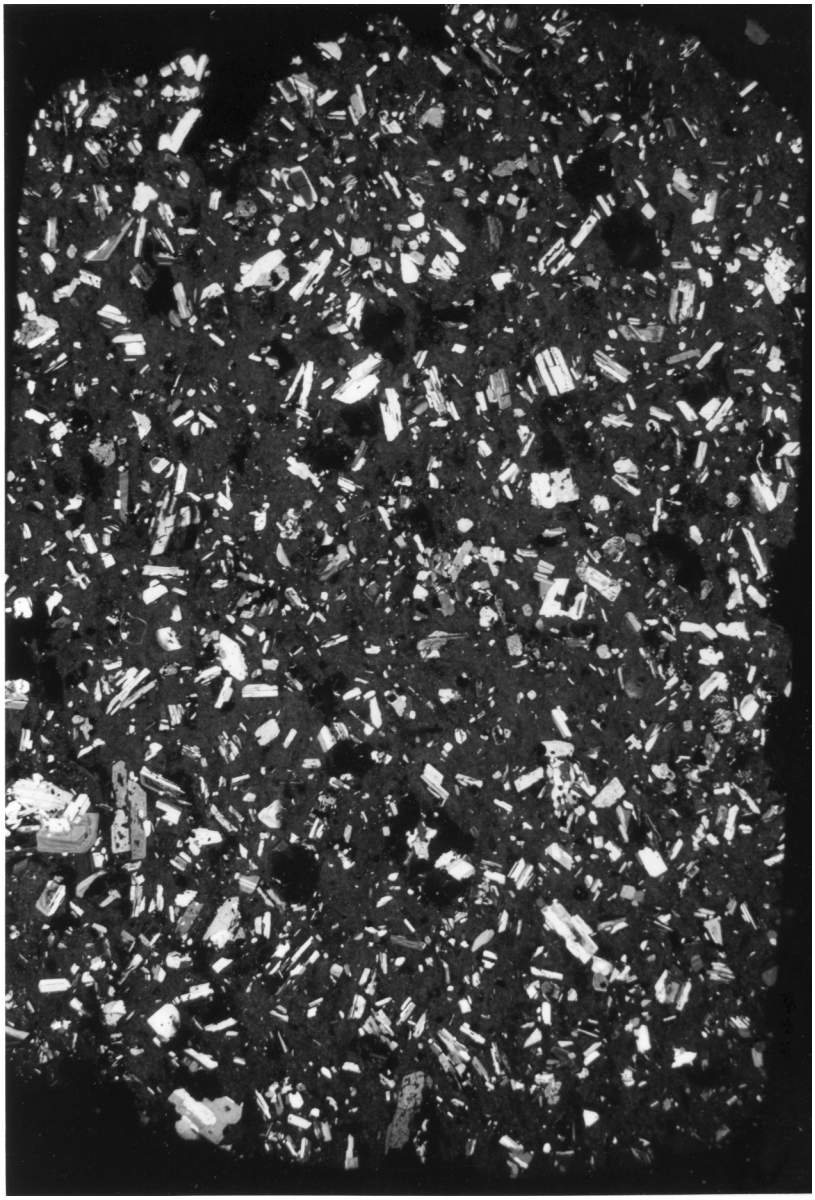

Figure A-8 Andesite sample No. 499.

DACITE

SAMPLE No. 501

Color and Texture

Light grey. Porphyritic and hypocrystalline.

Phenocryst Phases

Plagioclase - euhedral to subhedral crystals that range in size from about 0.5 to 2 mm. Complex twinning and zoning is common, as are inclusions of apatite and glass. Partial resorption of some crystals is noted.

Orthopyroxene - pale green, euhedral crystals up to 1.5 mm long. Apatite and plagioclase inclusions are abundant. A few are partially resorbed, and a few skeletal crystals were seen.

Clinopyroxene - anhedral to subhedral grains appear to be colorless. Grains may be up to 1.5 mm long and are usually twinned and zoned. Most crystals show resorption features, and all are inclusion-rich.

Magnetite - anhedral to euhedral phenocrysts and microphenocrysts up to about 0.5 mm. May show faint magnetite-ilmenite exsolution.

Oxyhornblende - small euhedral crystals up to about 0.75 mm long. Some anhedral and subhedral crystals are seen as well. All crystals show dark brown to light tan pleochroism. Inclusions of a clear mineral, probably apatite, occur in most grains.

Tridymite - very low birefringence and relief, scattered

throughout the section, but best seen near cavities and around the edges.

Groundmass

Feldspar microlites, magnetite and orthopyroxene are the major mineral phases of the groundmass. Minor tridymite also occurs. All of these minerals are set in a semi-trachytic matrix.

Other Observations

Crystal clots occur scattered throughout the section. Mineral phases in these clots are plagioclase, orthopyroxene, clinopyroxene and magnetite. No hornblende was seen in any of the clots. Crystals in these clots have the same optical characteristics as the crystals found throughout the rest of the sample.

Xenoliths are also found scattered throughout the section as inclusions of a fairly coarse rock. Mineral composition of these xenoliths appears to be feldspar laths and highly corroded clinopyroxene with some minor orthopyroxene and magnetite, brown glass, devitrified glass and tridymite. Small inclusions of apatite and zircon occur in some of these phases. The crystals in these xenoliths are all set in a clear brownish glass. They are easily distinguished from the scattered crystal clots.

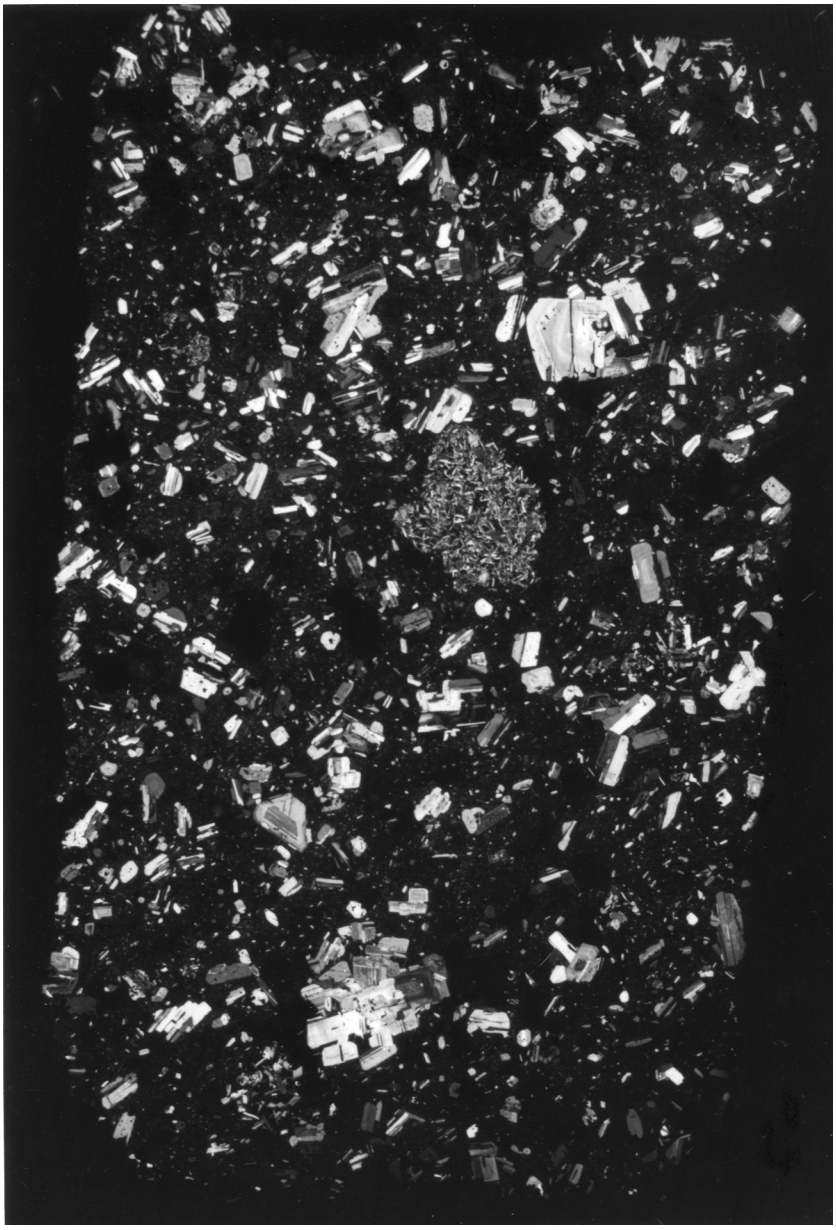

Figure A-9 Dacite sample No. 501. Note large xenolith in center of photograph and crystal clot at bottom center.

RHYODACITE

SAMPLE No. 495

Color and Texture

Light grey porphyritic and vesicular with a semi-trachytic texture.

Phenocryst Phases

Plagioclase - anhedral to subhedral crystals with complex twinning and zoning, up to 2 mm long. Some crystals are highly resorbed, and all contain abundant inclusions which may form rings paralleling the crystal outlines. Included phases are apatite, orthopyroxene, magnetite, hornblende and glass. Intergrown crystals are common.

Orthopyroxene - anhedral to euhedral inclusion-rich crystals up to 1.5 mm long. Apatite, magnetite and a little plagioclase are the included phases. Some crystals are slightly resorbed.

Oxyhornblende - dark brown to olive green to tan pleochroic crystals are anhedral to euhedral and up to 1 mm long. Some crystals are slightly resorbed. Inclusions are common, but identification is difficult.

Quartz - large anhedral fractured phenocrysts are a few mm in diameter. Most of these crystals are rounded, but one or two angular grains occur. Glass and apatite appear to be the included phases.

Magnetite - anhedral phenocrysts and microphenocrysts may reach a size of 0.75 mm. Slight magnetite-ilmenite exsolution may occur.

Clinopyroxene - large anhedral to euhedral phenocrysts up to 1.5 mm long, and smaller (0.5 mm) anhedral microphenocrysts. The larger grains are usually found alone, while the smaller ones usually occur together with orthopyroxene and hornblende. Both types contain inclusions of glass, apatite and magnetite, and both are twinned and zoned.

Groundmass

Mostly comprised of clear glass and many vesicles, but also contains feldspar microlites, needles of orthopyroxene, magnetite and quartz. In addition, apatite and zircon may be found in the groundmass, but identification of these phases, especially the latter, is difficult.

Other Observations

Crystal clots consisting of plagioclase, orthopyroxene, clinopyroxene, hornblende and magnetite occur throughout the section. In addition, clots that contain only plagioclase and magnetite also occur. The crystals found in both types of clots are optically indistinguishable from the crystals found within the rest of the section.

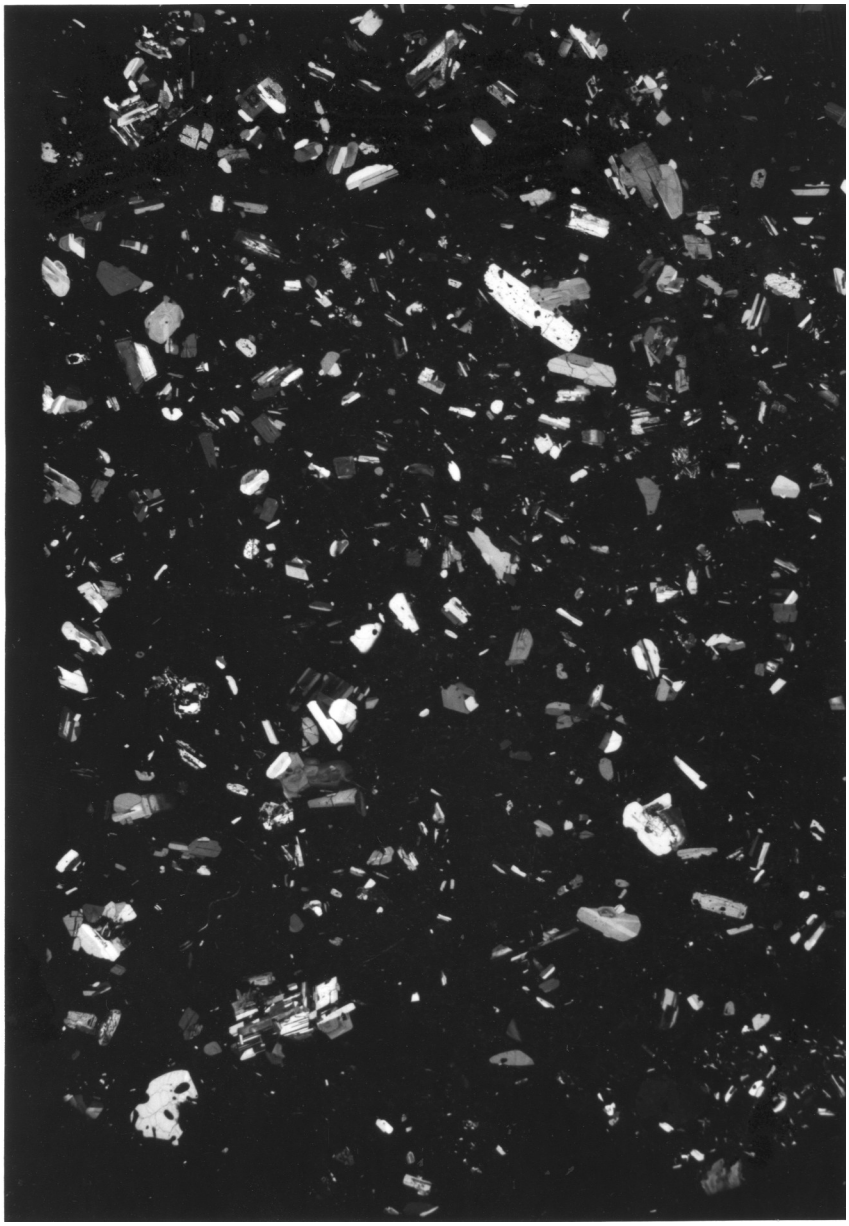

Figure A-10 Rhyodacite sample No. 495.

RHYODACITE

SAMPLE No. 489

Color and Texture

Light-medium grey. Porphyritic and highly vesicular, hypocrystalline.

Phenocryst Phases

Plagioclase - large subhedral crystals up to 4 mm long are clear, zoned and twinned. Inclusions, though not abundant, do occur in almost all of the grains. Apatite, orthopyroxene needles, magnetite and glass are the most abundant phases. Inclusions may be found as rings paralleling the crystal outlines, or, in a few cases, may be found in dusty, inclusion-rich cores. The glass included in the plagioclase appears to be pink.

Hornblende - anhedral to subhedral crystals up to 1 to 1.5 mm long show olive-green to brown, tan to dark brown, brown to brownish-red, and brown to very dark brown/black pleochroism. A few crystals have rims that are more pleochroic than their cores. Inclusions present are orthopyroxene, plagioclase and magnetite.

Orthopyroxene - commonly subhedral to euhedral and up to 2 mm long. It may also occur as needles with length:width ratios of 10:1 or so. Many of the crystals contain inclusions of apatite, magnetite, plagioclase and glass. Some crystals show

interference colors that are too high, but other features confirm these grains as orthopyroxene.

Magnetite - small anhedral to euhedral grains up to 0.5 mm in size. Very fine scale magnetite-ilmenite exsolution was noted.

Quartz - large crystals up to 2 to 3 mm in diameter are anhedral with conchoidal fracture. Most crystals are fairly inclusion-free, though a clear, pinkish glass is contained within many.

Groundmass

Very glassy and vesicular groundmass contains small orthopyroxene rods and magnetite granules. Some areas of the section show flow foliation, while in other areas this feature is absent. Small feldspar and hornblende grains are also found imbedded in the glass.

Other Observations

Crystal clots of plagioclase, orthopyroxene, hornblende, magnetite and quartz occur throughout the section. These crystal clots contain minerals that are optically identical to those contained within the rest of the sample. In addition, plagioclase is found in crystal clots by itself. The crystals in these monominerallic clots are also optically identical to the crystals within the rest of the sample.

One very large xenolith, about 1 cm in diameter, is contained within the sample. It is composed of two halves

with differing features. One half is light brown ad very sparsely porphyritic, while the other is a much darker brown and heavily porphyritic. The dividing line between the two sides is sharp.

The sparsely porphyritic side contains phenocrysts of plagioclase, clinopyroxene, orthopyroxene and magnetite. All of the non-opaque phases show some signs of resorption, and are fairly inclusion-rich. Apatite, orthopyroxene, magnetite and glass are the included phases. The plagioclase and clinopyroxene are both zoned and twinned.

The highly porphyritic side contains the same mineral phases as the other side, but in much greater quantities. In addition, the clinopyroxene:plagioclase ratio appears to be much higher. The pyroxenes are both pleochroic from pale pink to pale green, and inclusions of apatite, glass and magnetite are common. A few of the opaque grains in this half show well defined magnetite-ilmenite exsolution.

The groundmass on both sides of this composite xenolith is composed of a clear, brownish glass with magnetite, plagioclase, and both of the pyroxenes.

A few smaller xenoliths are found throughout the section. These bodies appear to be very similar to the heavily porphyritic side of the composite xenolith in both mineral composition and texture.

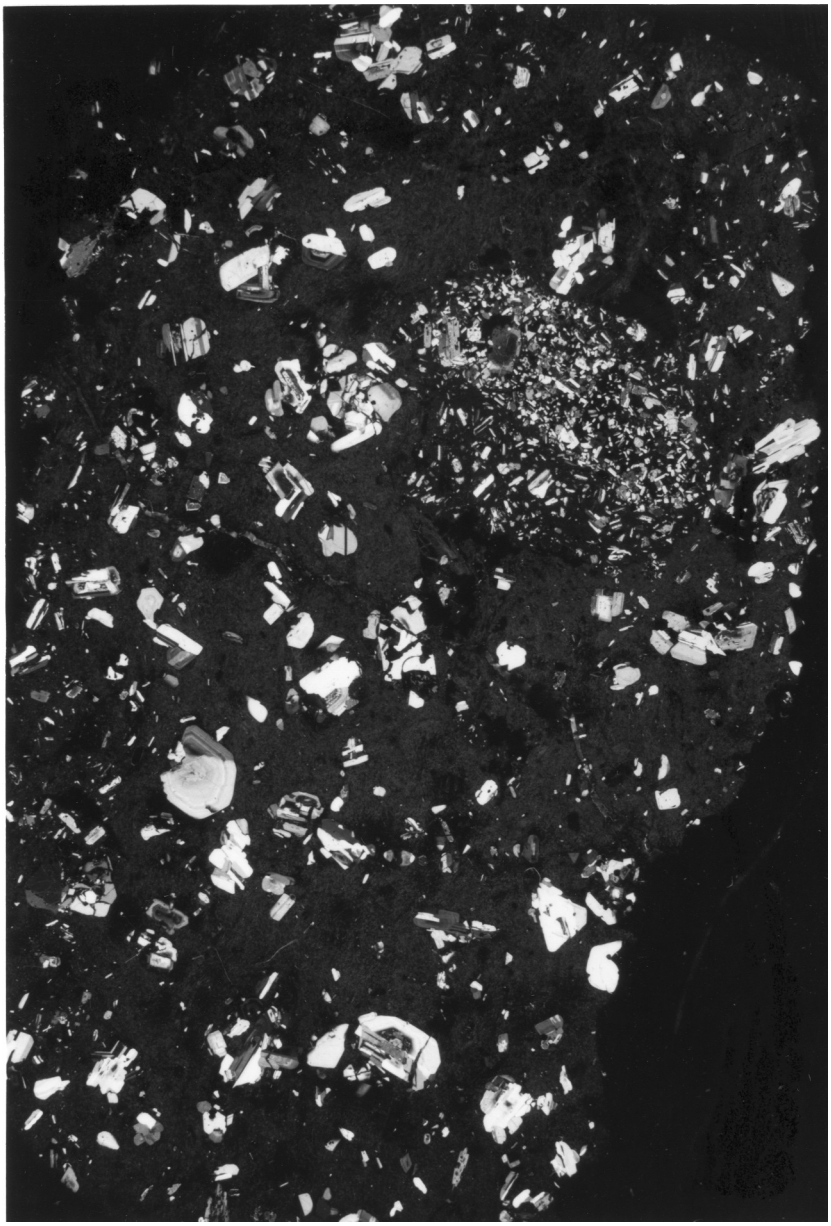

Figure A-11 Rhyodacite sample No. 489. Large composite xenolith is located above and to the right of center.

APPENDIX III

GROVE AND WALKER DIAGRAMS

THEORY AND EQUATIONS

Both the Grove and Walker diagrams discussed in chapter 5 and pictured in figures 5-1 and 5-2 are modifications of O'Hara's (1968a) so called CMAS diagram. The CMAS diagram was an attempt to project rock compositions that occur within the tetrahedron Quartz-Olivine-Diopside-Plagioclase onto the two-dimensional ternary defined by the points for enstatite, diopside and a point lying halfway between olivine and plagioclase. O'Hara (1968a) termed this the high pressure eclogite thermal divide plane. A set of formulae were developed to obtain this conversion and these formulae were based on the molecular proportions of the various major oxides.

Walker et al. (1979) simplified this system somewhat by developing a set of formulae to project points occurring in the tetrahedron Quartz-Olivine-Diopside-Plagioclase from plagioclase onto the ternary Quartz-Olivine-Diopside. CMAS components were calculated from the molar proportions of the major oxides as follows:

a-1 $C = CaO + 2Na_2O + 2K_2O$

a-2 $M = FeO^* + MgO$

a-3 $A = Al_2O_3 + Na_2O + K_2O$

a-4 $S = SiO_2 - 2Na_2O - 2K_2O$

The molar mineral components are then calculated from:

a-5 $Di = CMS_2 = C-A$

a-6 Silica = S = S - M/2 - A/2 - 3/2C

a-7 Ol = M_2S = (M + A - C)/2

a-8 Pl = CAS_2 = A

Substituting a-1 through a-4 into the four equations above yields the following equations:

a-9 Plag = $Al_2O_3 + Na_2O + K_2O$

a-10 Di = $CaO - Al_2O_3 + Na_2O + K_2O$

a-11 Ol = $(FeO^* + MgO + MnO + Al_2O_3 - CaO - Na_2O - K_2O)/2$

a-12 Silica = $SiO_2 - (Al_2O_3 + FeO^* + MgO + MnO + 3CaO + 11Na_2O + 11K_2O)/2$

These are the equations given in Walker et al. (1979) and are used to plot the whole-rock compositions of the rocks of Little Sitkin island as given in Appendix I and shown in figure 5-2.

The Grove diagram is very similar to the Walker diagram, with minor differences in the positions of the liquid line of descent and the boundary curves. The theory behind this diagram is similar to that of the Walker diagram as well, as it is also a modification of O'Hara's (1968a) original CMAS diagram. The formulae published in Grove et al. (1982) are also slightly different from those of Walker et al. (1979). They are the following:

a-13 Sum = $SiO_2 - CaO - 2(KO_{0.5} + NaO_{0.5} + Cr_2O_3 + TiO_2$

$$+ Cr_2O_3 + 0.5TiO_2)/Sum$$

a-15 Plag $= 0.5(AlO_{1.5} + NaO_{0.5} + KO_{0.5})/Sum$

a-16 Ol $= 0.5(FeO^* + MgO + 0.5(AlO_{1.5} - KO_{0.5} - NaO_{0.5}) - CaO - 2TiO_2 - Cr_2O_3)/Sum$

a-17 Cpx $= CaO - 0.5AlO_{1.5} + 0.5(KO_{0.5} + NaO_{0.5})/Sum$

Both diagrams are calculated at low pressure. The liquid line of descent and the boundary curves in the walker diagram were constructed using microprobe analyses of 3-phase saturated liquids at the QFM buffer. Glasses coexisting with olivine, pyroxene and plagioclase were used to construct the cotectics, reaction curves and points of the Grove diagram.

APPENDIX IV

REPRESENTATIVE PHASE CHEMICAL ANALYSES

Notes to Appendix IV

This appendix lists representative mineral analyses for all of the phases contained within the rocks of Little Sitkin island. Where there are two or more analyses listed for the same phase in the same rock it is because there is a significant variation in chemistry between grains in that sample. If there is only one analysis given, it is because the chemistry of all the grains in the given sample are very similar.

For each mineral, I have listed the analyses in order of increasing silica in the bulk rock. In other words all analyses of mineral 1 in basalt 491 come before analyses of mineral 1 in andesite 492, and so on.

Many of the analyses given are for both core and rims in the phenocryst. A typical analysis label may look like this:

491OL1c

where:
491 = Sample Number
OL = Mineral
1 = Grain Number
c = Core (r = rim and g = groundmass)

Mineral abbreviations are:

CPX = Clinopyroxene
OPX = Orthopyroxene
PIG = Pigeonite
OL = Olivine
P = Plagioclase
DP = Dirty Plagioclase
AMP = Amphibole
MT = Magnetite

ILM = Ilmenite
GL = Glass

PLAGIOCLASE ANALYSES

	491P2c	491P2r	491P4c	491P4r	491P1g
SiO2	45.81	48.42	49.78	53.37	53.51
Al2O3	34.97	32.96	31.79	29.13	28.94
FeO*	0.62	0.74	0.65	0.95	1.03
MnO	0.00	0.01	0.01	0.00	0.03
MgO	0.03	0.08	0.14	0.11	0.11
CaO	17.80	15.71	14.95	12.15	11.90
Na2O	1.24	2.38	2.92	4.26	4.31
K2O	0.09	0.16	0.15	0.37	0.41
Total	100.57	100.48	100.38	100.35	100.24

Number of ions per 8 oxygen

Si	2.1021	2.2119	2.2697	2.4177	2.4261
Al	1.8911	1.6957	1.7081	1.5553	1.5466
Fe	0.0239	0.0282	0.0246	0.0362	0.0392
Mn	0.0000	0.0005	0.0002	0.0000	0.0011
Mg	0.0020	0.0056	0.0095	0.0072	0.0075
Ca	0.8750	0.7691	0.7302	0.5900	0.5782
Na	0.1103	0.2112	0.2579	0.3743	0.3792
K	0.0052	0.0091	0.0088	0.0216	0.0235
Total	5.0097	5.0104	5.0091	5.0021	5.0014
An	88.34	77.74	73.25	59.85	58.95
Ab	11.14	21.35	25.87	37.96	38.66
Or	0.53	0.92	0.89	2.19	2.39

	491P3g	492P1c	492P1r	492P2c	492P2r
SiO2	49.22	54.15	56.59	50.58	54.44
Al2O3	32.07	29.73	27.74	31.88	28.81
FeO*	1.05	0.60	0.55	0.67	0.79
MnO	0.01	0.00	0.00	0.01	0.01
MgO	0.07	0.00	0.00	0.00	0.00
CaO	15.30	12.48	10.24	14.75	11.19
Na2O	2.63	4.40	5.26	3.03	4.81
K2O	0.16	0.15	0.19	0.12	0.23
Total	100.51	101.51	100.58	101.04	100.29

Number of ions per 8 oxygen

Si	2.2476	2.4165	2.5284	2.2847	2.4531
Al	1.7260	1.5634	1.4609	1.6969	1.5303
Fe	0.0402	0.0202	0.0184	0.0228	0.0268
Mn	0.0004	0.0001	0.0000	0.0005	0.0004
Mg	0.0047	0.0000	0.0000	0.0000	0.0000
Ca	0.7489	0.5964	0.4903	0.7139	0.5404
Na	0.2326	0.3809	0.4560	0.2650	0.4207
K	0.0095	0.0083	0.0110	0.0071	0.0131
Total	5.0099	4.9858	4.9650	4.9910	4.9848
An	75.57	60.51	51.22	72.40	55.47
Ab	23.48	38.64	47.63	26.88	43.18
Or	0.96	0.84	1.15	0.72	1.34

	492DP1c	492DP1r	492P4g	492P5g	496P1c
SiO2	48.43	52.63	46.98	52.36	58.36
Al2O3	33.21	29.22	33.72	29.41	27.28
FeO*	0.58	1.08	0.94	0.65	0.23
MnO	0.02	0.02	0.01	0.01	0.00
MgO	0.00	0.00	0.04	0.08	0.01
CaO	16.05	11.72	17.20	11.96	8.70
Na2O	1.85	4.37	1.76	4.36	6.35
K2O	0.07	0.26	0.06	0.17	0.22
Total	100.20	99.29	100.72	99.00	101.16

Number of ions per 8 oxygen

Si	2.2104	2.4045	2.1491	2.3971	2.5825
Al	1.7863	1.5730	1.8180	1.5870	1.4229
Fe	0.0239	0.0372	0.0322	0.0226	0.0084
Mn	0.0003	0.0006	0.0005	0.0006	0.0000
Mg	0.0000	0.0000	0.0031	0.0052	0.0010
Ca	0.7848	0.5736	0.8429	0.5867	0.4123
Na	0.1635	0.3870	0.1556	0.3869	0.5446
K	0.0038	0.0152	0.0036	0.0101	0.0124
Total	4.9696	4.9910	5.0049	4.9961	4.9841
An	82.43	58.79	84.11	59.65	42.54
Ab	17.18	39.66	15.53	39.33	56.18
Or	0.40	1.55	0.36	1.02	1.28

	496P1r	496P2c	496P2r	496DP1c	496DP1r
SiO2	61.72	54.71	52.80	51.90	54.77
Al2O3	25.51	29.54	29.96	31.07	28.98
FeO*	0.20	0.60	0.66	0.56	0.61
MnO	0.00	0.03	0.00	0.01	0.00
MgO	0.00	0.06	0.06	0.07	0.06
CaO	6.24	12.00	12.67	13.85	11.59
Na2O	7.18	4.38	4.26	3.11	4.19
K2O	0.37	0.20	0.14	0.09	0.15
Total	101.22	101.53	100.55	100.66	100.36

Number of ions per 8 oxygen

Si	2.7039	2.4384	2.3861	2.3427	2.4619
Al	1.3170	1.5515	1.5958	1.6530	1.5354
Fe	0.0074	0.0224	0.0249	0.0213	0.0230
Mn	0.0001	0.0010	0.0000	0.0002	0.0000
Mg	0.0003	0.0041	0.0042	0.0046	0.0040
Ca	0.2931	0.5731	0.6137	0.6699	0.5583
Na	0.6097	0.3788	0.3733	0.2719	0.3656
K	0.0207	0.0112	0.0081	0.0052	0.0088
Total	4.9523	4.9804	5.0062	4.9689	4.9571
An	31.73	59.51	61.67	70.74	59.86
Ab	66.02	39.33	37.51	28.71	39.20
Or	2.25	1.17	0.82	0.55	0.95

	496DP3c	496DP3r	496P1g	497P1c	497P1r
SiO2	54.74	51.24	53.91	49.55	56.41
Al2O3	29.27	31.50	29.78	32.31	28.46
FeO*	0.55	0.77	0.58	0.64	0.46
MnO	0.00	0.02	0.00	0.01	0.01
MgO	0.07	0.12	0.06	0.04	0.03
CaO	11.65	14.66	12.30	14.77	10.46
Na2O	4.54	2.81	4.23	2.73	4.89
K2O	0.20	0.10	0.16	0.03	0.16
Total	101.01	101.22	101.03	100.08	100.88

Number of ions per 8 oxygen

Si	2.4492	2.3093	2.4169	2.2609	2.5122
Al	1.5432	1.6732	1.5735	1.7378	1.4939
Fe	0.0206	0.0291	0.0218	0.0246	0.0172
Mn	0.0000	0.0006	0.0000	0.0003	0.0002
Mg	0.4800	0.0080	0.0043	0.0026	0.0021
Ca	0.5583	0.7078	0.5910	0.7219	0.4991
Na	0.3938	0.2451	0.3678	0.2416	0.4220
K	0.0113	0.0058	0.0090	0.0017	0.0091
Total	4.9812	4.9790	4.9843	4.9914	4.9559
An	57.95	73.83	61.06	74.79	53.65
Ab	40.88	25.57	38.00	25.03	45.37
Or	1.17	0.61	0.93	0.17	0.98

	497DP1c	497DP1r	497P1g	497P2g	501P3c
SiO2	54.68	51.44	52.37	60.62	53.43
Al2O3	29.09	30.77	30.65	25.33	29.50
FeO*	0.53	0.79	0.68	0.49	0.35
MnO	0.01	0.00	0.00	0.00	0.00
MgO	0.04	0.11	0.06	0.03	0.04
CaO	11.35	13.72	12.93	7.45	11.82
Na2O	4.34	2.96	3.71	6.57	4.57
K2O	0.21	0.13	0.11	0.38	0.17
Total	100.26	99.91	100.52	100.85	99.88

Number of ions per 8 oxygen

Si	2.4599	2.3414	2.3656	2.6785	2.4211
Al	1.5425	1.6508	1.6315	1.3189	1.5751
Fe	0.0198	0.0299	0.0258	0.0181	0.0133
Mn	0.0004	0.0000	0.0000	0.0000	0.0000
Mg	0.0030	0.0072	0.0038	0.0019	0.0024
Ca	0.5472	0.6691	0.6259	0.3528	0.5736
Na	0.3786	0.2617	0.3245	0.5628	0.4018
K	0.0123	0.0075	0.0065	0.0218	0.0098
Total	4.9637	4.9672	4.9837	4.9548	4.9971
An	58.33	71.34	65.41	37.64	58.22
Ab	40.36	27.87	33.91	60.04	40.78
Or	1.31	0.80	0.68	2.36	0.99

	501P3r	501P4c	501P4r	501P1g	501P2g
SiO2	57.14	56.96	59.36	57.32	51.42
Al2O3	27.32	27.31	25.91	27.43	30.90
FeO*	0.39	0.39	0.37	0.45	0.46
MnO	0.01	0.00	0.00	0.02	0.01
MgO	0.02	0.04	0.03	0.03	0.04
CaO	9.57	9.48	7.82	9.44	13.42
Na2O	5.98	5.67	6.21	6.06	3.87
K2O	0.16	0.21	0.22	0.19	0.10
Total	100.58	100.04	99.93	100.92	100.21

Number of ions per 8 oxygen

Si	2.5526	2.5550	2.6469	2.5407	2.3364
Al	1.4381	1.4435	1.3615	1.4328	1.6545
Fe	0.0148	0.0146	0.0139	0.0168	0.0164
Mn	0.0003	0.0000	0.0000	0.0008	0.0003
Mg	0.0013	0.0024	0.0019	0.0016	0.0025
Ca	0.4577	0.4555	0.3737	0.4480	0.6533
Na	0.5178	0.4926	0.5368	0.5204	0.3408
K	0.0092	0.0124	0.0124	0.0106	0.0054
Total	4.9918	4.9760	4.9471	4.9717	5.0096
An	46.48	47.42	40.49	45.76	65.36
Ab	52.58	51.29	58.16	53.16	34.10
Or	0.93	1.29	1.34	1.08	0.54

	495P1c	495P1r	495P7c	495P7r	495DP1c
SiO2	49.48	53.61	58.69	61.13	45.69
Al2O3	32.21	28.75	27.15	25.32	35.37
FeO*	0.60	0.67	0.24	0.18	0.67
MnO	0.00	0.01	0.00	0.02	0.01
MgO	0.06	0.07	0.02	0.01	0.04
CaO	15.18	11.86	8.40	6.63	18.44
Na2O	2.68	4.43	6.36	7.18	0.85
K2O	0.09	0.20	0.23	0.29	0.00
Total	100.30	99.61	101.09	100.75	101.07

Number of ions per 8 oxygen

Si	2.2541	2.4360	2.5941	2.6942	2.0848
Al	1.7294	1.5395	1.4143	1.3152	1.9020
Fe	0.0207	0.0231	0.0080	0.0059	0.0230
Mn	0.0000	0.0004	0.0001	0.0006	0.0030
Mg	0.0039	0.0049	0.0011	0.0009	0.0028
Ca	0.7410	0.5773	0.3976	0.3129	0.9014
Na	0.2367	0.3907	0.5448	0.6139	0.0756
K	0.0053	0.0113	0.0150	0.0164	0.0000
Total	4.9912	4.9832	4.9733	4.9599	4.9900
An	75.38	58.95	41.61	33.17	92.26
Ab	24.08	39.89	57.01	65.09	7.74
Or	0.53	1.14	1.39	1.74	0.00

	495DP1r	495P1g	495P4g
SiO2	53.61	50.81	58.43
Al2O3	28.81	32.00	27.14
FeO*	0.76	0.83	0.29
MnO	0.00	0.01	0.05
MgO	0.08	0.08	0.01
CaO	11.83	14.85	8.40
Na2O	4.14	2.73	6.68
K2O	0.16	0.13	0.29
Total	99.42	101.45	101.28

Number of ions per 8 oxygen

Si	2.4369	2.2845	2.5841
Al	1.5451	1.6960	1.4145
Fe	0.0260	0.0282	0.0095
Mn	0.0000	0.0005	0.0017
Mg	0.0054	0.0056	0.0010
Ca	0.5764	0.7156	0.3981
Na	0.3651	0.2376	0.5727
K	0.0092	0.0076	0.0161
Total	4.9642	4.9755	4.9978
An	60.63	74.48	40.34
Ab	38.40	24.73	58.03
Or	0.97	0.79	1.63

CLINOPYROXENE ANALYSES

	491CPX4c	491CPX4r	491MCPX2c	491MCPX2r	491CPX1g
SiO2	51.85	51.69	53.66	52.11	51.70
TiO2	0.37	0.50	0.12	0.77	0.50
Al2O3	2.98	2.32	1.26	1.56	0.78
Cr2O3	0.27	0.11	0.47	0.01	0.01
FeO*	7.46	10.19	3.55	13.49	14.70
MnO	0.20	0.27	0.09	0.30	0.33
MgO	16.77	16.76	17.95	14.50	13.56
CaO	19.57	17.05	22.42	17.25	17.03
Na2O	0.27	0.22	0.19	0.29	0.33
K2O	0.03	0.02	0.00	0.05	0.02
Total	99.77	99.13	99.72	100.33	98.95

Number of ions per 6 oxygen

Si	1.9144	1.9313	1.9596	1.9529	1.9770
Ti	0.0103	0.0140	0.0033	0.0217	0.0144
Al	0.1295	0.1021	0.0541	0.0687	0.0352
Cr	0.0080	0.0033	0.0135	0.0002	0.0003
Fe	0.2303	0.3182	0.1084	0.4228	0.4700
Mn	0.0064	0.0085	0.0029	0.0096	0.0107
Mg	0.9227	0.9332	0.9770	0.8102	0.7726
Ca	0.7741	0.6826	0.8772	0.6927	0.6976
Na	0.0193	0.0157	0.0135	0.0214	0.0248
K	0.0013	0.0011	0.0000	0.0024	0.0009
Total	4.0164	4.0101	4.0097	4.0025	4.0034
Wo	40.04	35.14	44.63	35.79	35.76
En	47.72	48.04	49.71	41.86	39.60
Fs	12.24	16.82	5.67	22.34	24.64

	491PIG1g	492CPX4c	492CPX4r	496CPX7c	496CPX7r
SiO2	53.20	53.04	49.97	52.19	51.91
TiO2	0.29	0.38	0.98	0.44	0.52
Al2O3	1.04	1.45	3.87	1.35	1.94
Cr2O3	0.03	0.04	0.02	0.00	0.01
FeO*	17.26	9.56	10.50	9.46	9.52
MnO	0.39	0.46	0.32	0.43	0.41
MgO	21.74	14.68	14.44	14.55	14.96
CaO	5.27	20.89	19.66	20.86	20.28
Na2O	0.10	0.30	0.29	0.26	0.26
K2O	0.01	0.00	0.02	0.01	0.01
Total	99.35	100.80	100.06	99.57	99.84

Number of ions per 6 oxygen

Si	1.9747	1.9618	1.8713	1.9567	1.9384
Ti	0.0081	0.0104	0.0275	0.0124	0.0147
Al	0.0455	0.0633	0.1707	0.0599	0.0855
Cr	0.0009	0.0011	0.0006	0.0000	0.0004
Fe	0.5359	0.2957	0.3288	0.2966	0.2974
Mn	0.0124	0.0144	0.0101	0.0138	0.0129
Mg	1.2027	0.8096	0.8062	0.8132	0.8328
Ca	0.2095	0.8279	0.7890	0.8381	0.8116
Na	0.0072	0.0217	0.0209	0.0191	0.0191
K	0.0007	0.0002	0.0009	0.0000	0.0005
Total	3.9976	4.0061	4.0260	4.0104	4.0134
Wo	10.69	42.51	40.79	42.73	41.52
En	61.35	41.57	41.68	41.45	42.61
Fs	27.97	15.92	17.52	15.82	15.87

	496CPX1g	497CPX3c	497CPX3r	497CPX1g	501CPX1c
SiO2	49.46	52.25	52.21	52.13	53.30
TiO2	0.64	0.47	0.52	0.48	0.23
Al2O3	4.46	1.85	1.69	1.70	1.01
Cr2O3	0.04	0.01	0.03	0.00	0.00
FeO*	8.02	10.01	10.51	9.65	9.85
MnO	0.19	0.43	0.55	0.38	0.59
MgO	16.23	14.14	14.02	14.62	14.16
CaO	20.43	20.70	20.32	21.10	21.29
Na2O	0.17	0.30	0.31	0.28	0.30
K2O	0.01	0.00	0.01	0.00	0.00
Total	99.65	100.15	100.17	100.35	100.73

Number of ions per 6 oxygen

Si	1.8438	1.9500	1.9522	1.9420	1.9781
Ti	0.0180	0.0131	0.0147	0.0134	0.0063
Al	0.1962	0.0812	0.0746	0.0747	0.0440
Cr	0.0012	0.0003	0.0008	0.0000	0.0000
Fe	0.2500	0.3124	0.3287	0.3007	0.3058
Mn	0.0060	0.0136	0.0175	0.0121	0.0187
Mg	0.9020	0.7866	0.7812	0.8115	0.7830
Ca	0.8158	0.8279	0.8139	0.8421	0.8463
Na	0.0120	0.0214	0.0224	0.0202	0.0219
K	0.0006	0.0000	0.0005	0.0002	0.0002
Total	4.0450	4.0065	4.0065	4.0170	4.0043
Wo	41.33	42.66	41.92	42.82	43.32
En	45.70	40.54	40.24	41.27	40.08
Fs	12.97	16.80	17.84	15.91	16.60

	501CPX1r	501CPX1g	495CPX3c	495CPX3r
SiO2	52.78	51.49	52.14	52.38
TiO2	0.26	0.48	0.42	0.46
Al2O3	1.17	1.97	1.72	1.75
Cr2O3	0.01	0.08	0.01	0.00
FeO*	9.62	9.92	10.04	9.51
MnO	0.64	0.48	0.44	0.38
MgO	14.38	14.34	14.63	14.81
CaO	21.35	20.79	20.55	20.42
Na2O	0.28	0.33	0.27	0.32
K2O	0.01	0.00	0.01	0.00
Total	100.50	99.88	100.23	100.03
	Number of ions per 6 oxygen			
Si	1.9643	1.9313	1.9453	1.9507
Ti	0.0073	0.0136	0.0118	0.0129
Al	0.0511	0.0870	0.0754	0.0769
Cr	0.0003	0.0024	0.0002	0.0001
Fe	0.2994	0.3111	0.3133	0.2961
Mn	0.0201	0.0151	0.0139	0.0121
Mg	0.7977	0.8018	0.8133	0.8223
Ca	0.8515	0.8357	0.8215	0.8147
Na	0.0203	0.0239	0.0194	0.0234
K	0.0006	0.0001	0.0006	0.0000
Total	4.0127	4.0220	4.0148	4.0092
Wo	43.25	42.56	41.87	41.88
En	40.52	40.83	41.45	42.27
Fs	16.23	16.61	16.67	15.85

ORTHOPYROXENE ANALYSES

	492OPX7c	492OPX7r	496OPX1c	496OPX1r	496OPX3g
SiO2	53.20	53.31	53.67	53.64	53.73
TiO2	0.20	0.37	0.21	0.17	0.31
Al2O3	1.24	1.46	0.72	0.62	1.70
Cr2O3	0.00	0.02	0.00	0.00	0.00
FeO*	19.41	19.77	19.46	19.85	17.26
MnO	0.70	0.70	0.80	0.80	0.52
MgO	23.43	23.26	24.03	24.18	24.47
CaO	1.41	1.62	1.32	1.34	2.02
Na2O	0.04	0.02	0.04	0.04	0.03
K2O	0.00	0.00	0.00	0.01	0.01
Total	99.62	100.47	100.24	100.65	100.05

Number of ions per 6 oxygen

Si	1.9681	1.9593	1.9737	1.9691	1.9598
Ti	0.0056	0.0086	0.0057	0.0046	0.0085
Al	0.0539	0.0634	0.0311	0.0267	0.0729
Cr	0.0000	0.0007	0.0000	0.0000	0.0000
Fe	0.6004	0.6077	0.5985	0.6096	0.5267
Mn	0.0219	0.0217	0.0250	0.0249	0.0162
Mg	1.2920	1.2739	1.3174	1.3232	1.3305
Ca	0.0558	0.0636	0.0518	0.0526	0.0789
Na	0.0026	0.0016	0.0026	0.0031	0.0022
K	0.0000	0.0000	0.0002	0.0005	0.0006
Total	4.0003	4.0005	4.0061	4.0143	3.9962
Wo	2.83	3.24	2.60	2.61	4.04
En	65.58	64.77	66.11	65.82	68.15
Fs	31.59	32.00	31.29	31.56	27.81

	497OPX1c	497OPX1r	501OPX5c	501OPX5r	501OPX1g
SiO2	53.71	53.08	53.67	53.26	53.30
TiO2	0.24	0.28	0.14	0.18	0.21
Al2O3	0.83	0.90	0.33	0.63	1.01
Cr2O3	0.01	0.00	0.00	0.00	0.00
FeO*	20.48	20.76	21.95	20.95	20.74
MnO	0.75	0.72	1.34	0.99	1.23
MgO	23.23	22.79	21.57	22.35	22.65
CaO	1.53	1.58	1.06	1.12	1.29
Na2O	0.01	0.03	0.02	0.03	0.00
K2O	0.00	0.01	0.00	0.01	0.00
Total	100.80	100.15	100.07	99.52	100.44

Number of ions per 6 oxygen

Si	1.9734	1.9678	2.0009	1.9870	1.9709
Ti	0.0066	0.0077	0.0038	0.0051	0.0058
Al	0.0358	0.0392	0.0144	0.0275	0.0442
Cr	0.0003	0.0000	0.0000	0.0000	0.0000
Fe	62.9300	0.6437	0.6845	0.6537	0.6415
Mn	0.0235	0.0226	0.0423	0.0313	0.0385
Mg	1.2721	1.2594	1.1986	1.2428	1.2486
Ca	0.0603	0.0627	0.0423	0.0449	0.0512
Na	0.0009	0.0024	0.0015	0.0021	0.0003
K	0.0000	0.0006	0.0000	0.0005	0.0000
Total	4.0020	4.0061	3.9884	3.9950	4.0010
Wo	3.04	3.16	2.15	2.28	2.59
En	64.08	63.33	60.91	63.00	63.07
Fs	32.88	33.51	36.94	34.73	34.35

	495OPX5c	495OPX5r	495OPX6c	495OPX6r
SiO2	51.58	51.46	54.20	53.73
TiO2	0.10	0.09	0.24	0.23
Al2O3	0.43	0.50	0.78	0.90
Cr2O3	0.01	0.00	0.00	0.00
FeO*	28.56	28.41	19.24	18.70
MnO	1.67	1.90	0.67	0.65
MgO	17.12	17.00	23.92	24.72
CaO	0.81	0.86	1.43	1.65
Na2O	0.03	0.01	0.02	0.03
K2O	0.00	0.00	0.00	0.00
Total	100.30	100.24	100.51	100.61

Number of ions per 6 oxygen

Si	1.9864	1.9845	1.9828	1.9630
Ti	0.0030	0.0026	0.0065	0.0064
Al	0.0196	0.0226	0.0338	0.0386
Cr	0.0002	0.0001	0.0000	0.0000
Fe	0.9199	0.9163	0.5886	0.5713
Mn	0.0544	0.0620	0.0208	0.0201
Mg	0.9825	0.9771	1.3040	1.3462
Ca	0.0334	0.0354	0.0562	0.0645
Na	0.0019	0.0010	0.0014	0.0018
K	0.0000	0.0000	0.0000	0.0001
Total	4.0013	4.0016	3.9941	4.0119
Wo	1.68	1.78	2.85	3.22
En	49.37	49.08	66.21	67.24
Fs	48.96	49.14	30.94	29.54

OLIVINE ANALYSES

	491OL1c	491OL1r	491OL2c	491OL2r	491OL4g
SiO2	39.53	37.02	37.09	36.18	35.18
TiO2	0.01	0.01	0.02	0.01	0.04
Al2O3	0.02	0.01	0.01	0.02	0.01
FeO*	17.84	30.91	31.54	33.56	39.30
MnO	0.25	0.40	0.40	0.42	0.49
MgO	42.14	32.18	31.92	30.28	26.09
CaO	0.19	0.20	0.20	0.21	0.23
Total	99.97	100.74	101.17	101.08	101.95
	Number of ions per 4 oxygen				
Si	1.0055	0.9975	0.9975	0.9952	0.9939
Ti	0.0001	0.0002	0.0003	0.0002	0.0007
Al	0.0005	0.0002	0.0004	0.0006	0.0002
Fe	0.3795	0.6965	0.7090	0.7638	0.9122
Mn	0.0054	0.0091	0.0090	0.0098	0.0115
Mg	1.5977	1.2924	1.2793	1.2283	1.0796
Ca	0.0052	0.0059	0.0057	0.0062	0.0068
Total	2.9939	3.0019	3.0017	3.0041	3.0050
Fo	80.59	64.69	64.04	61.36	53.89
F/(F+M)	0.1941	0.3531	0.3596	0.3864	0.4611

	4910L8g	4920L1c	4920L1r	4920L2	4920L7
SiO2	36.38	38.04	38.43	37.08	38.11
TiO2	0.01	0.01	0.01	0.01	0.02
Al2O3	0.01	0.03	0.03	0.03	0.03
FeO*	35.83	22.80	22.57	29.89	22.23
MnO	0.46	0.40	0.40	0.53	0.40
MgO	28.41	38.91	38.72	32.74	38.98
CaO	0.24	0.17	0.17	0.17	0.17
Total	101.64	100.36	100.33	100.45	99.94
	Number of ions per 4 oxygen				
Si	1.0023	0.9898	0.9978	0.9977	0.9930
Ti	0.0003	0.0002	0.0001	0.0002	0.0005
Al	0.0004	0.0010	0.0010	0.0008	0.0008
Fe	0.8190	0.4960	0.4901	0.6726	0.4844
Mn	0.0106	0.0087	0.0087	0.0122	0.0089
Mg	1.1572	1.5088	1.4987	1.3132	1.5141
Ca	0.0072	0.0048	0.0049	0.0048	0.0049
Total	2.9969	3.0093	3.0013	3.0015	3.0061
Fo	58.25	74.93	75.03	65.73	75.43
F/(F+M)	0.4175	0.2507	0.2497	0.3427	0.2457

	497OL1	497OL2	497OL3
SiO2	38.61	38.26	38.83
TiO2	0.02	0.03	0.03
Al2O3	0.03	0.03	0.03
FeO*	21.25	24.04	21.11
MnO	0.31	0.52	0.30
MgO	40.22	37.33	40.07
CaO	0.18	0.14	0.20
Total	100.62	100.35	100.57

Number of ions per 4 oxygen

Si	0.9933	1.0005	0.9981
Ti	0.0003	0.0005	0.0006
Al	0.0009	0.0010	0.0008
Fe	0.4571	0.5257	0.4537
Mn	0.0068	0.0115	0.0064
Mg	1.5423	1.4551	1.5353
Ca	0.0051	0.0039	0.0055
Total	3.0057	2.9983	3.0006
Fo	76.88	73.04	76.94
F/(F+M)	0.2312	0.2696	0.2306

AMPHIBOLE ANALYSES

	496AMP1c	496AMP1r	496AMP2c	496AMP2r	495AMP1
SiO2	43.73	45.02	46.42	48.05	43.49
TiO2	2.02	2.12	1.33	1.18	2.06
Al2O3	11.15	12.42	6.72	6.67	11.39
Na2O	2.14	2.00	1.28	1.34	2.18
K2O	0.27	0.28	0.24	0.25	0.28
Cr2O3	0.00	0.02	0.02	0.00	0.00
FeO*	13.85	11.98	17.42	16.72	14.07
MnO	0.37	0.32	0.63	0.67	0.33
MgO	13.76	12.31	12.05	13.12	12.80
CaO	11.16	10.38	10.22	10.08	11.35
OH	2.04	2.05	1.98	2.03	2.03
Total	100.49	98.89	98.32	100.12	99.97

Number of ions per 24 oxygen

Si	6.4132	6.5922	7.0167	7.0819	6.4209
Ti	0.2226	0.2334	0.1513	0.1313	0.2282
Al	1.9279	2.1424	1.1966	1.1589	1.9815
Na	0.6072	0.5663	0.3757	0.3821	0.6236
K	0.0512	0.0520	0.0467	0.0478	0.0522
Cr	0.0000	0.0019	0.0019	0.0000	0.0003
Fe	1.6988	1.4670	2.2024	2.0613	1.7376
Mn	0.0459	0.0400	0.0810	0.0840	0.0409
Mg	3.0070	2.6864	2.7147	2.8813	2.8165
Ca	1.7543	1.6282	1.6555	1.5922	1.7948
OH	1.0000	1.0000	1.0000	1.0000	1.0000
Total	16.7280	16.4099	16.4425	16.4208	16.6964
F/(F+M)	0.3672	0.3594	0.4569	0.4268	0.3870

	495AMP2	495AMP3	495AMP4	495AMP5	495AMP6
SiO2	48.11	48.23	47.78	42.13	40.83
TiO2	1.29	1.07	1.16	2.43	2.50
Al2O3	6.75	6.48	6.49	11.41	12.28
Na2O	1.42	1.35	1.35	2.24	2.20
K2O	0.21	0.20	0.23	0.34	0.52
Cr2O3	0.01	0.00	0.02	0.00	0.00
FeO*	17.98	17.38	17.46	18.32	20.12
MnO	0.69	0.68	0.71	0.56	0.61
MgO	12.46	12.79	12.24	9.73	8.49
CaO	9.94	9.81	10.02	10.87	10.82
OH	2.04	2.03	2.01	1.99	1.97
Total	100.89	100.02	99.46	100.03	100.34

Number of ions per 24 oxygen

Si	7.0720	7.1267	7.1150	6.3570	6.2114
Ti	0.1422	0.1188	0.1304	0.2756	0.2864
Al	1.1703	1.1277	1.1395	2.0286	2.2015
Na	0.4038	0.3870	0.3884	0.6557	0.6476
K	0.0398	0.0379	0.0428	0.0663	0.1010
Cr	0.0015	0.0000	0.0024	0.0000	0.0000
Fe	2.2105	2.1482	2.1740	2.3120	2.5591
Mn	0.0854	0.0848	0.0896	0.0710	0.0787
Mg	2.7296	2.8171	2.7167	2.1892	1.9248
Ca	1.5654	1.5533	1.5990	1.7574	1.7639
OH	1.0000	1.0000	1.0000	1.0000	1.0000
Total	16.4203	16.4016	16.3978	16.7127	16.7744
F/(F+M)	0.4568	0.4422	0.4545	0.5212	0.5781

	495AMP7	501AMP1	501AMP2	501AMP3	501AMP4
SiO2	48.55	42.22	41.74	42.00	43.24
TiO2	1.09	2.07	1.99	1.68	2.01
Al2O3	6.49	12.29	12.91	13.03	11.97
Na2O	1.35	2.15	2.27	2.19	2.18
K2O	0.21	0.32	0.29	0.34	0.33
Cr2O3	0.00	0.01	0.00	0.00	0.00
FeO*	16.61	12.91	13.24	14.12	12.61
MnO	0.64	0.19	0.20	0.18	0.15
MgO	13.06	14.33	14.25	13.08	14.31
CaO	10.18	11.22	10.86	11.50	11.54
OH	2.04	2.03	2.03	2.03	2.05
Total	100.20	99.73	99.77	100.16	100.39

Number of ions per 24 oxygen

Si	7.1373	6.2283	6.1620	6.2039	6.3204
Ti	0.1200	0.2295	0.2209	0.1866	0.2206
Al	1.1248	2.1365	2.2459	2.2683	2.0615
Na	0.3842	0.6153	0.6485	0.6278	0.6188
K	0.0393	0.0605	0.0540	0.0638	0.0615
Cr	0.0000	0.0007	0.0003	0.0002	0.0000
Fe	2.0416	1.5925	1.6344	1.7450	1.5418
Mn	0.0794	0.0234	0.0249	0.0229	0.0184
Mg	2.8608	3.1503	3.1353	2.8806	3.1169
Ca	1.6031	1.7731	1.7175	1.8207	1.8072
OH	1.0000	1.0000	1.0000	1.0000	1.0000
Total	16.3906	16.8101	16.8438	16.8197	16.7670
F/(F+M)	0.4258	0.3390	0.3461	0.3803	0.3336

	501AMP5	501AMP6c	501AMP6r
SiO2	43.33	42.96	41.36
TiO2	2.29	2.54	2.32
Al2O3	11.78	11.16	12.73
Na2O	2.04	2.05	2.16
K2O	0.28	0.27	0.34
Cr2O3	0.04	0.01	0.00
FeO*	13.07	12.48	14.31
MnO	0.20	0.23	0.33
MgO	14.57	14.30	12.14
CaO	10.78	10.85	11.25
OH	2.05	2.02	2.00
Total	100.44	98.88	98.95

Number of ions per 24 oxygen

Si	6.3263	6.3653	6.2004
Ti	0.2518	0.2833	0.2614
Al	2.0279	1.9493	2.2482
Na	0.5785	0.5882	0.6288
K	0.0514	0.0508	0.0654
Cr	0.0049	0.0010	0.0003
Fe	1.5956	1.5465	1.7939
Mn	0.0248	0.0293	0.0425
Mg	3.1712	3.1576	2.7114
Ca	1.6867	1.7230	1.8074
OH	1.0000	1.0000	1.0000
Total	16.7190	16.6943	16.7596
F/(F+M)	0.3382	0.3329	0.4038

OPAQUE ANALYSES

	491ILM4	491ILM8	491MT1	491MT7	492MT4
SiO2	0.28	0.07	0.04	0.96	0.08
TiO2	51.54	48.93	6.22	12.80	15.17
Al2O3	0.00	0.02	1.32	2.12	1.96
FeO	44.26	47.37	35.36	40.58	43.16
Fe2O3	0.00	0.00	53.88	38.64	38.01
MnO	0.43	0.50	0.17	0.26	0.42
MgO	1.82	2.10	0.46	0.59	1.22
CaO	0.06	0.09	0.07	0.15	0.01
Total	98.40	99.09	97.53	96.11	100.04

Number of ions per 32 oxygen

Si	0.0758	0.0199	0.0139	0.2969	0.0242
Ti	10.4882	10.0592	1.4526	2.9680	3.3918
Al	0.0000	0.0079	0.4812	0.7714	0.6872
Fe+2	10.0171	10.8292	9.1828	10.4670	10.7322
Fe+3	0.0000	0.0000	12.5875	8.9695	8.5028
Mn	0.0994	0.1163	0.0458	0.0688	0.1070
Mg	0.7350	0.8567	0.2110	0.2706	0.5393
Ca	0.0183	0.0258	0.0228	0.0509	0.0031
Total	21.4339	21.9150	23.9977	23.8631	23.9875

	496MT5	497ILM1	497MT1	501MT4	495MT3
SiO2	0.07	0.00	0.15	0.07	0.09
TiO2	10.99	45.51	13.02	9.64	11.61
Al2O3	3.18	0.18	2.33	2.48	3.16
FeO	37.47	50.24	41.08	37.30	38.13
Fe2O3	46.24	0.00	41.85	48.44	43.93
MnO	0.43	0.69	0.57	0.49	0.35
MgO	2.75	2.40	1.25	1.73	2.46
CaO	0.00	0.01	0.05	0.02	0.02
Total	101.14	99.02	100.31	100.16	99.75

Number of ions per 32 oxygen

Si	0.0211	0.0000	0.0437	0.0216	0.0271
Ti	2.3973	9.5265	2.9017	2.1497	2.5697
Al	1.0885	0.0601	0.8141	0.8664	1.0982
Fe+2	9.0914	11.6950	10.1797	9.2502	9.3881
Fe+3	10.0945	0.0000	9.3306	10.8090	9.7314
Mn	0.1053	0.1626	0.1426	0.1232	0.0869
Mg	1.1894	0.9948	0.5535	0.7637	1.0791
Ca	0.0009	0.0025	0.0147	0.0058	0.0066
Total	23.9886	22.4415	23.9807	23.9896	23.9870

GLASS ANALYSES

	496GL1	496GL2	496GL3	496GL4	497GL1
SiO2	73.51	72.35	73.50	71.24	79.36
TiO2	0.58	0.61	0.55	0.58	0.58
Al2O3	15.68	14.42	15.58	17.05	11.63
FeO*	1.91	3.26	1.97	1.31	2.04
MnO	0.06	0.12	0.00	0.05	0.02
MgO	0.50	1.14	0.00	0.15	0.12
CaO	3.74	3.63	2.75	3.49	0.65
Na2O	2.65	2.58	4.48	4.82	1.44
K2O	0.95	1.92	1.10	1.19	3.61
P2O5	0.15	0.19	0.11	0.16	0.06
Total	99.73	100.22	100.44	100.04	99.51

Number of ions

Si	0.2528	0.2499	0.2506	0.2438	0.2736
Ti	0.0015	0.0016	0.0014	0.0015	0.0015
Al	0.0636	0.0587	0.0626	0.0688	0.0472
Fe	0.0055	0.0094	0.0056	0.0038	0.0059
Mn	0.0002	0.0003	0.0001	0.0001	0.0001
Mg	0.0026	0.0059	0.0016	0.0008	0.0006
Ca	0.0138	0.0135	0.0100	0.0128	0.0024
Na	0.0176	0.0173	0.0296	0.0320	0.0096
K	0.0042	0.0084	0.0048	0.0052	0.0159
P	0.0004	0.0006	0.0003	0.0005	0.0002
O	0.6379	0.6344	0.6333	0.6309	0.6431
Mg#	31.8	38.3	22.3	17.3	9.6

	497GL2	497GL3	497GL4	497GL6	501GL1
SiO2	78.58	78.44	78.32	78.13	73.59
TiO2	0.59	0.56	0.57	0.59	0.32
Al2O3	11.29	11.37	11.34	11.53	15.78
FeO*	2.03	2.11	1.98	1.85	1.15
MnO	0.04	0.07	0.03	0.08	0.03
MgO	0.11	0.10	0.07	0.08	0.17
CaO	0.64	0.67	0.63	0.62	3.09
Na2O	1.90	1.83	2.09	2.74	4.85
K2O	3.64	3.77	3.58	3.49	1.63
P2O5	0.11	0.09	0.10	0.05	0.07
Total	98.93	99.01	98.70	99.16	100.68

Number of ions

Si	0.2726	0.2721	0.2721	0.2701	0.2499
Ti	0.0015	0.0015	0.0015	0.0015	0.0008
Al	0.0461	0.0465	0.0464	0.0470	0.0631
Fe	0.0059	0.0061	0.0057	0.0053	0.0033
Mn	0.0001	0.0002	0.0001	0.0002	0.0001
Mg	0.0006	0.0005	0.0004	0.0004	0.0009
Ca	0.0024	0.0025	0.0024	0.0023	0.0112
Na	0.0128	0.0123	0.0141	0.0184	0.0319
K	0.0161	0.0167	0.0159	0.0154	0.0071
P	0.0003	0.0003	0.0003	0.0001	0.0002
O	0.6416	0.6414	0.6412	0.6392	0.6315
Mg#	9.0	7.9	5.9	7.3	21.1

	501GL2	501GL3	501GL4	501GL5	495GL1
SiO2	79.38	74.40	72.24	76.62	77.42
TiO2	0.46	0.58	0.29	0.42	0.11
Al2O3	11.13	11.99	17.35	13.31	12.53
FeO*	1.33	2.87	1.15	1.48	1.07
MnO	0.04	0.11	0.02	0.00	0.09
MgO	0.07	0.70	0.12	0.09	0.14
CaO	0.64	0.74	3.87	1.69	1.09
Na2O	3.12	3.24	5.14	2.48	3.38
K2O	3.41	3.59	1.34	3.19	3.13
P2O5	0.08	0.19	0.05	0.08	0.05
Total	99.66	98.41	101.57	99.37	99.01

Number of ions

Si	0.2722	0.2608	0.2434	0.2643	0.2669
Ti	0.0018	0.0015	0.0007	0.0011	0.0003
Al	0.0450	0.0495	0.0689	0.0541	0.0509
Fe	0.0038	0.0084	0.0033	0.0043	0.0031
Mn	0.0001	0.0003	0.0001	0.0000	0.0003
Mg	0.0003	0.0037	0.0006	0.0005	0.0007
Ca	0.0024	0.0028	0.0140	0.0062	0.0040
Na	0.0208	0.0220	0.0336	0.0166	0.0226
K	0.0149	0.0161	0.0059	0.0141	0.0138
P	0.0002	0.0006	0.0001	0.0002	0.0001
O	0.6392	0.6344	0.6296	0.6387	0.6373
Mg#	8.0	30.4	15.2	9.8	18.5

	495GL3	495GL4	495GL5a	495GL5b	495GL6b
SiO2	78.27	76.41	77.54	78.02	77.80
TiO2	0.12	0.16	0.13	0.12	0.12
Al2O3	12.87	12.65	12.95	12.60	12.62
FeO*	1.11	0.97	1.10	1.10	1.16
MnO	0.05	0.05	0.08	0.05	0.08
MgO	0.14	0.15	0.16	0.13	0.14
CaO	1.10	1.05	1.08	1.05	1.09
Na2O	3.54	3.35	3.61	3.39	3.68
K2O	3.20	3.12	3.18	3.19	3.07
P2O5	0.01	0.03	0.02	0.04	0.03
Total	100.40	97.94	99.85	99.69	99.89

Number of ions

Si	0.2661	0.2662	0.2652	0.2671	0.2661
Ti	0.0003	0.0004	0.0003	0.0003	0.0003
Al	0.0516	0.0519	0.0522	0.0508	0.0509
Fe	0.0032	0.0028	0.0031	0.0032	0.0033
Mn	0.0002	0.0002	0.0002	0.0001	0.0002
Mg	0.0007	0.0008	0.0008	0.0007	0.0007
Ca	0.0040	0.0039	0.0040	0.0039	0.0040
Na	0.0233	0.0226	0.0239	0.0225	0.0244
K	0.0139	0.0139	0.0136	0.0139	0.0134
P	0.0000	0.0001	0.0001	0.0001	0.0001
O	0.6368	0.6372	0.6365	0.6374	0.6365
Mg#	18.7	21.4	20.6	17.2	17.5

GLASS INCLUSION ANALYSES

	497PGL1	497PGL2	497PGL3	501PGL1	501PGL2
SiO2	76.92	77.73	77.36	69.81	75.91
TiO2	0.56	0.58	0.54	0.35	0.52
Al2O3	11.00	10.79	11.24	16.74	12.46
FeO*	2.37	2.86	2.25	1.89	2.09
MnO	0.06	0.08	0.05	0.11	0.06
MgO	0.14	0.31	0.29	0.44	0.36
CaO	0.84	0.81	0.94	4.48	1.15
Na2O	2.60	2.81	2.94	5.08	3.32
K2O	3.60	3.78	3.33	0.96	3.49
P2O5	0.11	0.11	0.05	0.03	0.11
Total	98.20	99.84	99.00	99.89	99.47

Number of ions

Si	0.2694	0.2684	0.2684	0.2403	0.2623
Ti	0.0015	0.0015	0.0014	0.0009	0.0014
Al	0.0454	0.0439	0.0460	0.0679	0.0504
Fe	0.0069	0.0083	0.0065	0.0055	0.0060
Mn	0.0002	0.0002	0.0002	0.0003	0.0002
Mg	0.0007	0.0016	0.0015	0.0022	0.0019
Ca	0.0032	0.0030	0.0035	0.0165	0.0042
Na	0.0177	0.0188	0.0198	0.0339	0.0222
K	0.0161	0.0167	0.0147	0.0042	0.0154
P	0.0003	0.0003	0.0002	0.0001	0.0003
O	0.6386	0.6373	0.6379	0.6281	0.6354
Mg#	9.5	19.2	18.6	29.2	23.5

	495PGL1	495PGL2	497OPXGL1	501OPXGL1	495OPXGL1
SiO2	78.75	74.00	73.26	73.74	76.15
TiO2	0.13	0.96	0.46	0.44	0.08
Al2O3	12.70	12.45	15.59	14.54	12.22
FeO*	1.09	2.49	1.62	1.99	0.54
MnO	0.06	0.10	0.05	0.07	0.07
MgO	0.15	0.42	0.24	0.14	0.02
CaO	1.16	2.25	2.35	1.01	1.34
Na2O	3.09	3.13	2.72	4.35	2.88
K2O	3.10	2.34	1.75	3.84	2.46
P2O5	0.03	0.29	0.27	0.07	0.07
Total	100.26	98.43	98.32	100.18	95.82

Number of ions

Si	0.2680	0.2590	0.2549	0.2532	0.2702
Ti	0.0003	0.0025	0.0012	0.0011	0.0002
Al	0.0510	0.0514	0.0639	0.0588	0.0511
Fe	0.0031	0.0073	0.0047	0.0057	0.0016
Mn	0.0002	0.0003	0.0002	0.0002	0.0002
Mg	0.0007	0.0022	0.0013	0.0007	0.0001
Ca	0.0043	0.0084	0.0088	0.0037	0.0051
Na	0.0204	0.0213	0.0184	0.0290	0.0198
K	0.0135	0.0104	0.0078	0.0168	0.0111
P	0.0001	0.0009	0.0008	0.0002	0.0002
O	0.6385	0.6363	0.6381	0.6306	0.6404
Mg#	19.3	23.3	21.1	11.4	4.8

	496CPXGL1	496CPXGL2	497CPXGL1	497CPXGL2
SiO2	74.72	76.13	75.07	76.23
TiO2	0.67	0.57	0.49	0.35
Al2O3	15.81	14.05	14.49	14.00
FeO*	1.38	0.80	0.69	1.05
MnO	0.09	0.05	0.09	0.05
MgO	0.09	0.11	0.17	0.50
CaO	0.80	1.65	1.43	2.22
Na2O	1.63	2.37	2.80	3.59
K2O	3.84	2.83	2.77	2.54
P2O5	0.18	0.14	0.11	0.14
Total	99.22	98.70	98.10	100.69

Number of ions

Si	0.2583	0.2634	0.2610	0.2588
Ti	0.0018	0.0015	0.0013	0.0009
Al	0.0644	0.0573	0.0594	0.0560
Fe	0.0040	0.0023	0.0020	0.0030
Mn	0.0003	0.0001	0.0003	0.0002
Mg	0.0004	0.0006	0.0009	0.0026
Ca	0.0030	0.0061	0.0053	0.0081
Na	0.0109	0.0159	0.0189	0.0236
K	0.0169	0.0125	0.0123	0.0110
P	0.0005	0.0004	0.0003	0.0004
O	0.6395	0.6400	0.6384	0.6355
Mg#	18.0	19.4	30.6	46.2

APPENDIX V

LEAST-SQUARES MIXING MODELS

Notes to Appendix V

This appendix contains the results of some least-squares mixing calculations as discussed in chapter 7. Modelled attempts to generate the composition of sample 491 by adding various mineral phases to the bulk composition of andesite 493 are given in the first two listings. The next four listings represent attempts to generate the composition of andesite sample 496 by mixing together endmembers of the hypothetical mixing pairs given in chapter 7.

Listings seven through eleven show the results of least-squares calculations that attempted to reproduce the proposed fractionation trend of figure 3-5. Listing twelve is an example of the results of least-squares mixing calculations that use orthopyroxene as a fractionating phase. It can be seen in this example that orthopyroxene must be added to, not subtracted from, the bulk composition of andesite 492 in order to form andesite 499, thereby causing some problems in any proposed fractionation scheme (see chapter 7 for a more complete discussion of this point).

The last four listings show the results of possible whole-rock mixes that may have formed andesite sample 497. Taken along with petrographic evidence (chapter 4 and appendix II) these results suggest that a mixing event may have formed this sample.

491

	OBSERVED	CALCULATED
SiO2	52.77	53.12
TiO2	0.57	0.63
Al2O3	12.00	11.47
FeO*	8.44	6.77
MnO	0.17	0.17
MgO	11.03	9.29
CaO	12.50	13.61
Na2O	1.78	1.82
K2O	0.64	0.53
P2O5	0.11	0.09

ESTIMATED WEIGHT PERCENTAGES

493	55.97
491AVGMEGACPX	41.53

SUM OF SQUARES OF RESIDUALS

7.4489

491

	OBSERVED	CALCULATED
SiO2	52.77	52.77
TiO2	0.57	0.73
Al2O3	12.00	12.00
FeO*	8.44	8.41
MnO	0.17	0.16
MgO	11.03	11.04
CaO	12.50	12.49
Na2O	1.78	1.82
K2O	0.64	0.52
P2O5	0.11	0.09

ESTIMATED WEIGHT PERCENTAGES

493	55.40
491AVGMEGACPX	33.63
491MEGAOL	7.10
491P2c	2.61
491MT3	1.29

SUM OF SQUARES OF RESIDUALS

0.0416

496

	OBSERVED	CALCULATED
SiO2	59.46	59.67
TiO2	0.76	0.76
Al2O3	17.28	16.65
FeO*	6.94	6.86
MnO	0.15	0.15
MgO	3.24	3.25
CaO	7.25	7.01
Na2O	3.42	3.44
K2O	1.35	1.44
P2O5	0.15	0.15

ESTIMATED WEIGHT PERCENTAGES

491	2.30
497	97.08

SUM OF SQUARES OF RESIDUALS

0.5176

496

	OBSERVED	CALCULATED
SiO2	59.46	59.44
TiO2	0.76	0.77
Al2O3	17.28	17.39
FeO*	6.94	6.37
MnO	0.15	0.16
MgO	3.24	3.32
CaO	7.25	7.52
Na2O	3.42	3.63
K2O	1.35	1.27
P2O5	0.15	0.16

ESTIMATED WEIGHT PERCENTAGES

492	63.63
501	36.41

SUM OF SQUARES OF RESIDUALS

0.4637

496

	OBSERVED	CALCULATED
SiO2	59.46	59.44
TiO2	0.76	0.75
Al2O3	17.28	17.51
FeO*	6.94	6.29
MnO	0.15	0.15
MgO	3.24	3.41
CaO	7.25	7.39
Na2O	3.42	3.48
K2O	1.35	1.22
P2O5	0.15	0.16

ESTIMATED WEIGHT PERCENTAGES

493	61.88
501	37.91

SUM OF SQUARES OF RESIDUALS

0.5541

496

	OBSERVED	CALCULATED
SiO2	59.46	59.47
TiO2	0.76	0.74
Al2O3	17.28	17.20
FeO*	6.94	6.96
MnO	0.15	0.15
MgO	3.24	3.33
CaO	7.25	7.27
Na2O	3.42	3.49
K2O	1.35	1.35
P2O5	0.15	0.17

ESTIMATED WEIGHT PERCENTAGES

495	15.82
X	84.31

SUM OF SQUARES OF RESIDUALS

0.0240

X

	OBSERVED	CALCULATED	ESTIMATED WEIGHT PERCENTAGES	
SiO2	57.50	57.50	492	127.97
TiO2	0.81	0.98	492AVGPL	-18.80
Al2O3	17.55	17.56	492AVGCPX	-6.66
FeO*	7.57	7.53	492AVGOL	-1.32
MnO	0.15	0.18	492AVGMT	-0.90
MgO	3.73	3.76		
CaO	7.97	7.97	SUM OF SQUARES OF RESIDUALS	
Na2O	3.33	3.32		
K2O	1.21	1.26	0.0371	
P2O5	0.18	0.22		

497

	OBSERVED	CALCULATED	ESTIMATED WEIGHT PERCENTAGES	
SiO2	60.22	60.21	492	171.96
TiO2	0.77	0.93	492AVGPL	-48.43
Al2O3	16.87	16.92	492AVGCPX	-15.06
FeO*	6.86	6.83	492AVGOL	-4.57
MnO	0.15	0.20	492AVGMT	-3.52
MgO	3.08	3.12		
CaO	6.92	6.93	SUM OF SQUARES OF RESIDUALS	
Na2O	3.51	3.32		
K2O	1.47	1.63	0.1137	
P2O5	0.15	0.30		

499

	OBSERVED	CALCULATED	ESTIMATED WEIGHT PERCENTAGES	
SiO2	61.64	61.62	492	188.53
TiO2	0.74	0.74	492AVGPL	-56.80
Al2O3	17.29	17.37	492AVGCPX	-21.13
FeO*	5.82	5.82	492AVGOL	-4.84
MnO	0.13	0.19	492AVGMT	-5.43
MgO	2.76	2.78		
CaO	6.21	6.24	SUM OF SQUARES OF RESIDUALS	
Na2O	3.80	3.45		
K2O	1.45	1.78	0.2734	
P2O5	0.16	0.33		

501

	OBSERVED	CALCULATED
SiO2	65.13	65.12
TiO2	0.53	0.55
Al2O3	16.35	16.36
FeO*	4.75	4.75
MnO	0.13	0.11
MgO	1.98	2.01
CaO	5.10	5.11
Na2O	4.15	4.15
K2O	1.72	1.93
P2O5	0.15	0.20

ESTIMATED WEIGHT PERCENTAGES	
497	132.40
497AVGPL	-17.61
497AVGCPX	-6.59
497AVGOPX	-4.66
497AVGMT	-3.25

SUM OF SQUARES OF RESIDUALS

0.0484

495

	OBSERVED	CALCULATED
SiO2	69.50	69.50
TiO2	0.38	0.39
Al2O3	15.15	15.16
FeO*	3.68	3.68
MnO	0.12	0.13
MgO	1.16	1.16
CaO	3.48	3.48
Na2O	4.34	4.29
K2O	2.07	2.12
P2O5	0.11	0.19

ESTIMATED WEIGHT PERCENTAGES	
501	126.46
501AVGPL	-15.89
501AVGHBL	-7.15
501AVGCPX	-2.02
501AVGMT	-1.30

SUM OF SQUARES OF RESIDUALS

0.0128

499

	OBSERVED	CALCULATED
SiO2	61.64	61.64
TiO2	0.74	0.68
Al2O3	17.29	17.37
FeO*	5.82	5.83
MnO	0.13	0.23
MgO	2.76	2.75
CaO	6.21	6.21
Na2O	3.80	3.38
K2O	1.45	1.60
P2O5	0.16	0.29

ESTIMATED WEIGHT PERCENTAGES	
492	167.17
492AVGOPX	11.27
492AVGPLAG	-43.63
492AVGCPX	-19.68
492AVGOL	-10.38
492AVGMT	-4.76

SUM OF SQUARES OF RESIDUALS

0.2275

497

	OBSERVED	CALCULATED
SiO2	60.22	60.09
TiO2	0.77	0.77
Al2O3	16.87	17.49
FeO*	6.86	6.46
MnO	0.15	0.14
MgO	3.08	3.06
CaO	6.92	6.83
Na2O	3.51	3.63
K2O	1.47	1.36
P2O5	0.15	0.16

ESTIMATED WEIGHT PERCENTAGES

500	25.48
499	74.51

SUM OF SQUARES OF RESIDUALS

0.6039

497

	OBSERVED	CALCULATED
SiO2	60.22	60.11
TiO2	0.77	0.78
Al2O3	16.87	17.45
FeO*	6.86	6.20
MnO	0.15	0.14
MgO	3.08	3.11
CaO	6.92	6.91
Na2O	3.51	3.67
K2O	1.47	1.33
P2O5	0.15	0.17

ESTIMATED WEIGHT PERCENTAGES

492	26.42
499	73.44

SUM OF SQUARES OF RESIDUALS

0.8283

497

	OBSERVED	CALCULATED
SiO2	60.22	60.12
TiO2	0.77	0.77
Al2O3	16.87	17.48
FeO*	6.86	6.16
MnO	0.15	0.14
MgO	3.08	3.13
CaO	6.92	6.83
Na2O	3.51	3.61
K2O	1.47	1.32
P2O5	0.15	0.16

ESTIMATED WEIGHT PERCENTAGES

493	24.60
499	75.11

SUM OF SQUARES OF RESIDUALS

0.9292

497

	OBSERVED	CALCULATED
SiO2	60.22	60.16
TiO2	0.77	0.71
Al2O3	16.87	17.13
FeO*	6.86	6.57
MnO	0.15	0.14
MgO	3.08	3.12
CaO	6.92	6.96
Na2O	3.51	3.62
K2O	1.47	1.39
P2O5	0.15	0.17

ESTIMATED WEIGHT PERCENTAGES

501	35.11
X	64.87

SUM OF SQUARES OF RESIDUALS

0.1769